MODELING, ANALYSIS, AND EVALUATION OF RANKINE CYCLE PROPULSION SYSTEMS

VOLUME I: FINAL REPORT

By

J. H. Skinner, R. P. Shah, and W. A. Boothe

February 1972

Prepared for

OFFICE OF AIR PROGRAMS
ENVIRONMENTAL PROTECTION AGENCY
ANN ARBOR, MICHIGAN 48105

Contract No. EHS-70-111

Mechanical Engineering Laboratory
Corporate Research and Development
General Electric Company
Schenectady, New York 12305

FOREWORD

This report, "Modeling, Analysis, and Evaluation of Rankine Cycle Propulsion System," describes work carried out under Contract No. EHS-70-111 for the Office of Air Programs, Environmental Protection Agency at Ann Arbor, Michigan. The work was conducted by the Mechanical Engineering Laboratory of Corporate Research and Development of the General Electric Company in Schenectady, New York.

The report consists of two volumes:

Volume I -- Final Report
Volume II -- Users Manual

Volume I includes the derivation of the models and their application to specific designs. Steady-state and transient results are presented. Volume II includes copies of the computer programs, FORTRAN nomenclature, flow diagrams, and other user information.

The Project Officer for this contract was Mr. William Zeber of the Environmental Protection Agency. The Deputy Project Officer was Mr. Kent Jefferies of the National Aeronautics and Space Administration Lewis Research Center in Cleveland, Ohio.

ACKNOWLEDGMENTS

The authors gratefully acknowledge assistance from the following people:

Mr. Robert Barber and his associates of Barber-Nichols Engineering Corporation, Arvada, Colorado, for turbine expander data and analyses. Barber-Nichols was a subcontractor in this project.

Mr. Dale H. Brown, Thermal Branch, General Electric Corporate Research and Development, for advice and assistance on transient thermodynamics.

Dr. Thomas Kerr of the Information Studies Branch, Corporate Research and Development, and Mr. William Keltz of the Specialty Fluidics Operation, General Electric Company, for assistance in controls analysis.

Mrs. Barbara Kuhn, Contract Administrator, General Electric Corporate Research and Development.

Mr. Peter M. Meenan and Mr. Robert C. Rustay of the Information Studies Branch, General Electric Corporate Research and Development, for assistance in modeling and simulation.

Dr. Dean Morgan and his associates in the Thermo Electron Corporation, Waltham, Massachusetts, for reciprocating expander data and analyses. Thermo Electron was a subcontractor on this project.

Professor Wen-Jei Yang of the University of Michigan for consultation in the area of transient thermal analysis.

TABLE OF CONTENTS

TABLE OF CONTENTS (Cont'd)

TABLE OF CONTENTS (Cont'd)

LIST OF ILLUSTRATIONS

LIST OF ILLUSTRATIONS (Cont'd)

LIST OF ILLUSTRATIONS (Cont'd)

LIST OF TABLES

Section 1

SUMMARY

BACKGROUND

The increasing concern for a cleaner environment has led to serious consideration of the Rankine cycle engine for low-pollution automotive propulsion. Typical driving cycles clearly indicate that automobiles are always in transient operation; therefore, engine loading is continuously changing. The Rankine cycle power plant is characterized by a number of thermal inertias which significantly affect the ability of the vehicle to respond to varying demands. Furthermore, engine transients are transmitted through the controls to the combustor fuel and air supply system. High emission levels and inadequate vehicle performance can result if the propulsion system dynamics are not understood and properly controlled.

OBJECTIVE

The objective of the program described in this report was to develop a generalized computer model of a Rankine-cycle automotive propulsion system to be used for the analysis of propulsion system dynamics.

RESULTS

Digital computer models were developed for the following propulsion system components:

- Working fluid -- water and organic
- Combustor
- Vapor generator
- Expander -- reciprocating and turbine
- Condenser
- Regenerator
- Feedpump
- Controls

The major criteria in the development of the component dynamic models were:

- Applicability to the several alternative propulsion system designs under development by the Office of Air Programs, Environmental Protection Agency
- Validity over the full range of vehicle operating conditions

Other vehicle system models were developed to permit analysis of engine dynamics during realistic driving transients. These included models of:

Transmission

Vehicle motion

Route mission profiles

Driver

The programming language is FORTRAN IV. The models were run on the General Electric 635 computer and were calibrated with experimental data when such data were available.

A module-linkage approach was employed for the modeling. Each of the component models is a self-contained module with several input and output information signals. Linkage of the information signals forms a total system model which can be employed for transient analysis of the entire propulsion system.

The computer models that have been developed are described in Volume I of this report. The basic equations are derived, solution techniques are discussed, and preliminary results are presented. Volume II, the Users Manual, contains copies of the computer programs, nomenclature lists, flow diagrams, and other important user information.

The component models have been provided with input data for a propulsion system with a reciprocating expander and organic working fluid designed by the Thermo Electron Corporation (TECO) in Reference 1. The component models have been linked together to form a total system model, which has been run without controls to derive the system steady-state condition.

The models were developed so that design modifications and different working fluids can be easily analyzed by changing the input data. The models are applicable to many alternative propulsion system designs, including:

- Simple reciprocating expander with water as working fluid
- Compound reciprocating expander with water as working fluid
- Turbine expander with organic working fluid

The most comprehensive models developed are for the heat exchangers (vapor generator, condenser, and regenerator). These components play a very significant role in determining dynamic system performance, and their transient behavior is not well understood. A major effort was therefore directed toward developing full-range dynamic heat exchanger models involving a minimum number of assumptions and limitations.

RECOMMENDATIONS

Although most of the effort to date has been concerned with development of the models, and only a limited number of computer runs have been made to obtain definitive results, several recommendations can be made. These recommendations are listed below and are fully developed and discussed in Section 6 of this volume.

Recommendation 1: Because the thermal inertia of the heat exchanger components will determine propulsion system response, the following work is recommended in order to more accurately establish heat exchanger dynamics.

- Sensitivity analyses should be carried out for

  Heat transfer coefficients

  Two-phase/vapor transition point

  Water-jacket resistance

  These analyses would employ the models for parametric variation of the above items to determine their effect on steady-state and dynamic performance.

- The correlation of two-phase flow and heat transfer should be expanded to account for the various two-phase flow regimes.

- The heat exchanger models should be validated with transient experimental data.

Recommendation 2: In order to improve the run-time economy of the computer simulation it is recommended that:

- The fluid property models be utilized more efficiently.

- Fixed time steps and lump sizes be employed in the heat exchanger models.

- A set of "parametric models" be developed.

Recommendation 3: The following control system development plan is recommended:

- The instantaneous control models that have been developed should be employed to bring the total system to steady state at the design condition, and small perturbation transients around this point should be analyzed. This will establish the basic validity of the control scheme.

- Acceptable limits on the variation of system parameters during transients should be established.

- The full-range dynamic models should be used to derive limited-range parametric models as described above.
- The instantaneous control scheme should be modified to include control dynamics. The controls should be developed by means of the parametric models.
- The final control scheme should be checked out with the full-range dynamic models.

Recommendation 4: The models developed are highly flexible and general. They can be used to simulate the dynamics of many alternative Rankine cycle propulsion-system configurations. It is recommended that the models be employed for transient analysis of the systems under development by the Environmental Protection Agency and the results used to support and guide the design and experimentation.

Section 2

INTRODUCTION

BACKGROUND

Since the exhaust emissions of internal combustion engines are a major source of air pollution, serious consideration is being given to other automotive propulsion systems with low pollution characteristics. The Rankine cycle engine appears to be a most promising near-term alternative. This engine, using components of reasonable size, weight, and cost, is capable of providing required vehicle performance with minimum contamination.

Automobile operation is distinctly transient; this is due to the repetitive accelerations and decelerations that are required in most driving situations. Propulsion systems rarely operate in steady state, and engine designs based solely on steady-state considerations will have serious deficiencies. Propulsion system dynamics must be analyzed in order to determine the size and capacity of engine components, the vehicle performance and emissions, and the control system requirements.

In order to illustrate the importance of understanding Rankine cycle dynamics, consider the highway passing situation. Initially, the vehicle is cruising at a constant velocity, the engine speed is constant, and the vapor mass flow rate is uniform throughout the cycle. The torque required for acceleration is several times the torque at cruise. As a result the vapor demand during the acceleration period is also several times higher than at steady state. Therefore, the size and capacity of all the engine components (vapor generator, expander, regenerator, condenser, pumps, and fans) must be based on the transient operating condition.

In order to execute the passing maneuver the driver depresses the accelerator pedal, which opens the throttle, or increases the expander cut-off. This produces a demand for a rapid increase in vapor flow from the vapor generator. If the flow through the feedpump is not increased to maintain vapor generator inventory, the pressure will drop and consequently the engine torque capability will be reduced. Therefore, the acceleration rate of the vehicle depends upon the dynamic response of the vapor generator and pump. Furthermore a control linkage is required between the accelerator pedal, expander, and feedpump.

As the mass flow rate through the system increases, the vapor generator exit temperature will drop and the cycle efficiency will be impaired, unless there is a simultaneous increase in combustor fuel flow. However, the emission levels are highly sensitive to air/fuel ratio. If the airflow rate is not increased proportionately to the fuel, the air/fuel ratio will deviate from its optimum value and the air pollution level will be high. The rate at which the air and fuel flows change depends upon the dynamics of the air and fuel supply systems.

Therefore, in order to maintain low emission levels during transients the combustor dynamics must be controlled.

From the above discussion it should be apparent that understanding of the propulsion system dynamics is essential in order to develop high-performance low-emission Rankine cycle engines.

OBJECTIVE

The objective of this program carried out for the Office of Air Programs, Environmental Protection Agency was:

- To develop a generalized computer model of a Rankine cycle automotive propulsion system to be used for analysis of propulsion system dynamics.

APPROACH

A mathematical model of an engine component is a set of analytical expressions, equations, or algorithms which describe the component's operation. The approach taken in the present program was the development of digital computer models of the major components of the Rankine cycle propulsion system. The following components were modeled:

Working Fluid -- water and organics

Combustor

Vapor Generator

Expander -- reciprocating and turbine

Condenser

Regenerator

Feedpump

Controls -- power, flow rate, combustor

In addition to the propulsion system models, other models were constructed for the analysis of dynamics in realistic driving situations. These included models for:

- Transmission
- Vehicle -- motion resistance, traction
- Route mission profiles consisting of

  Start-up
  Accelerations
  Cruise at various speeds
  Decelerations
  High-speed pass
  Grades

- Driver -- compares the vehicle performance to reference conditions and adjusts the acceleration pedal or brake accordingly.

The models have been written in computer language FORTRAN IV and have been run on the General Electric 635 high-speed digital computer. The models can be used on any computer that employs a FORTRAN IV compiler.

The procedure used for the modeling is referred to as the module-linkage approach. Each of the individual component models is formulated in a modular or building-block manner. That is, each component model is a unit in itself, and the equations describing it are independent of those describing other components. These modules are linked together by statements expressing the interplay or communication between components. For example, in the expander model, the torque is expressed as a function of inlet pressure and temperature, exit pressure, cut-off, and expander speed.

The expander model is linked to:

a. The transmission model, by rpm and torque linkages
b. The vapor generator model, by pressure temperature and mass flow linkages
c. The control system, by the cut-off linkage

Linking together all of the component models forms a total system model that is capable of simulating steady-state and dynamic performance over the entire vehicle operating range.

The module-linkage approach allows rapid examination of alternative engine and control system configurations. The component models were developed to permit simulation of the performance of four systems:

- Reciprocating engine with CP-34 as working fluid
- Reciprocating engine with water as working fluid
- Turbine engine with FC-75 as working fluid
- Compound reciprocating engine with water as working fluid

The first engine configuration, with CP-34 as working fluid, is the system designed by the Thermo Electron Corporation under Contract CPA 22-69-162 (Ref. 1). Data for this system have been input into the models, the models have been checked out, and component transient analyses have been run. The total system model has been formulated, linking together the components, and has been brought to steady state at the design condition.

The total system model can now be employed for system transient analyses. A preliminary control scheme has been developed for this purpose.

For the remaining three systems, preliminary designs have been completed, and data generated suitable for input into the component and system models. As of this writing the models have not been exercised for these three alternative systems.

ADVANTAGES AND LIMITATIONS OF MODELING AND SIMULATION

Modeling and simulation are extremely powerful analytical techniques, widely used for the investigation of dynamic systems. They are especially suited to the analysis of complex systems containing many interacting components -- such as Rankine cycle engines. Use of the digital computer makes possible the numerical solution of equations describing component dynamics.

The accuracy and validity of modeling and simulation are limited by the theoretical basis for describing the physical processes involved. This is an inherent limitation of all analytical techniques. The models developed in this program have been calibrated with experimental data, whenever available, in order to represent realistic engine designs.

The vapor generator is one of the most important components to be accurately modeled, as it has a significant effect on system dynamics. This is also the most difficult component to model, since it is necessary to simultaneously solve the nonlinear partial differential equations for mass, momentum, and energy conservation. As will be brought out in later sections, vapor generator dynamics are fairly sensitive to the assumptions made in describing the two-phase flow during transients. Therefore, at the end of this report, future work is recommended which will improve the capability of the vapor generator model in predicting the dynamic behavior of this critical component. This work consists of using the model to run sensitivity studies on the heat transfer parameters in order to isolate those which have a strong influence on dynamic response. The studies should be followed by experimentation to accurately determine these parameters, and this information should be factored back into the vapor generator model.

The above recommendation provides a good example of how modeling and simulation can be employed to complement experimentation. In any experimental program there are limitations on the parameters that can be measured. For the vapor generator, for example, pressure, temperature, and mass flow rates are fairly easy to measure, while it is difficult to sense the motion of the liquid two-phase interface which causes changes in pressure, temperature, and flow. However, the vapor generator model can be used to predict the interface motion and isolate the cause of the experimentally measured effects.

Simulation can also be used for investigations of hazardous conditions or conditions outside the range of the experimental apparatus. Finally, simulation is usually much less costly than actual experimentation, and should therefore be used to direct and focus an experimental program.

One of the requirements of the models developed in this program was flexibility. The models readily accept design changes, different working fluids, different component configurations, and alternative control linkages. This requirement increased the complexity of the models, the development time, the computer memory size, and the run time. Simpler special-purpose models would have been easier and individually less expensive, but a separate model would be required for each component of each system to be studied. Furthermore, design changes would probably require internal model modifications rather than just change of input data as in the present case. The more flexible modeling is valuable in development programs where there are many alternatives to be considered.

Throughout this program, efforts were made to minimize the limitations and weaknesses of the digital simulation approach and increase its accuracy and utility.

In Section 3, the propulsion system models are derived and transient results are presented. This is followed by discussion of the other vehicle component models (Section 4) and the total system model (Section 5). Finally, at the end of Volume I (Section 6), the results are discussed and recommendations are made for future work.

Section 3

PROPULSION SYSTEM

Models have been developed for the following propulsion system components:

- Working fluid

  Thermodynamic properties
  Transport and metal properties

- Reciprocating expander
- Turbine expander
- Vapor generator
- Regenerator
- Condenser
- Feedpump
- Combustor
- Controls

Dimensional and geometric data have been input into these models, and steady-state and transient analyses have been made. In most instances, the component design has been based on the propulsion system specified in Reference 1 -- a reciprocating expander with CP-34 as working fluid.

The models were developed so that different engine designs could be readily analyzed. Input data for the following three alternative propulsion systems have been generated employing a parametric design procedure described in Appendix I, "Parametric Propulsion System Designs," at the end of this volume.

- Reciprocating expander with water as working fluid
- Turbine expander with FC-75 as working fluid
- Compound reciprocating expander with water as a working fluid

In the following subsections, the propulsion system models will be derived and results of their application will be discussed.

WORKING FLUID

Models have been developed for the thermodynamic and transport properties of the working fluid. These models are employed throughout the Rankine cycle and used to determine various properties of the working fluid when other properties are known.

THERMODYNAMIC PROPERTIES

Models have been developed which yield thermodynamic properties in the saturated and superheated regions. These models are based upon tabular thermodynamic data which are entered and stored in the program. These data can then be searched to determine the properties needed. The models apply to any working fluid for which thermodynamic data are available. Data for CP-34, FC-75, and water are presented in the Appendix, "Working Fluid Thermodynamic Properties for CP-34, Water, and FC-75," of Volume II of this report.

Saturated Properties

The saturated property model consists of three elements: a fluid property listing, a reading program, and an interpolation program.

Saturated Fluid Property Listing. Each line of the saturated fluid property listing contains a temperature value and the corresponding values of pressure, specific volume of the liquid, specific volume of the vapor, enthalpy of the liquid, and enthalpy of the vapor. The property listing can easily be extended on both the lower and upper ends or filled in so that the intervals between temperature steps are smaller. A variable temperature interval can also be used to increase accuracy without necessitating any change in the interpolation program. The amount of data in the fluid property listing is the factor which establishes the accuracy of the interpolation.

Saturated Reading Program. The saturated reading program reads the values in the saturated fluid properties listing and assigns subscripted labels to these values. It stores these dimensioned arrays for subsequent use. The reading program needs to be loaded only once during the execution of any one computer run.

Saturated Interpolation Program. In the saturated region, specification of one fluid property establishes the values of all remaining properties. The saturated interpolation program was developed to determine these remaining properties. The interpolation program is so constructed that it can be entered with a value of temperature, pressure, or enthalpy of the liquid. A logic input code is used to direct the computer to the correct portion of the interpolation program for the given input property.

Based on the input property, the interpolation program starts at one end of the saturated property array and searches in sequence for the interval in which the input value falls. Then a linear interpolation is carried out across this interval. This method of search works satisfactorily but can be inefficient if the interpolation program has to be entered a great many times. Alternative methods, employing memory or binary search, could be used so that the entire array does not have to be searched each time.

If an input value exceeds the range of that particular fluid property array, the interpolation program extrapolates to that value.

Interrelationship Between the Reading and Interpolation Programs. Figure 1 is a diagram of the program steps for obtaining interpolated saturated property values. The interpolation program is entered with a value of a saturated fluid property. Before interpolation can take place, a check must be made to ascertain whether the reading program has already been entered. If it has not previously been entered, it is now called. The reading program, in turn, reads and stores the saturated fluid property values in their individual arrays. The appropriate logic variable in the interpolation program prevents any subsequent entering of the reading program. The saturated fluid property values are now available to the interpolation program, which uses them in its process.

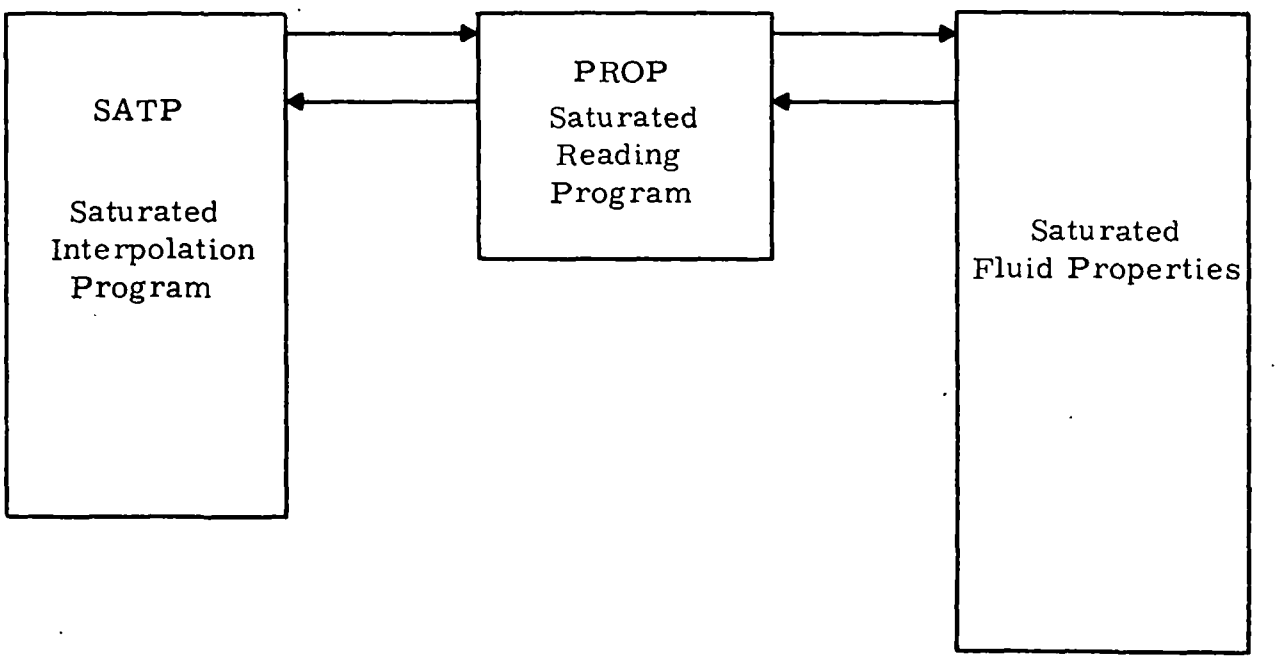

Figure 1. Linkage of Saturated Fluid Property Model (SATP and PROP are the names of programs which are described in Volume II)

Results. Table 1 shows the results of the test case of the saturated property model for water. Data from the American Society of Mechanical Engineers steam table (Ref. 2) are printed next to the interpolated computer values for comparison. A good agreement can be seen.

Superheated Properties

The superheated property model also consists of three elements: a fluid property listing, a reading program, and an interpolation program.

Table 1

RESULTS OF SATURATED PROPERTY MODEL FOR WATER
(Values in Parentheses are from Reference 2)

Temperature = 202°F		
Pressure, psi	12.0236	(12.011)
Temperature, °F	202.0000	(202.0)
Liquid Specific Volume, ft^3/lb	0.0167	(0.01665)
Vapor Specific Volume, ft^3/lb	32.4090	(32.367)
Liquid Enthalpy, Btu/lb	170.1020	(170.10)
Vapor Enthalpy, Btu/lb	1146.7600	(1146.7)
Temperature = 518°F		
Pressure, psi	798.5500	(798.55)
Temperature, °F	518.0000	(518.0)
Liquid Specific Volume, ft^3/lb	0.0209	(0.02086)
Vapor Specific Volume, ft^3/lb	0.5701	(0.57006)
Liquid Enthalpy, Btu/lb	509.6000	(509.6)
Vapor Enthalpy, Btu/lb	1199.4000	(1199.4)
Temperature = 468°F		
Pressure, psi	504.8940	(504.83)
Temperature, °F	468.0000	(468.0)
Liquid Specific Volume, ft^3/lb	0.0198	(0.01976)
Vapor Specific Volume, ft^3/lb	0.9188	(0.91862)
Liquid Enthalpy, Btu/lb	450.6500	(450.7)
Vapor Enthalpy, Btu/lb	1204.6500	(1204.6)
Pressure = 1000 psi		
Pressure, psi	1000.0000	(1000.0)
Temperature, °F	544.5693	(544.58)
Liquid Specific Volume, ft^3/lb	0.0216	(0.02159)
Vapor Specific Volume, ft^3/lb	0.4461	(0.446)
Liquid Enthalpy, Btu/lb	542.5758	(542.55)
Vapor Enthalpy, Btu/lb	1192.9292	(1192.9)

Table 1 (Cont'd)

Pressure = 50 psi		
Pressure, psi	50.0000	(50.0)
Temperature, °F	280.9965	(281.02)
Liquid Specific Volume, ft^3/lb	0.0173	(0.01727)
Vapor Specific Volume, ft^3/lb	8.5199	(8.514)
Liquid Enthalpy, Btu/lb	250.1789	(250.21)
Vapor Enthalpy, Btu/lb	1174.0989	(1174.1)
Liquid Enthalpy = 405.7		
Pressure, psi	336.5195	(336.463)
Temperature, °F	428.0000	(428)
Liquid Specific Volume, ft^3/lb	0.0191	(0.01906)
Vapor Specific Volume, ft^3/lb	1.3786	(1.3782)
Liquid Enthalpy, Btu/lb	405.7000	(405.7)
Vapor Enthalpy, Btu/lb	1203.7500	(1203.7)

Superheated Fluid Property Listings. There are three superheated fluid property listings. The first contains the pressure and temperature steps for which the other two listings supply the corresponding specific volume, enthalpy, entropy, and specific heat values. The property data can easily be extended on both the lower and upper ends, or filled in so that the intervals between pressure steps and temperature steps are smaller. Variable temperature or pressure steps can also be used to increase interpolation accuracy without necessitating any change in the interpolation program. The amount of data available, and also the amount of computer memory space, are the limiting factors in determining the accuracy of the superheated interpolation program.

Superheated Reading Program. The superheated reading program reads the values in the superheated fluid property listings and assigns subscripted labels to these values. It stores these dimensioned arrays in COMMON for subsequent use. It is necessary to enter the reading program only once during the execution of the system's program.

Superheated Interpolation Program. In the superheated region specification of two independent fluid properties establishes the values of all remaining properties. The superheated interpolation program was developed to determine these remaining properties. The interpolation program is constructed

so that it can be entered with values for any of the following pairs of fluid properties:

- Pressure and temperature
- Pressure and entropy
- Pressure and enthalpy
- Specific volume and entropy

A value of a logic input code is also entered and used to direct the computer to the correct portion of the interpolation program for the given input properties.

Each pressure block of the superheated table contains superheated properties for a wide temperature range. For temperatures below the saturation temperature (for that particular pressure block) subcooled data were employed to fill out the pressure block.

As already mentioned in the discussion of the saturated interpolation program, the method of search used in the interpolation programs would not be efficient enough if the program was to be entered a great many times. Here, as in the saturated interpolation program, appropriate messages are printed if an input value falls outside the range of the superheated listings. This message may be suppressed by the use of the appropriate printing logic variable.

Interrelationship Between Reading and Interpolation Programs. Figure 2 is a diagram of the program steps in obtaining interpolated superheated property values. The interpolation program is entered with values of two superheated fluid properties.

As in the discussion of the saturated reading and interpolation programs, a check must be made to determine whether the reading program has already been entered and the superheated fluid property values stored in arrays in COMMON for use by the interpolation program. The appropriate logic variable prevents any subsequent entering of the reading program.

Results. Table 2 shows the results of a test case of the superheated property model for FC-75. Data from Reference 3 are written beside the interpolated computer values for comparison. It is seen that agreement is good. Where there is a discrepancy it is due to difficulty in reading the pressure enthalpy diagram in Reference 3.

TRANSPORT PROPERTIES

Fluid transport properties such as the following were obtained as a function of pressure and temperature from many sources (Refs. 2 - 7):

Specific heat

Viscosity

Conductivity

Density

Surface tension

These were curve-fitted with polynomials by a least squares technique.

In many cases the data available did not cover the entire operating range and had to be extended by extrapolation. The transport properties are listed in Volume II, and the comparison with available data is indicated. Metal, air, and combustion gas properties are handled in a similar manner.

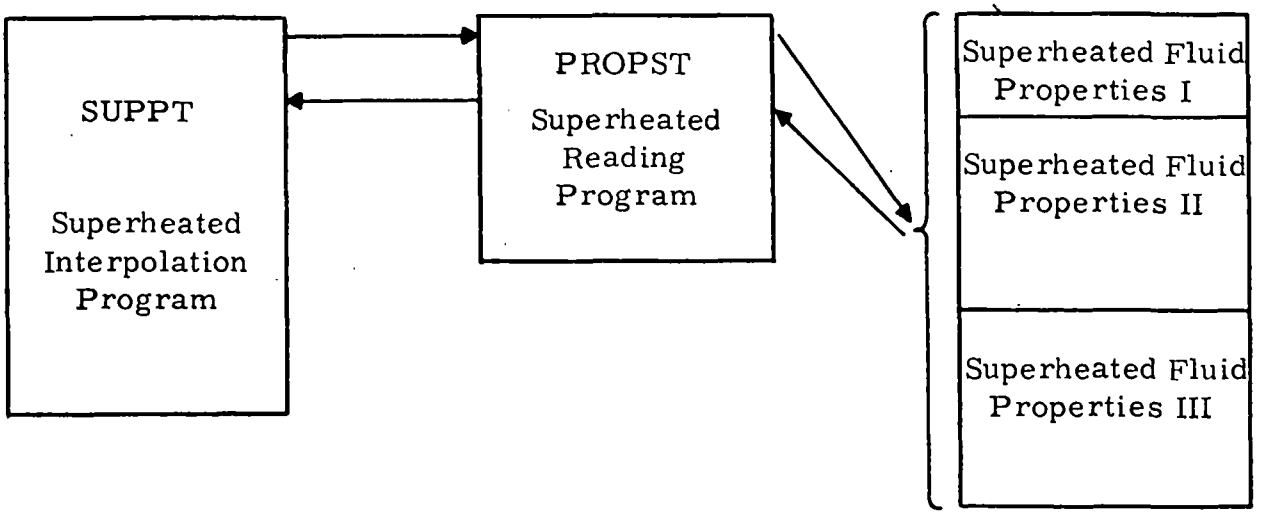

Figure 2. Linkage of Superheated Property Model (SUPPT and PROPST are the names of programs which are described in Volume II)

Table 2

RESULTS OF SUPERHEATED PROPERTY MODEL FOR FC-75
(Values in Parentheses are from Reference 3)

Pressure = 4 atm; Temperature = 170 °C		
Pressure, atm	4.0000	(4.00)
Temperature, °C	170.0000	(170.0)
Enthalpy, Kcal/mole	25.4000	(25.40)
Entropy, cal/mole °C	68.7000	(68.70)
Specific Volume, liters/mole	7.8730	(7.873)
Pressure = 38 atm; Temperature = 294 °C		
Pressure, atm	38.0000	(38.0)
Temperature, °C	294.0000	(294.0)

Table 2 (Cont'd)

Pressure = 38 atm; Temperature = 294°C (Cont'd)		
Enthalpy, Kcal/mole	35.5332	(35.5)
Entropy, cal/mole °C	85.9364	(86.0)
Specific Volume, liters/mole	0.6544	(.708)
Pressure = 12 atm; Entropy = 88 cal/mole °K		
Pressure, atm	12.0000	(12.0)
Temperature, °C	272.4402	(275.)
Enthalpy, Kcal/mole	35.8431	(35.9)
Entropy, cal/mole °C	88.0000	(88.0)
Specific Volume, liters/mole	3.0474	(3.25)
Pressure = 32 atm, Entropy = 78 cal/mole °K		
Pressure, atm	32.0000	(32.0)
Temperature, °C	256.1174	(257.)
Enthalpy, Kcal/mole	31.0467	(31.0)
Entropy, cal/mole °C	78.0000	(78.0)
Specific Volume, liters/mole	0.4994	(.583)
Pressure = 8 atm; Enthalpy = 32 Kcal/mole		
Pressure, atm	8.0000	(8.0)
Temperature, °C	235.1327	(236.)
Enthalpy, Kcal/mole	32.0000	(32.0)
Entropy, cal/mole °C	81.3446	(81.5)
Specific Volume, liters/mole	4.3750	(4.79)
Specific Volume = 39.25 liters/mole; Entropy = 81.22 cal/mole °K		
Pressure, atm	1.0000	(1.000)
Temperature, °C	210.0000	(210.0)
Enthalpy, Kcal/mole	30.0500	(30.05)
Entropy, cal/mole °C	81.2200	(81.22)
Specific Volume, liters/mole	39.2500	(39.25)

EXPANDER

Models have been developed for a reciprocating and turbine expander. These models are quasi-steady in that they instantaneously predict torque and fluid properties at the outlet, as a function of inlet properties, throttle (or cut-off) setting and rpm. The time rate of change of rpm depends upon the engine loading, and is therefore determined in the vehicle model, which is discussed in Section 4 of this volume.

RECIPROCATING EXPANDER

Nomenclature

Alphabetical Symbols	
A_{e1}	Area of blowdown exhaust ports
A_{e2}	Area of auxiliary exhaust ports
A_i	Average inlet valve area
A_p	Piston cross section area
C_{e1}	Flow coefficient of blowdown exhaust ports
C_{e2}	Flow coefficient of auxiliary exhaust ports
C_i	Inlet valve flow coefficient
h_a	Enthalpy after intake
h_b	Enthalpy at end of stroke
h_e	Exhaust enthalpy
h_i	Inlet enthalpy
J	Torque
k	Working fluid conductivity
$\dot{m}$	Mass flow rate through engine
N_p	Number of pistons
p_a	Pressure after intake

Alphabetical Symbols (Cont'd)

p_b	Pressure at end of stroke
p_e	Exhaust pressure
p_i	Inlet pressure
p_m	Indicator mean effective pressure
Q	Heat loss (Btu/lb)
R	Cut-off - fraction of stroke
RPM	Expander rotational speed
s_e	Exhaust entropy
s_i	Inlet entropy
S_p	Stroke
T	Average working fluid temperature
T_b	Temperature at end of stroke
T_e	Exhaust temperature
T_i	Inlet temperature
T_w	Average wall temperature
v_a	Specific volume after intake
v_b	Specific volume at end of stroke
v_e	Exhaust specific volume
v_i	Inlet specific volume
V_p	Piston speed
W_i	Indicator work
W_s	Isentropic work
W_{sh}	Shaft work
x_e	Exhaust quality

Greek Symbols

η_m	Mechanical efficiency
η_{th}	Thermal efficiency
θ_e	Crank angle at which blowdown exhaust ports are uncovered
θ_i	Crank angle for intake opening
μ	Working fluid viscosity

Derivation of Equations

A schematic and indicator diagram for a simple reciprocating vapor expander is shown as Figure 3. The piston starts at the left end of the cylinder and moves to the right, taking in vapor at inlet pressure. When the vapor flow is cut off at point a by closing the inlet valve, the piston continues moving as the vapor trapped in the cylinder expands. When the piston reaches the end of the stroke at point b, the exhaust valve opens and the pressure drops to the exhaust pressure. The piston then moves to the left, discharging the remaining vapor, the exhaust valve is closed, the inlet valve is opened, and the cycle is repeated.

The basic equations for the reciprocating expander model are the relationships for

Torque:

$$J = \frac{W_{shaft\ m}}{RPM} \tag{1}$$

Mass flow:

$$\dot{m} = \frac{N_p A_p V_p}{v_b} \tag{2}$$

Shaft work:

$$W_{shaft} = \eta_{th} \eta_m W_s \tag{3}$$

Isentropic work:

$$W_s = (h_i - h_b) - v_b (p_b - p_e) \tag{4}$$

The properties h_b, p_b, and v_b in Equation 4 are determined for an isentropic expansion from inlet conditions to point b at the end of the stroke.

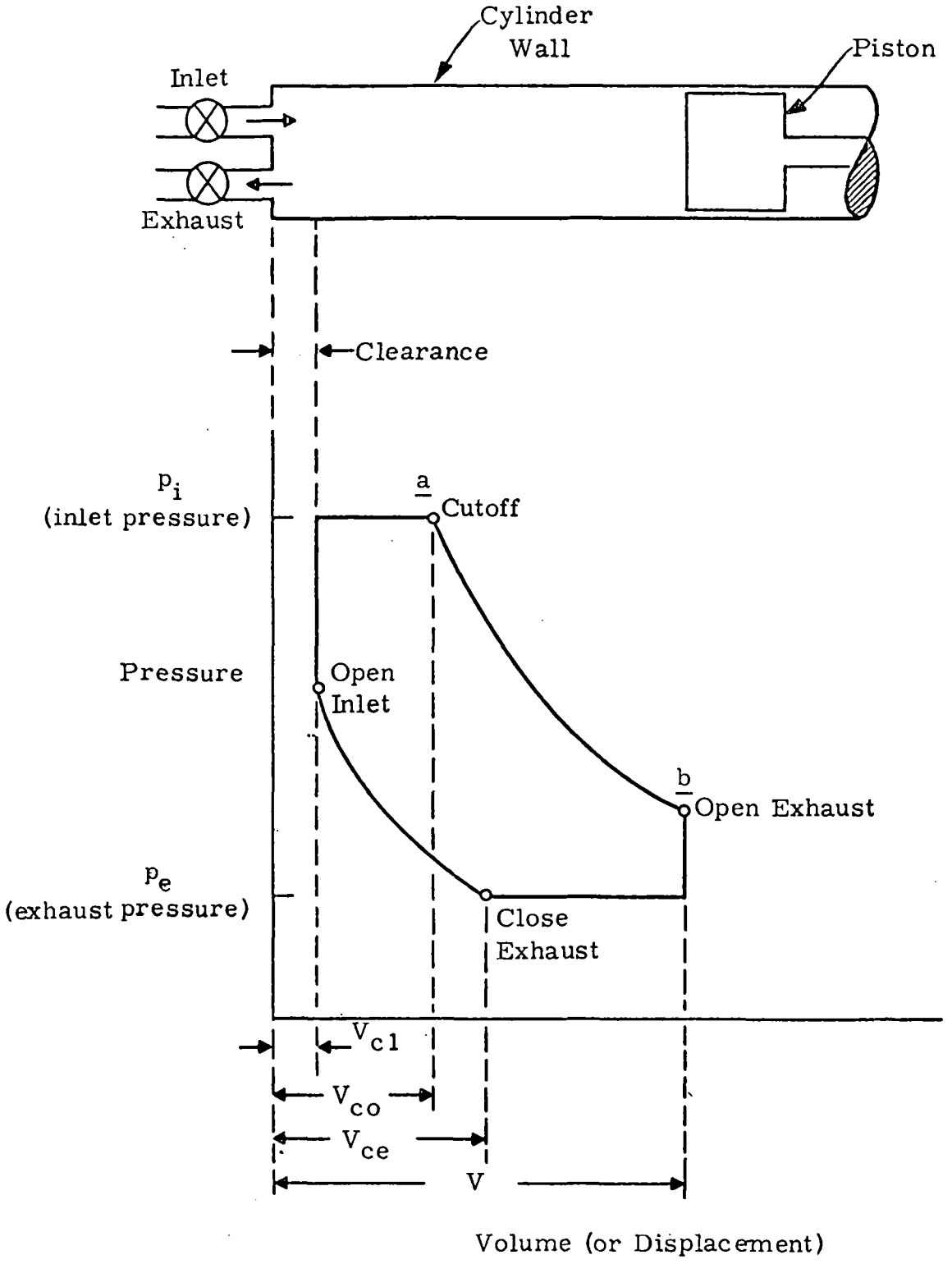

Figure 3. Simple Reciprocating Engine Cylinder Schematic and Indicator Diagram

Mechanical Efficiency. The mechanical efficiency is related to piston speed and indicator mean effective pressure by the following relation derived from expander data by the Thermo Electron Corporation:

$$\eta_m = 1 - V_p \left[\frac{174}{p_m} + 1.6\right] 10^{-5} + \frac{5.46}{p_m} + 0.012 \qquad (5)$$

The above relationship is derived for the dimensions of V_p in feet per minute and p_m in pounds per square inch. The piston speed is defined as

$$V_p = 2 S_p \, RPM \qquad (6)$$

while the mean effective pressure is defined as

$$p_m = W_i / v_b \qquad (7)$$

where v_b is the specific volume at the end of the stroke for the actual non-isentropic expansion.

Thermal Efficiency. The thermal efficiency is defined as

$$\eta_{th} = W_i / W_s \qquad (8)$$

The indicator work is defined as

$$W_i = W_s - \Delta p_i v_i - \Delta p_e v_b - Q \qquad (9)$$

where $\Delta p_i v_i$ is the work loss during intake, $\Delta p_e v_b$ is the work loss during exhaust, and Q is the heat loss.

For incompressible flow through the inlet valve, the following relation can be derived for the pressure loss during intake:

$$\Delta p_i = \frac{1}{8} \left(\frac{A_p}{A_i}\right)^2 \left(\frac{V_p}{C_i}\right)^2 \frac{R}{v_b} \left(\frac{360}{\theta_i}\right)^2 \qquad (10)$$

where the crank angle for intake opening is

$$\theta_i = \text{Arcos}\,(1 - 2R) \qquad (11)$$

The ratio of piston area to average inlet valve area depends upon the valving arrangement and schedule. The relationship employed in this model is the one given for the Thermo Electron expander design in Reference 1. The pressure loss during exhaust for this design can be expressed as:

$$\Delta p_e = \frac{1}{2} \left(\frac{A_p}{A_{e2}}\right)^2 \left(\frac{1}{C_{e2}}\right)^2 \frac{S_p^2}{v_b} - \left(\frac{\theta_e}{360}\right) \left(\frac{A_p A_{e1}}{A_{e2}^2}\right) \left(\frac{C_{e1}}{C_{e2}^2}\right) S_p \sqrt{\frac{p_b - p_e}{v_b}} \qquad (12)$$

The heat loss correlation is

$$Q = \frac{K\, v_b\, k}{V_p \sqrt{A_p}\, S_p} \left(\frac{V_p \sqrt{A_p}}{v_b\, \mu} \right)^{0.75} (T - T_w) \qquad (13)$$

where K is an empirical constant.

The average working fluid temperature was taken as the arithmetic mean of the inlet temperature, and the value at the end of the stroke (point b), assuming a straight line temperature drop during expansion,

$$T = T_i\, R + 0.5(1 - R)\, (T_i + T_b) \qquad (14)$$

The average wall temperature relation is based on Thermo Electron Corporation test data for an engine operating under 550°F inlet conditions. This relationship, normalized with inlet temperature, is

$$T_w = \frac{T_i}{550} (400 + 156\, R^2) \qquad (15)$$

Model Development

The reciprocating expander model is entitled ENGINE and is listed in Volume II of this report. Inputs to the model are:

$$R,\ RPM,\ p_i,\ T_i,\ h_i,\ s_i,\ v_i,\ \text{and}\ p_e.$$

The following geometric and dimensional data must be supplied:

$$N_p,\ A_p,\ S_p,\ C_i,\ C_{e1},\ C_{e2},\ A_{e1},\ \text{and}\ A_{e2}.$$

The model was developed for fixed values of

$$C_i = C_{e1} = C_{e2} = 0.6$$

$$(A_p/A_{e1}) = 16.7$$

$$\frac{A_p\, A_{e1}}{A_{e2}^2} = 6.5$$

which are based on the Thermo Electron expander design. The number of pistons, stroke, and bore are variable.

If the equations derived above are to be employed, the specific volume at the end of the stroke (v_b) must be known. This is determined through an iterative procedure. A first estimate of v_b is obtained by assuming an isentropic intake and expansion and employing the relation

$$v_b = v_i/R \qquad (16)$$

Then Equations 10 and 13 are solved for the pressure drop and heat loss. The pressure and enthalpy after intake are calculated by

$$p_a = p_i - \Delta p_i \tag{17}$$

and

$$h_a = h_i - \left(\frac{\theta_i}{180}\right) Q\left(\frac{T_i - T_w}{T - T_w}\right) \tag{18}$$

The fluid property models are then employed to determine v_a, and a second approximation on v_b is obtained from

$$v_b = v_a/R \tag{19}$$

This is repeated until the successive iterations converge.

The flow through the expander can end in either the superheated or the saturated region, depending on the working fluid and cut-off valve. The fluid quality is therefore calculated and the appropriate working fluid property model is employed.

The outputs from the reciprocating expander model are

$$J,\ \dot{m},\ T_e,\ h_e,\ s_e,\ v_e,\ x_e$$

Other alternative outputs are

$$W_s,\ \eta_m,\ \eta_{th},\ W_i,\ W_{shaft},\ \text{and}\ p_m$$

Results

The reciprocating expander model was run with CP-34 as a working fluid for the following conditions:

$R = 0.137$
$RPM = 2000$
$p_i = 500$ psi
$T_i = 550°F$
$h_i = 123$ Btu/lb
$s_i = 0.0315$ Btu/lb °F
$v_i = 0.1873$ ft^3/lb
$p_e = 25$ psi
$N_p = 4$
$A_p = 15.3$ in.^{2}
$S_p = 3$ in.

The results obtained are:

J = 365 ft-lb

$\dot{m}$ = 7301 lb/hr

T_e = 348°F

h_e = 77 Btu/hr

v_e = 4.05 ft^3/lb

x_e = 1

W_s = 48.3 Btu/lb

η_m = 0.915

η_{th} = 0.849

W_i = 41.0 Btu/lb

W_{sh} = 37.5 Btu/lb

p_m = 126.8 psi

The fluid properties at the engine exit, flow rate, efficiencies, and mean effective pressure are presented in Reference 1 for the same engine design and working fluid. The model results compare very well with these values.

Figure 4 presents a parametric plot of the model results for overall expander efficiency (product of η_m and η_{th}) versus expander speed for several different intake ratios. The results from Reference 1 are also plotted on this figure for R = 0.137. The comparison demonstrates that the model provides a valid representation of expander performance over this range.

TURBINE EXPANDER

Nomenclature

Alphabetical Symbols	
A_e	Nozzle exit area
A_t	Nozzle throat area
C_o	Isentropic spouting velocity
C_1	Flow velocity relative to turbine blades
D_r	Turbine rotor diameter
h_i	Inlet enthalpy

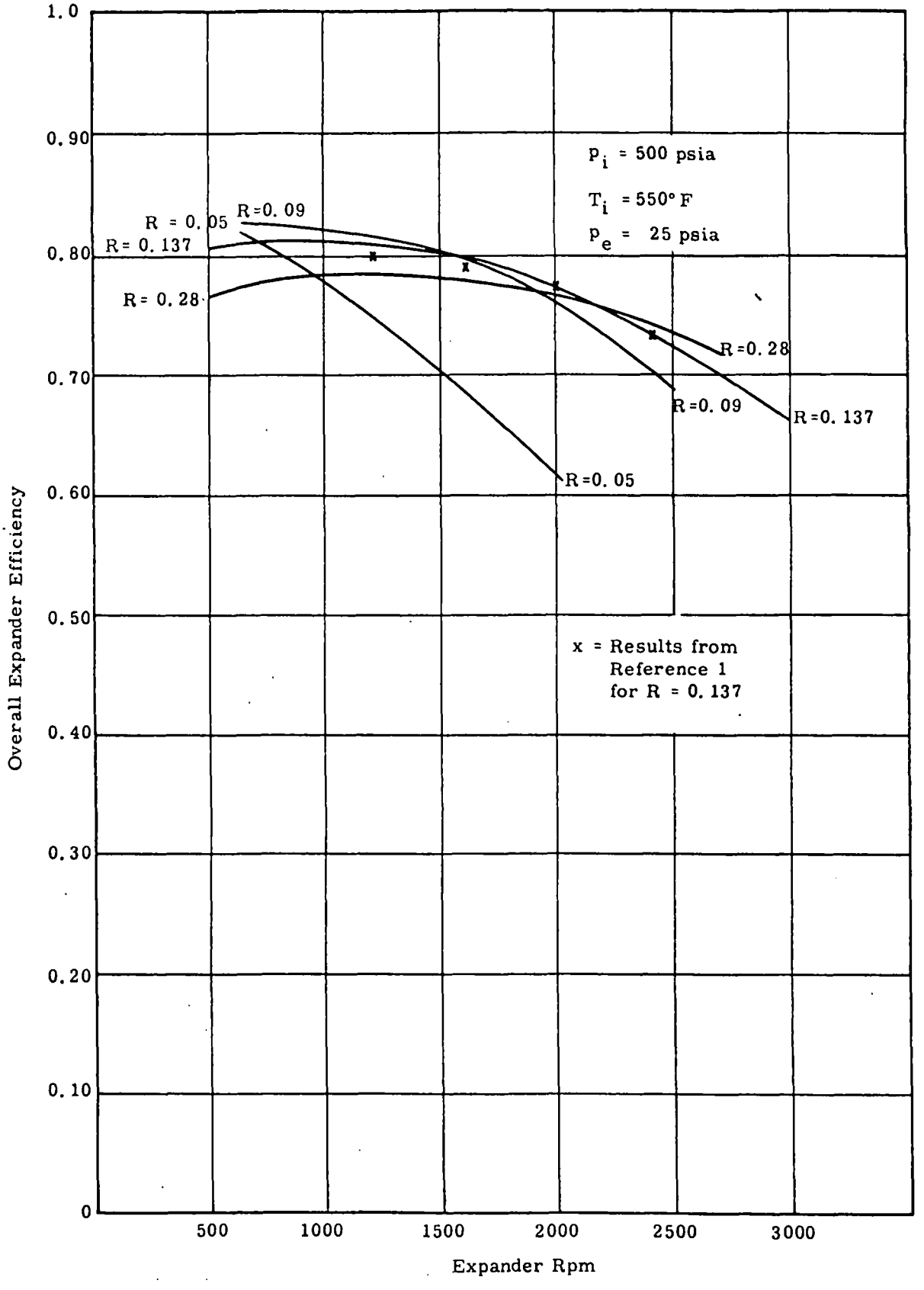

Figure 4. Reciprocating Expander Model -- Efficiency vs Rpm

Alphabetical Symbols (Cont'd)

h_o	Exit enthalpy
J	Torque
$\dot{m}$	Mass flow
M_d	Design Mach number
M_e	Exit Mach number
M_i	Isentropic Mach number
p_i	Inlet pressure
p_o	Exhaust pressure
R	Gas constant
RPM	Rotational speed
T_i	Inlet temperature
U	Turbine tip speed

Greek Symbols

α	Inlet angle
γ	Ratio of specific heats
Δh_s	Enthalpy change for isentropic expansion from p_i to p_o
ΔM_d	Design Mach number correction employed in determining nozzle coefficient
Δp_c	Critical pressure ratio
$\Delta\gamma$	Specific heat correction employed in determining nozzle coefficient
η_h	Hydraulic efficiency
Ψ_n	Nozzle coefficient
Ψ_{nd}	Design nozzle coefficient
Ψ_r	Rotor coefficient

Derivation of Equations

The following equations were derived for an axial impulse turbine expander. The basic equations are the relationships for:

Torque:

$$J = \frac{(h_i - h_o)\,\dot{m}}{RPM} \tag{20}$$

Enthalpy change:

$$h_i - h_o = \eta_h(\Delta h_s) \tag{21}$$

and the equation for mass flow rate, which is derived from compressible flow relations.

Mass Flow Rate. The mass flow rate through the nozzle depends on the pressure ratio across the turbine. The following equations apply to a converging diverging nozzle. The critical pressure ratio is defined as (Ref. 8)

$$\Delta p_c = \left(\frac{2}{\gamma + 1}\right)^{\gamma/\gamma-1} \tag{22}$$

For (p_o/p_i) greater than Δp_c the mass flow rate is equal to

$$\dot{m} = A_e\sqrt{\frac{\gamma}{R}}\;\frac{p_i}{\sqrt{T_i}}\;\frac{M_e}{\left(1 + \frac{\gamma-1}{2}\,M_e^2\right)^{\frac{\gamma+1}{2(\gamma-1)}}} \tag{23}$$

where

$$M_e = \left\{\left[\left(\frac{p_i}{p_o}\right)^{\frac{\gamma-1}{\gamma}} - 1\right]\;\frac{2}{\gamma - 1}\right\}^{1/2} \tag{24}$$

For (p_e/p_i) less than Δp_c

$$\dot{m} = A_t\sqrt{\frac{\gamma}{R}}\;\frac{p_i}{\sqrt{T_i}}\Bigg/\left(1 + \frac{(\gamma-1)}{2}\right)^{\frac{\gamma+1}{2(\gamma-1)}} \tag{25}$$

Hydraulic Efficiency. The hydraulic efficiency can be expressed as (Ref. 9)

$$\eta_h = \frac{2U}{C_o}\,(1 + \Psi_r)\left[\Psi_n \cos\alpha - \frac{U}{C_o}\right] \tag{26}$$

The tip speed is equal to:

$$U = \frac{RPM\,D_r}{2} \tag{27}$$

The spouting velocity is equal to:

$$C_o = \sqrt{2\,\Delta h_s} \tag{28}$$

The rotor coefficient is a function of the flow velocity relative to the blades:

$$\Psi_r = f(C)$$

where

$$C = \left[(C_o \sin \alpha)^2 + (C_o \cos \alpha - U)^2\right]^{1/2} \tag{29}$$

The nozzle coefficient is a function of the specific heat, isentropic Mach number ratio, and design Mach number. The manner in which the nozzle and rotor coefficients were determined will be discussed for a particular nozzle below.

Model Development

The turbine model is entitled TURBIN and is listed in Volume II of this report.

The input to the turbine model is:

$$p_i,\ T_i,\ p_e,\ \text{and RPM}$$

The following geometric and dimensional data must be supplied:

$$\gamma,\ D_r,\ A_t,\ \alpha,\ M_d,\ \Psi_{nd},\ \text{and } R$$

The main outputs are:

$$J,\ \dot{m},\ \text{and } h_o$$

The rotor coefficient relationship employed is that given in Reference 10.

The turbine model was developed for FC-75 as a working fluid with

$$\gamma = 1.02 \text{ and } R = 3.72\ \frac{\text{ft lb}_f}{\text{lb}_m\ ^\circ\text{F}}$$

The isentropic Mach number at design was $M_d = 2.626$, and the design rotor coefficient was $\Psi_{nd} = 0.918$. The other geometric parameters are variable as long as they are consistent with the above design conditions. To run the model with a different working fluid and different design conditions, the nozzle coefficient equations must be changed.

The nozzle coefficient was obtained from Reference 11, which presents curves of normalized nozzle coefficient versus normalized Mach numbers for various design Mach numbers and ratios of specific heats. Typical curves are presented on Figures 5 and 6. These figures cannot be used directly,

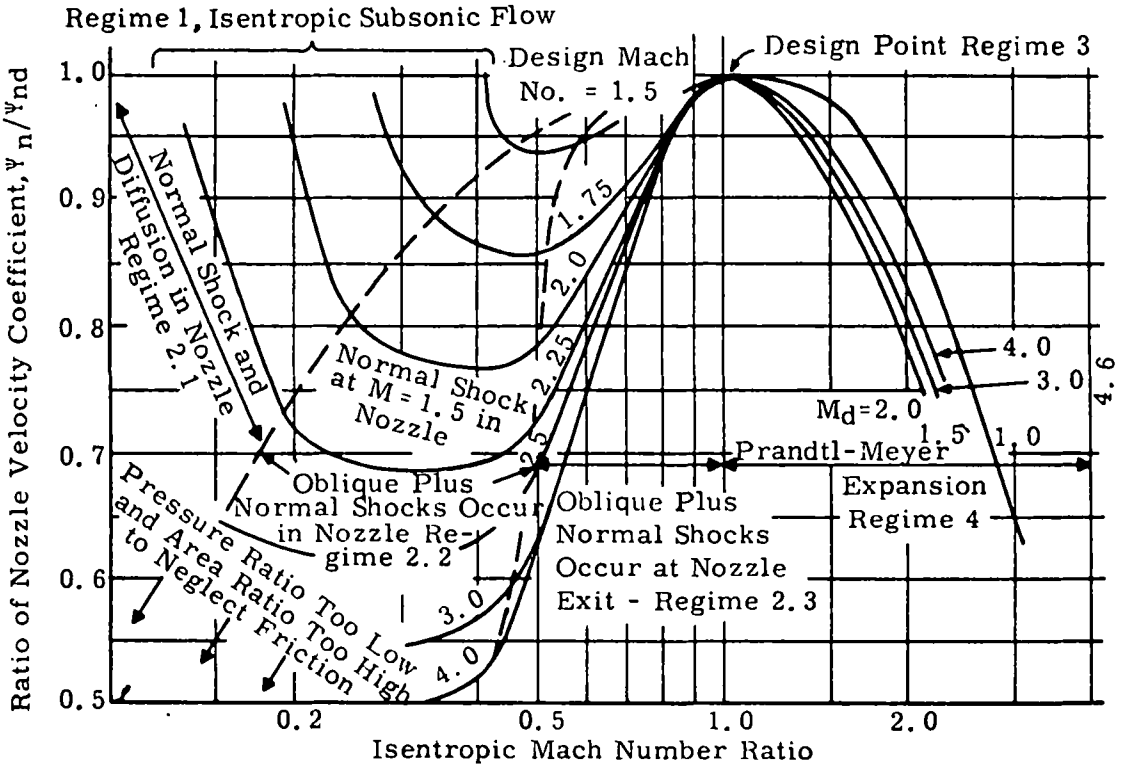

Figure 5. Theoretical Nozzle Performance (γ = 1.4)

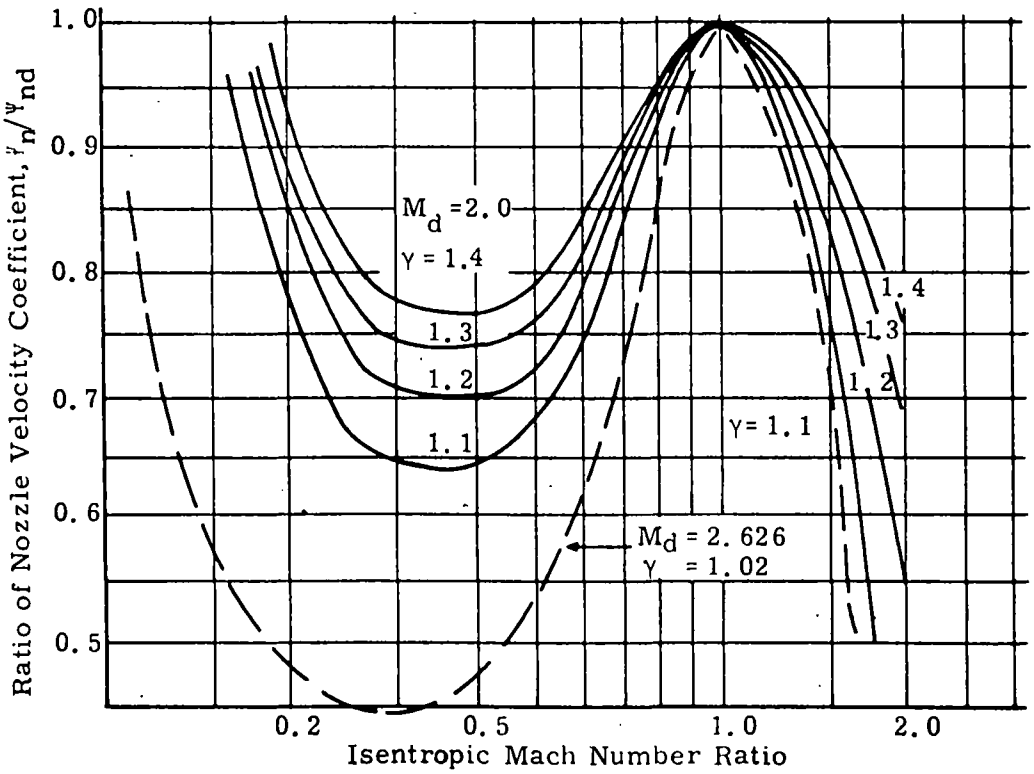

Figure 6. Effect of Gas Ratio of Specific Heats on Calculated Nozzle Performance

since the selected ratios of specific heats and design Mach number are not directly represented. A new curve had to be generated for these conditions; this was done in the following manner.

Figure 6 shows the effect of the ratio of specific heats on the nozzle coefficient for a design Mach number of 2.0. Corrections for $\gamma = 1.02$ were obtained by linear extrapolation from $\gamma = 1.2$ at each Mach number ratio. The specific heat correction will be referred to as $\Delta\gamma$.

Figure 5 shows the effect of design Mach number on nozzle coefficient for a ratio of specific heat of 1.4. It was assumed that the effect of the design Mach number is independent of the ratio of specific heats. The curve for $M_d = 2.5$ was considered to be close enough to the actual value of $M_d = 2.626$. Therefore, a second correction, ΔM_d, was obtained from the difference in the curves for $M_d = 2.0$ and $M_d = 2.5$ in Figure 5.

Finally, the overall correction to obtain a curve for $M_d = 2.626$ and $\gamma = 1.02$ from the curve for $M_d = 2.0$ and $\gamma = 1.2$ was obtained by employing both corrections, $\Delta\gamma$ and ΔM_d, for each isentropic Mach number ratio. This final curve is plotted in Figure 5. A curve fit was obtained and has been provided in the model in the form

$$\frac{\Psi_n}{\Psi_{nd}} = f\left(\frac{M_i}{M_d}\right) \tag{30}$$

where M_i is the isentropic Mach defined as

$$M_i = \left\{\left[\left(\frac{p_i}{p_o}\right)^{\frac{\gamma-1}{\gamma}} - 1\right]\frac{\gamma}{\gamma-1}\right\}^{1/2} \tag{31}$$

The isentropic Mach number M_i and the exit Mach number M_e are equivalent for subsonic flow through the nozzle.

Results

The turbine expander model was run with FC-75 as working fluid, for the following conditions:

$\gamma = 1.02$
$M_d = 2.626$
$D_r = 7.65$ in.
$\alpha = 10°$
$A_t = 0.039$ in.^{2}
$A_e = 2.62$ in.^{2}
$\Psi_{nd} = 0.918$

The inlet conditions and turbine speed at design were

p_i = 220 psi

T_i = 446°F

p_o = 7.35 psi

RPM = 12,870

The pressure ratio (p_i/p_o) was varied from 5 to 200 at fixed RPM = 12,870. The RPM was then varied at fixed pressure ratio. The results, which are plotted in terms of torque coefficient and velocity ratio, are shown in Figure 7. The torque coefficient is defined as

$$\frac{J}{C_o \dot{m} D_r}$$

and the velocity ratio is U/C_o.

These results were compared with turbine performance calculations provided by the Barber-Nichols Engineering Company. Barber-Nichols employed test data from Reference 12 in calibrating their calculation procedure. Figure 8 shows a comparison of the torque coefficient plotted against velocity ratio for the Barber-Nichols and General Electric calculations. This figure indicates that for a given velocity ratio the Barber-Nichols performance averages about ten percent higher than that predicted by the General Electric model. The slope of the curves is also slightly different. It is felt, however, that these differences are not significant, and the Barber-Nichols Company recommends that the General Electric model be used for the full-admission turbine.

The reason for the accuracy of the model calculations is the high specific speed application where the parasitic losses are only about 2%. If a different working fluid were used where the specific speed is lower, the parasitic losses would be higher and the model predictions would be less accurate.

FEEDPUMP

NOMENCLATURE

Alphabetical Symbols	
A_p	Piston area
A_v	Valve area
D	Maximum displacement
HP	Pump power

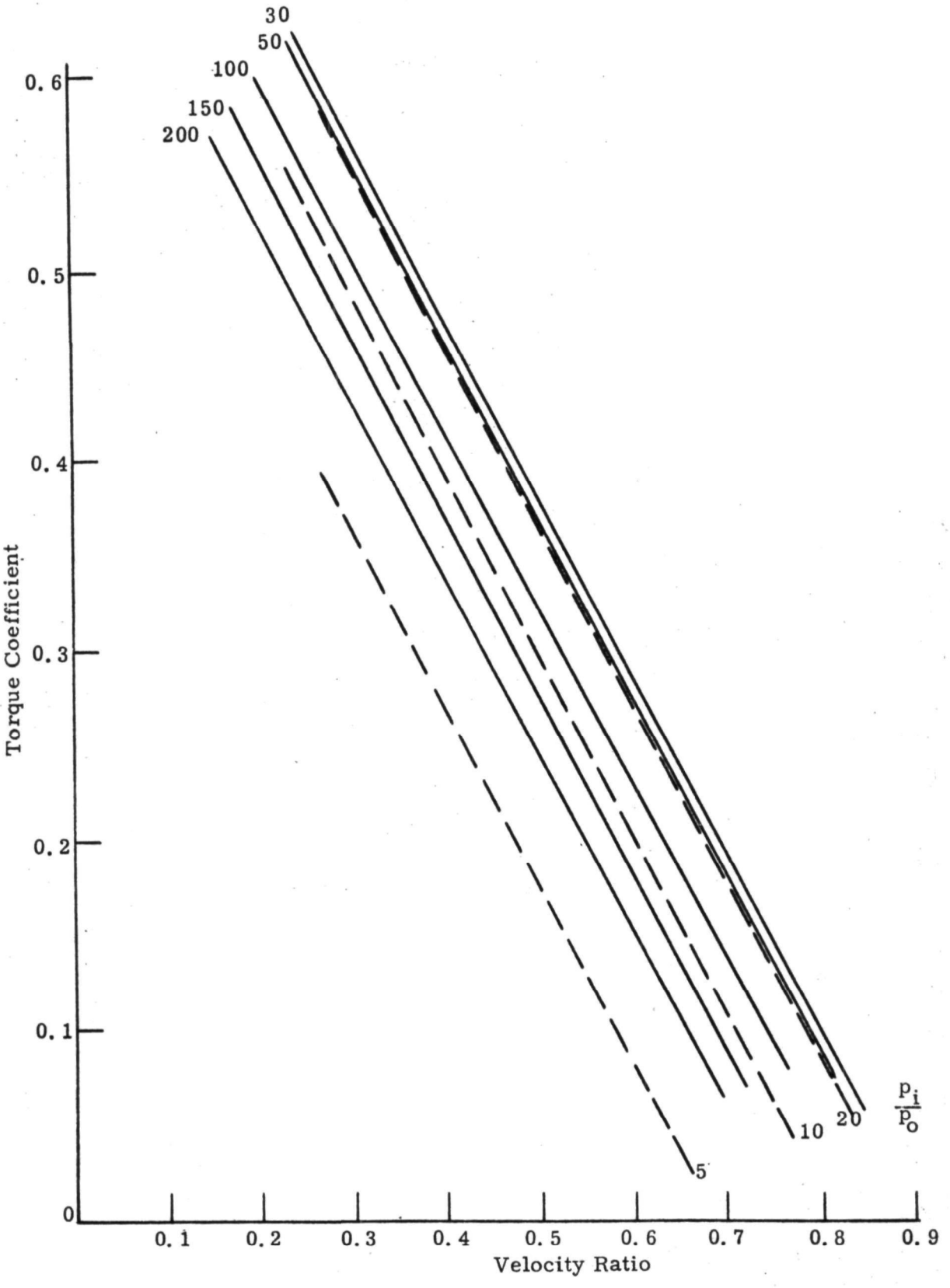

Figure 7. Turbine Model Results (Single-stage Axial Turbine: FC-75 Working Fluid)

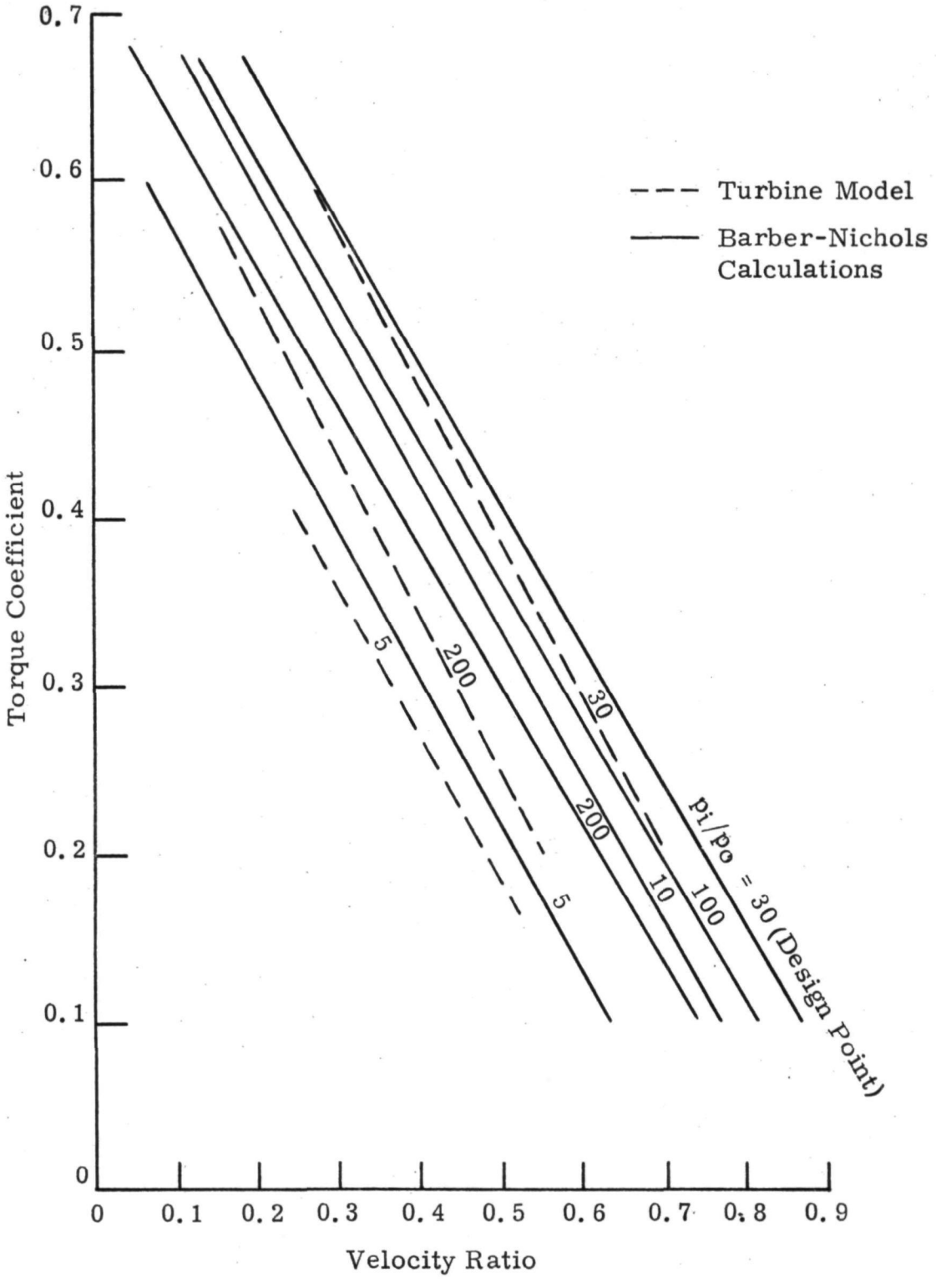

Figure 8. Comparison of Turbine Model with Barber-Nichols Engineering Company Calculations

Alphabetical Symbols (Cont'd)	
K	Flow coefficient
$\dot{m}$	Mass flow rate
N_c	Number of cylinders
NPSH	Net positive section head
p_i	Inlet pressure
p_o	Exit pressure
p_s	Saturation pressure at inlet temperature
R	Variable displacement ratio
RPM	Rotational speed
T_i	Inlet temperature
V	Average flow velocity through inlet valve
v	Specific volume
W	Flow work

Greek Symbols	
η_m	Mechanical efficiency
η_v	Volumetric efficiency
Δp_i	Pressure drop across inlet valve

DERIVATION OF EQUATIONS

The basic equations for the positive-displacement feedpump model are the relationships for the following:

Power:

$$HP = W\dot{m}/\eta_m \tag{32}$$

Mass flow:

$$\dot{m} = \frac{R\ D\ RPM\ \eta_v}{v} \tag{33}$$

Flow work:

$$W = v(p_o - p_i) \tag{34}$$

The volumetric efficiency was derived from data supplied by the Thermo Electron Corporation for the Hypro-Pump, Model 5420.

$$\eta_v = 1 - 0.05 \left(\frac{RPM}{600}\right) \tag{35}$$

The mechanical efficiency was obtained as:

$$\eta_m = 1/\left(1 + 115/[\eta_v (p_o - p_i)]\right) \tag{36}$$

Pump Cavitation

Cavitation is local vaporization at the pump inlet and can cause severe pump damage. The pump will cavitate if the pressure drop across the inlet valve is greater than the net positive suction head, defined as

$$NPSH = p_i - p_s \tag{37}$$

Using the incompressible pressure drop relation of the form

$$\Delta p = \frac{K V^2}{2v} \tag{38}$$

where K is an empirical constant, the following approximate relation can be derived:

$$\Delta p_i = \left(\frac{K}{2v}\right) \left(\pi \left(\frac{D}{A_p}\right) \left(\frac{A_p}{A_v}\right) RPM\right)^2 \tag{39}$$

MODEL DEVELOPMENT

The feedpump model is entitled PUMP and is described in Volume II of this report. Inputs to the model are:

$$R,\ RPM,\ p_i,\ p_o,\ \text{and}\ T_i$$

The following geometric and dimensional data must be supplied:

$$N_c,\ D,\ K,\ A_p,\ \text{and}\ A_v$$

The model was developed for fixed values of

$$\frac{A_p}{A_v} = 4.0$$

$K = 2.8$

$A_p = 1 \text{ in.}^2$

The number of cylinders and maximum displacement are variables.

Initially, the NPSH and pressure drop across the inlet valve are calculated and compared to check for cavitation. If cavitation occurs, the model sets the mass flow at zero. In reality, there is some mass flow during cavitation, but it is very difficult to predict analytically. If the pump does not cavitate, the mass flow and power are calculated, employing the equations listed in the previous subsection.

RESULTS

The positive displacement pump model was run with both water and CP-34 as a working fluid. For water, the following input conditions were supplied:

$R = 1$

$RPM = 342$

$p_i = 236 \text{ psi}$

$p_o = 1000 \text{ psi}$

$T_i = 217°F$

$N_c = 1$

$D = 1.36 \text{ in.}^3$

The results obtained are

$\Delta p_i = 1.185 \text{ psi}$

$NPSH = 7.43$

$\eta_v = 0.971$

$\eta_m = 0.891$

$\dot{m} = 0.26 \text{ lb/sec}$

$HP = 1.04 \text{ hp}$

For CP-34, two cases were run with different inlet temperatures to check the cavitation calculation. In the first case the input was:

$R = 1$

$RPM = 800$

$p_i = 250 \text{ in.}^3$

$p_o = 500 \text{ in.}^3$

$N_c = 5.$

$D = 4.78 \text{ in}^3$

$T_i = 196°F$

and the results were:

$\Delta p_i = 3.26$ psi

NPSH = 6.75 psi

$\eta_v = 0.933$

$\eta_m = 0.794$

$\dot{m} = 2.09$ lb/sec

HP = 4.51

In the second case the inlet temperature was changed to $T_i = 210°F$ and the pump cavitated

$\Delta p_i = 3.23$ psi

NPSH = 2.21 psi

$\dot{m} = 0$

Figure 9 presents a comparison of the pump model results with experimental data for a Hypro Pump 5530, obtained from Steam Engine Systems, Incorporated. As can be seen, the model is within 5% of complete agreement with the data. It is therefore felt that the model provides a valid representation of a positive displacement pump.

HEAT EXCHANGERS

NOMENCLATURE

Alphabetical Symbols	
A	Flow cross-section area
C	Energy storage capacity per unit length
c_p	Specific heat at constant pressure
E	Energy-transport parameter (= mass flow rate x specific heat)
F1, F2, F3, F4	Parameters for dynamic relations
G2, G3, G4	Parameters for quasi-steady relations
H	Heat transfer coefficient x surface area/unit length
h	Enthalpy

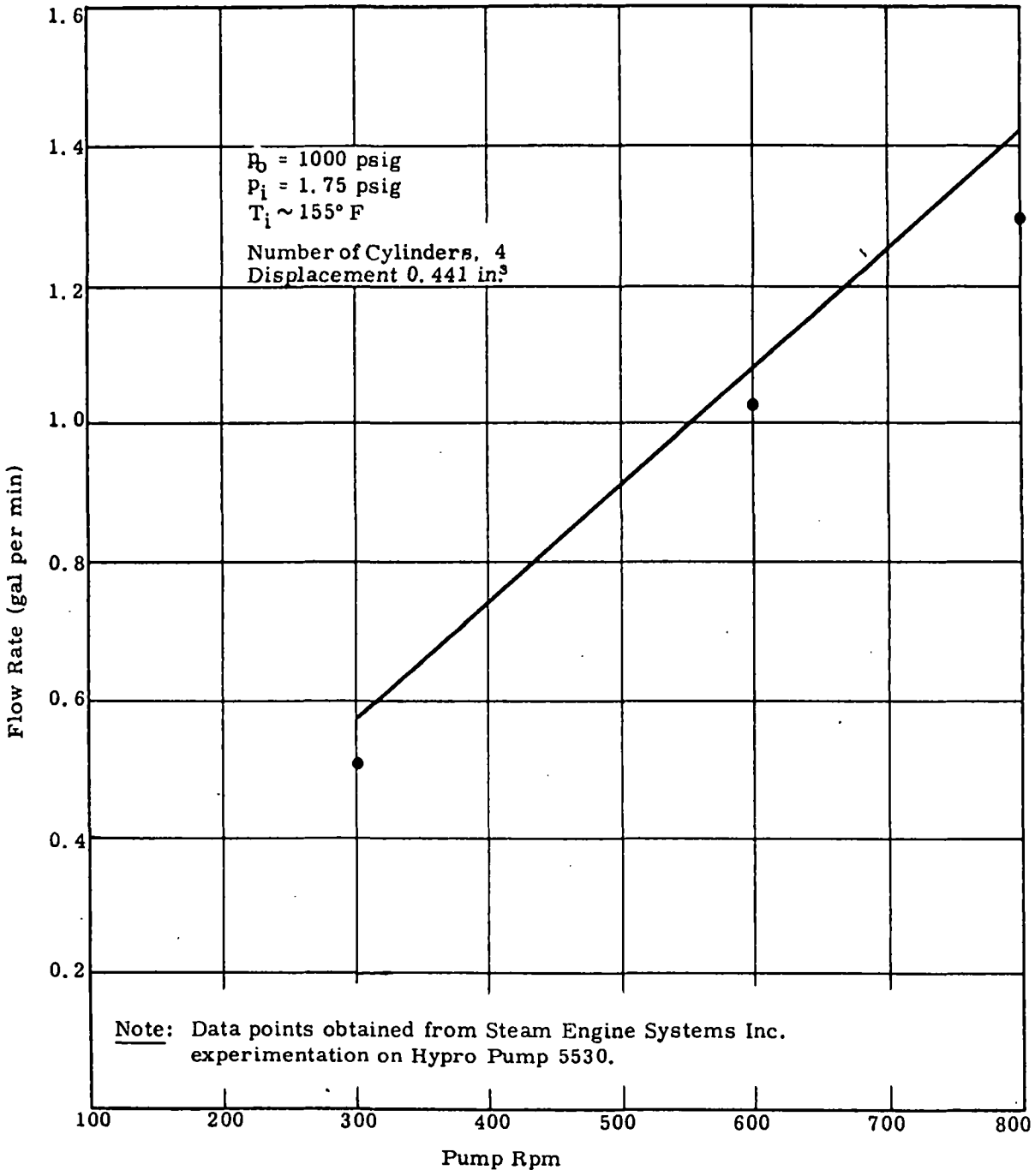

Figure 9. Pump Model -- Volumetric Flow Rate Versus Rpm

Alphabetical Symbols (Cont'd)

J	Joule's constant
M	Captive fluid mass per unit length
$\dot{m}$	Mass flow rate
N	Required number of iterations for gas-side energy transient
P	Pressure
$\dot{Q}$	Energy transfer rate, Btu/sec, per unit length
T	Temperature
t	Time
u	Internal energy
V	System volume
v	Specific volume for fluid
x	Flow direction

Subscripts

con	Constant
f	Fluid
f_2f_1	Between f2 and f1 nodes
f_2f_2	At f2 node
f_2t	Between f2 and t nodes
fg	Saturated fluid/saturated vapor interphase
g	Gas
gf	Saturated vapor/saturated fluid interphase
g_2g_1	Between g2 and g1 nodes
g_2t	Between g2 and t nodes
gs	Saturated vapor/superheated vapor interphase
gt	Between gas and tube
ℓ	Subcooled liquid phase
o	At design condition
r, ref	Reference condition
s	Superheated vapor

Subscripts (Cont'd)

sg	Superheated vapor/saturated vapor interphase
st	Stability limit
t	Tube metal
tf	Between tube and fluid
tg	Between tube and gas
tt	At tube node
1,2	Node locations (2 at upstream location)

Greek Symbols

Δt	Time increment
Δx	Distance step
ρ	Density

(Note: A dot ($\cdot$) above any quantity denotes its time-derivative (d/dt))

TRANSIENT THERMAL ANALYSIS

Dynamic models of the heat exchanger consider the conservation of mass, momentum, and energy simultaneously on a time-dependent basis. This requirement increases the model complexity, even for simple geometric configurations. In most practical cases, a number of simplifying assumptions are needed to obtain manageable results.

The equations describing the physical processes must be valid over a wide range of off-design operating conditions. This means that the linearization of process equation about the design point may not be acceptable.

The final selection of an appropriate transient model will depend upon these and other factors described in the following pages.

Methods of Transient Analysis

For any dynamic system, the dynamic relations describing the physical processes with its boundary conditions are written first. In cases where lumped parameter representation is adequate, the resulting relations are ordinary differential equations. For long tubular thermal components such as vapor generators, regenerators, or condensers, both the time and distance are variable parameters and the resulting relations are partial differential equations.

Several methods are available for solving these equations (Refs. 13-23) and are listed in Table 3. The choice depends upon the end use and scope of

Table 3

METHODS OF TRANSIENT THERMAL ANALYSIS

Method	Basis	Comments	References
Exact Solution Method	Solution by standard solution techniques for differential equations	a. Standard solution available for limited cases only b. Solutions for equations with variable coefficients generally not available or extremely complex	17, 22
Laplace Transform Method	Transformation in time and space variables, then inverse transformation	a. Inverse transform generally very complex; can be done through numerical techniques b. Variable coefficients not admissible	14, 17, 21, 22
State Variable Method	Distributed system solution technique of Brown	Same as for Laplace Transform Method	13, 16
Analog Method	Use of analog computer	a. Partial differential equations are required to be approximated as total differential equations b. Analog computer size limits the problem scope c. Variable coefficients are admissible though might not prove practical	17, 18, 19, 20, 23
Finite-difference Digital Method	Dusinberre method used on digital computer	a. Lumping errors exist but can be made practically insignificant b. Numerical instability should be watched c. Computing time and memory size depend on the selection of time and distance lumps d. Can readily admit variable coefficients e. Applicable to any complex geometry or design conditions	15, 17

the model. In the present case of the Rankine cycle simulation, the method should have the ability to:

a. Accept any design changes with minimum change in program

b. Predict dynamic behavior over a much wider range, even from cold start-up condition to full-load design operation

c. Incorporate nonlinearities and any variation of physical properties reflected in the variable nature of the coefficients of the differential equations

d. Handle variable operating conditions (e.g., a condenser with variable superheat inlet condition and existing in a subcooled state, with the location of the two-phase boundaries depending on the operating conditions)

In addition to the above characteristics, the selected method should also be:

e. Capable of giving results of acceptable accuracy

f. Economical in run-time requirement

g. Reasonable in machine size requirement

Beyond these considerations, any other characteristics of the method do not really pose any limitation on its usefulness. Thus, if an elegant closed solution method or a simple numerical method are weighed almost equally on the above considerations, neither possesses any superiority above the other method.

Closed-form Solution Methods. The set of conservation equations are solved in a closed-form method, satisfying appropriate boundary conditions for each section of the heat exchanger. The first three approaches given in Table 3 fall into this category. This method would yield explicit relations for variation in fluid pressure, enthalpy, and mass flow for any given input disturbance. Some of the customary assumptions required in this method are:

- Small perturbations (hence linear range) about any operating point
- Linear variation in fluid properties (equations-of-state linearized)
- Constant or uniform heat input rates and heat transfer coefficients
- Frictionless fluids

Some of these assumptions might be unduly restrictive. Further, a simple change in geometric layout may void the entire solution applicable to a previous geometry. Even then, though the final relations are in closed form, they are usually quite complex even for a simple geometry with a linearized range, and may require approximate numerical methods for their evaluation (Ref. 13-17).

Analog and hybrid methods are presented in Table 3 for completeness but were not considered for this simulation.

Finite-difference Method. The finite-difference digital method is a simple and most effective method, and it meets all the essential criteria with a surprising simplicity and brevity. Its drawbacks -- possible numerical instability, run time, and memory size requirements -- can be overcome. Dusinberre (Ref. 15) outlines a simple way of avoiding any numerical instability, and the resulting limits on time and distance increments are neither unreasonably restrictive nor overly demanding in machine-size and computing-time requirements.

In this method, the differential equations are approximated by finite difference equations. In Dusinberre's method of explicit solutions, the difference equation with respect to time (which represents a time derivative) is evaluated by using the present (or known) values of all required parameters. This method, which does not require any of the assumptions mentioned above, was selected for the simulation approach. Some of the very powerful features of this method are briefly mentioned in Table 4. It will be shown later that the method differs very little when applied to heat transfer equipments with such diverse geometrical and functional characteristics as the vapor generator, the regenerator, or the condenser. Further, computer memory size requirement can be significantly reduced through special programming methods.

Table 4

FEATURES OF FINITE-DIFFERENCE DIGITAL METHOD

Flexibility	1. Not limited to any arbitrary range of operation
	2. Complex flow phenomena (e.g., superheat, condensing, and subcooling existing in one pass) can be handled.
	3. Stiff system (with a wide range of heat capacities) can be identified, simplified (by ignoring negligible heat capacities), and the program suitably modified through very minor changes to achieve run-time economy.
Adaptability	1. Can be used for any complex geometry (e.g., counterflow, parallel flow, cross flow, multipass) with equal ease.
	2. Variable properties can be handled with the same program.
	3. Other process features -- conservation of mass and momentum -- can be readily included.

Table 4 (Cont'd)

Versatility	1. Same dynamic program can be used for computing the initial steady-state condition. Even a crude guess on initial distribution is acceptable.

Basic Approach

In any transient thermal process involving fluid flow, all the physical conservation laws -- conservation of mass, momentum, and energy -- should be satisfied simultaneously. However, if the primary interest is in the dynamics of thermal phenomena rather than the details of fluid dynamic phenomena, the problem is simplified. This is because the flow disturbances propagate rapidly (at the speed of sound) compared to propagation of thermal disturbances; hence, the fluid phenomena such as fluid inertia or liquid-phase compliance are of secondary importance and can be neglected.

Consider the case of a fluid flowing through the tube section (Figure 10). Assume:

1. Flow is one-dimensional.
2. Fluid inertia is neglected.
3. Geometry is uniform within a section.
4. Thermal conductivity of tube and fluid is infinite in the radial direction and zero in the longitudinal direction.
5. Fluid is radially homogeneous, and the relative velocity between liquid and vapor phases is neglected.
6. Fluid pressure is uniform within a section and time increment.
7. There are no internal heat sources or heat sinks.
8. Fluid and wall properties are constant within a section and time increment.

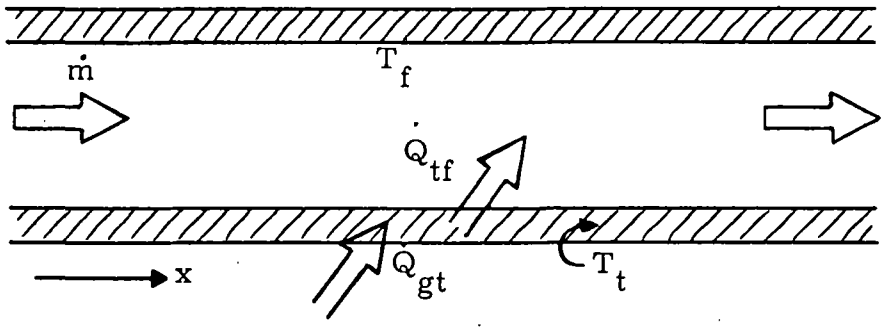

Figure 10. Schematic of Flow Through a Tube

The only essential assumption is one-dimensional flow. The other assumptions are neither restrictive nor essential; they merely allow a simple treatment of the problem.

Basic Process Equations. For the above case, the conservation equations are

Mass Balance:

$$\frac{\partial \dot{m}}{\partial x} = \frac{A}{v_f^2} \frac{\partial v_f}{\partial t} \tag{40}$$

Force Balance:

$$\frac{\partial P_f}{\partial x} = f \text{ (friction and momentum pressure drop)} \tag{41}$$

Energy Balance and Heat Transfer:

$$\dot{Q}_{tf} = H_f (T_t - T_f) \tag{42}$$

$$\dot{Q}_{tf} = \frac{\partial(\dot{m}h_f)}{\partial x} + A \frac{\partial(h_f/v_f)^*}{\partial t} \tag{43}$$

Tube Heat Capacity:

$$\dot{Q}_{gt} - \dot{Q}_{tf} = C \frac{\partial T_t}{\partial t} \tag{44}$$

Equations of State:

$$\begin{aligned} v_f &= f(P_f, T_f) \\ h_f &= f(P_f, T_f) \end{aligned} \tag{45}$$

Application of Finite-difference Method to Energy Equation. As an example of the application of the finite-difference method, consider a tube of length Δx. This tube section satisfies the assumptions given earlier.

*The general energy balance relation is

$$\dot{Q}_{tf} - \frac{\partial}{\partial x}(\dot{m}h) = \frac{\partial}{\partial t}(Mu) + P\dot{V}$$

where M is the captive fluid mass per unit length ($=\rho A = A/v$) and u is internal energy ($= h - PV$). Substituting these definitions and using assumption 3,

$$\dot{Q}_{tf} - \frac{\partial}{\partial x}(\dot{m}h) = A \frac{\partial(h/v)}{\partial t} - V\dot{P}$$

which reduces to Equation 43 when assumption 6 is used.

Expanding Equation 43 and combining with Equation 40 yields

$$\dot{Q}_{tf} = \dot{m} \frac{\partial h_f}{\partial x} + \frac{A}{v_f} \frac{\partial h_f}{\partial t} \tag{46}$$

Assume that the tube section refers to an economizer. Then take $v_f = v_o$ as average fluid specific volume. In combination with Equation 42

$$H_f (T_t - T_f) = \dot{m} \frac{\partial h_f}{\partial x} + \frac{A}{v_o} \frac{\partial h_f}{\partial t} \tag{47}$$

Before the finite-difference approximation is applied to Equation 47, it should be modified to base the relation in terms of either fluid temperature or fluid enthalpy. While in the case of an economizer or superheater the choice is not crucial, the boiling or condensing section can be represented with the enthalpy terms only. This is a crucial observation.

To achieve this transformation, define

$$(T_f - T_{ref}) = \left(\frac{h_f - h_{ref}}{c_{p_f}} \right) \tag{48}$$

where c_{p_f} is the mean specific heat of the fluid. Further, define

$$C_f = \frac{A}{v_o} c_{p_f}$$

$$E_f = \dot{m} c_{p_f}$$

Then Equations 47 and 48 give

$$E_f \frac{\partial h_f}{\partial x} + C_f \frac{\partial h_f}{\partial t} + H_f \left[(h_f - h_{ref}) - c_{p_f} (T_t - T_{ref}) \right] = 0 \tag{49}$$

The node pattern (Figure 11) must still be selected. For a tube section Δx, the fluid nodes 1 and 2 are designated at the upstream and downstream, respectively, and the tube metal node is taken midway between two fluid nodes. The length Δx is called the lump length.

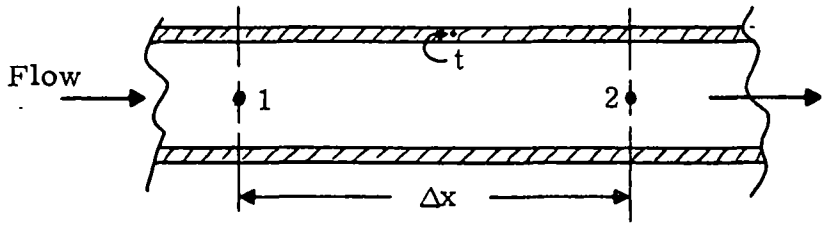

Figure 11. Node Pattern

Now, following Dusinberre's method, the forward-finite-difference approximation of the differential terms of Equation 49 is

$$\frac{\partial h_f}{\partial x} = \frac{h_{f_2}(t) - h_{f_1}(t)}{\Delta x}$$

$$\frac{\partial h_f}{\partial t} = \frac{h_{f_2}(t+\Delta t) - h_{f_2}(t)}{\Delta t} \qquad (50)$$

and

$$h_f = \frac{h_{f_1}(t) + h_{f_2}(t)}{2}$$

Equation 49 now becomes

$$h_{f_2}(t+\Delta t) = F1 \cdot h_{f_2}(t) + F2 \cdot h_{f_1}(t) + F3\ T(t) + F4 \qquad (51)$$

where

$$F1 = 1 - \frac{E_f}{C_f}\frac{\Delta t}{\Delta x} - \frac{\Delta t}{2}\frac{H_f}{C_f} = 1 - \frac{\Delta t}{\Delta x}\frac{E_f}{C_f}\left(1 + \frac{\Delta x}{2}\frac{H_f}{E_f}\right)$$

$$F2 = \frac{E_f}{C_f}\frac{\Delta t}{\Delta x} - \frac{\Delta t}{2}\frac{H_f}{C_f} = \frac{\Delta t}{\Delta x}\frac{E_f}{C_f}\left[1 - \frac{\Delta x}{2}\frac{H_f}{E_f}\right]$$

$$F3 = \Delta t \cdot \frac{H_f}{C_f} \cdot c_{p_f}$$

$$F4 = \Delta t \cdot \frac{H_f}{C_f}\left(h_{ref} - c_{p_f} \cdot T_{ref}\right)$$

Equation 51 computes the fluid enthalpy at the exit node at a future time, based on the present fluid enthalpy and tube temperature distribution; hence, this method is called explicit. Note also that all the coefficients associated with the distribution terms add up to a value of unity; thus the future enthalpy is a weighted sum of the present values of the surrounding elements.

An important feature of the explicit finite-difference approximation is that the lump size Δx and time step Δt should be selected for numerical stability. The upper and lower limits on Δx and Δt are required to minimize errors associated with the conversion of differential to difference equations. A simple rule to avoid the numerical instability requires that all F coefficients associated with the present distribution terms should be non-negative. A mathematical basis for this rule is given in Appendix II, "Stability and Error Criteria for Finite-difference Solution of Partial Differential Equations."

Applying the stability criteria for F2:

$$0 < \left(1 - \frac{\Delta x}{2} \frac{H_f}{E_f}\right)$$

$$\text{i.e.,} \quad \Delta x < \left(2 \frac{E_f}{H_f}\right) \tag{52}$$

for F3:

$$0 < \left[1 - \frac{\Delta t}{\Delta x} \frac{E_f}{C_f} \left(1 + \frac{\Delta x}{2} \frac{H_f}{E_f}\right)\right]$$

$$\Delta t < \left[\frac{2\, C_f/H_f}{1 + \frac{2}{\Delta x} \frac{E_f}{H_f}}\right] \tag{53}$$

Note that

1. These stability limits are time-dependent, since they require heat transfer coefficient and mass flow rate at a given location and time.
2. These limits are from the energy equation for the fluid only. Similar limits would arise from the conservation equations applied to other subsystems of the equipment, such as the tube, the outer fluid, and the shell.
3. The selected values of Δt and Δx should consider all the stability limits for the system, and also external constraints such as geometrical layout, maximum system time increment, etc.
4. While the stability criterion prefers smaller lump and time-step sizes, the requirements of simulation on a digital computer are that
   - Smaller lump and time-step sizes are associated with increased memory size and run-time requirements
   - The truncation errors grow in proportion to the number of lumps and time steps.

   Hence, the final choice of Δt and Δx should reflect all of the above considerations.

Small Time Constant (High Frequency) Situations. In certain dynamic situations involving more than one energy subsystem (e.g., a tube subjected to internal and external fluid flows) conditions could arise when the energy-storage-capacity to heat-transfer-coefficient ratio for some subsystems is very much smaller than that for the remaining subsystems. In the mathematical representation, this would require a much lower limit on allowable time step, as can be seen from Equation 53.

In physical terms, such a small quantity results from the fact that the corresponding capacity to film-coefficient ratio is small; i. e., the thermal capacity of the fluid or metal is very small or its surface heat-transfer resistance is negligible. In either case, the fluid can be treated as capable of assuming its steady state at a much faster rate; hence, the steady-state energy relations can be assumed applicable at any time during the transient operation of the equipment, without any appreciable error. This procedure effectively eliminates the term representing a fast transient -- a high-frequency term, and allows a reasonable value of the time step Δt based on remaining terms.

The previous dynamic equation, 51, is here recast for its steady-state representation. The quasi-steady behavior implies that

$$\frac{\partial h_f}{\partial t} = 0$$

that is,

$$h_{f2}(t + \Delta t) = h_{f2}(t)$$

Hence,

$$h_{f2} = G2\, h_{f1} + G3\, T_t + G4 \tag{54}$$

where

$$G2 = F2/(1 - F1)$$

$$G3 = F3/(1 - F1)$$

$$G4 = F4/(1 - F1)$$

or

$$G2 = \frac{1 - \frac{\Delta x}{2}\frac{H_f}{E_f}}{1 + \frac{\Delta x}{2}\frac{H_f}{E_f}}$$

$$G3 = \frac{\Delta x \frac{H_f}{E_f} \cdot c_{p_f}}{1 + \frac{\Delta x}{2}\frac{H_f}{E_f}} \tag{55}$$

$$G4 = \frac{\Delta t \cdot \frac{H_f}{E_f} \cdot (h_{ref} - c_{p_f} \cdot T_{ref})}{1 + \frac{\Delta x}{2}\frac{H_f}{E_f}}$$

The stability limit on Δx associated with Equation 54 is

$$\Delta x < \frac{2 E_f}{H_f} \tag{56}$$

This limit is identical to that in Equation 52 for the dynamic relation. Of course, the time-step size does not enter into the picture in this case.

VAPOR GENERATOR

The finite-difference approach outlined earlier will now be applied to simulate the dynamic behavior of a specific class of vapor generators. In the automotive application, a once-through monotube vapor generator has significant advantages. In the majority of such units, the hot-gas flow is arranged so that, overall, it resembles cross-flow arrangement. The mathematical model developed in this section refers to this specific type of unit.

General Description of Model

The overall system simulation requires a certain input-output arrangement for each system component. For each component, the input-output variables (also called information signals) indicate a preferred representation of the dynamic situation, and do not signify the flow directions.

The complete once-through vapor generator treated as a single unit has input-output conditions as shown in Figure 12. Note that the direction of the signals at each end always satisfies one primary energy requirement of the two flow quantities, pressure and mass flow rate: one is an output quantity, and the other is an input quantity.

Note that the signal-flow arrangement in Figure 12 is selected for convenience in overall system simulation. If the dynamic simulation of vapor generator alone is desired, it would be necessary to switch the signal-flow

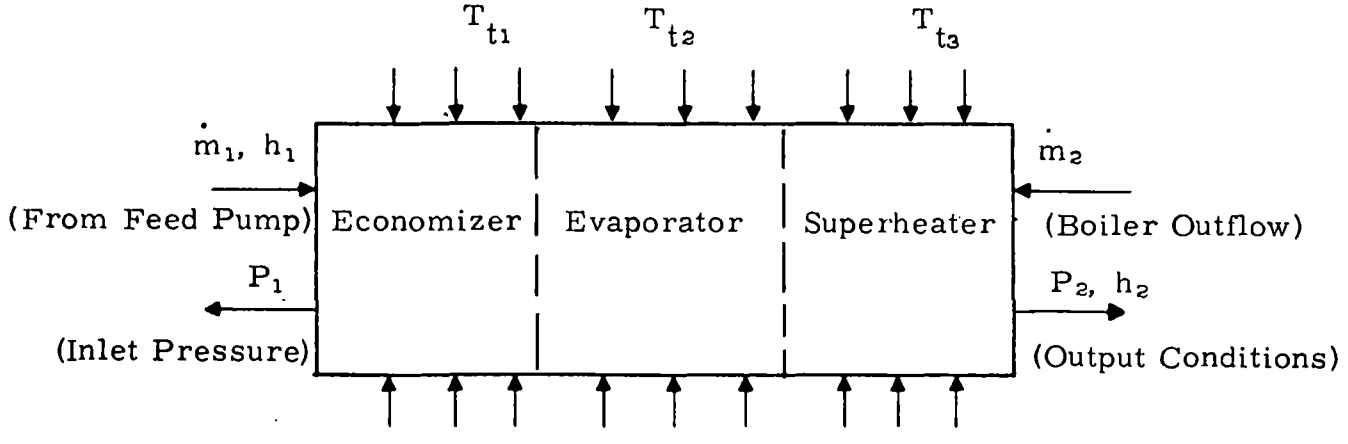

Figure 12. Information Signals for Vapor Generator Model

directions at the superheater outlet: the exit pressure would be an input signal, and the exit mass flow would be suitably governed by the difference in boiler pressure and exit pressure.

While Figure 12 indicates the existence of three distinct fluid zones, the boundaries separating them need not remain at a fixed location. During the transient operation, the last fluid zone may disappear. (Because this situation is not desirable, even transiently, the control system acts to prevent this.) The mathematical model should be such that it remains valid under these dynamic conditions.

In the present approach, the decision as to the state of the fluid (subcooled, two-phase or superheated) is based on the average values of fluid enthalpy and pressure at any time within a section of the tube (called a lump); the proper relations are then used to compute the transient behavior of the fluid within the lump. The exit fluid conditions of any lump are then transmitted as entrance fluid conditions for the next lump.

In the following subsection, the relations are developed for three distinct fluid states. Note, again, that these do not necessarily coincide with the geometric zones derived from a steady-state basis, but change continuously during transient operation.

Transient Analysis

Conservation Equations for the Fluid. The basic conservation equations given above are now applied to different fluid states.

For Subcooled Fluid: Assume that the fluid compressibility is negligible. Then,

$$v_f = \text{constant } (= v_o), \quad \frac{\partial v_f}{\partial t} = 0, \quad \frac{\partial v_f}{\partial x} = 0.$$

Consequently,

$$\frac{\partial \dot{m}_f}{\partial x} = 0 \tag{57}$$

$$\frac{\partial P_f}{\partial x} = f \text{ (friction)} \tag{58}$$

$$\dot{Q}_{tf} = \dot{m}_f \frac{\partial h_f}{\partial x} + \frac{A}{v_o} \frac{\partial h_f}{\partial t} \tag{59}$$

For two-phase or superheated fluid:

$$\frac{\partial \dot{m}_f}{\partial x} = \frac{A}{v^2} \frac{\partial v_f}{\partial t} \tag{60}$$

$$\frac{\partial P_f}{\partial x} = f \text{ (friction and momentum pressure drop) for two-phase}$$

$$= f \text{ (friction) for superheat} \tag{61}$$

$$\dot{Q}_{tf} = \frac{\partial(\dot{m}_f h_f)}{\partial x} + A \frac{\partial(h_f/v_f)}{\partial t}$$

$$= \dot{m}_f \frac{\partial h_f}{\partial x} + h_f \frac{\partial \dot{m}_f}{\partial x} + \frac{A}{v_f} \frac{\partial h_f}{\partial t} - \frac{A h_f}{v_f^2} \frac{\partial v_f}{\partial t}$$

Combining this relation with Equation 60 gives

$$\dot{Q}_{tf} = \dot{m}_f \frac{\partial h_f}{\partial x} + \frac{A}{v_f} \frac{\partial h_f}{\partial t} \tag{62}$$

Conservation Equations for the Tube. The major dynamic effect from the tube is that it retains a portion of the energy received from the hot fluid stream, and transmits the remaining energy to the cold fluid stream. In the absence of axial thermal conductivity of the tube material, the storage capacity of tube metal can be considered on a lumped-parameter basis. Hence,

$$\dot{Q}_{gt} - \dot{Q}_{tf} = C_t \frac{\partial T_t}{\partial t} \tag{63}$$

$$\dot{Q}_{gt} = h_{gt} \cdot A_{gt} (T_g - T_t) \tag{64}$$

$$\dot{Q}_{tf} = h_{tf} \cdot A_{tf} (T_t - T_f) \tag{65}$$

where T_g, T_t, and T_f are bulk temperatures for the gas, tube, and fluid respectively; A_{gt} and A_{tf} are heat transfer surfaces per unit length for the gas side and fluid side respectively.

Conservation Equations for the Gas. It is assumed here that the total mass flow rate of the gas is constant in both the time and space coordinates. Then

$$\frac{\partial P_g}{\partial x_2} = f \text{ (friction)} \tag{66}$$

$$\dot{Q}_{gt} = \dot{m}_g \frac{\partial h_g}{\partial x_2} + \left(\frac{A}{v_o}\right)_g \frac{\partial h_g}{\partial t} \tag{67}$$

Finite-difference Approximation of Energy Equations. The method already outlined for transforming energy equations is applied to Equations 59, 62, 63, and 67, transforming them into equivalent explicit finite-difference representation. Figure 13 defines the node pattern.

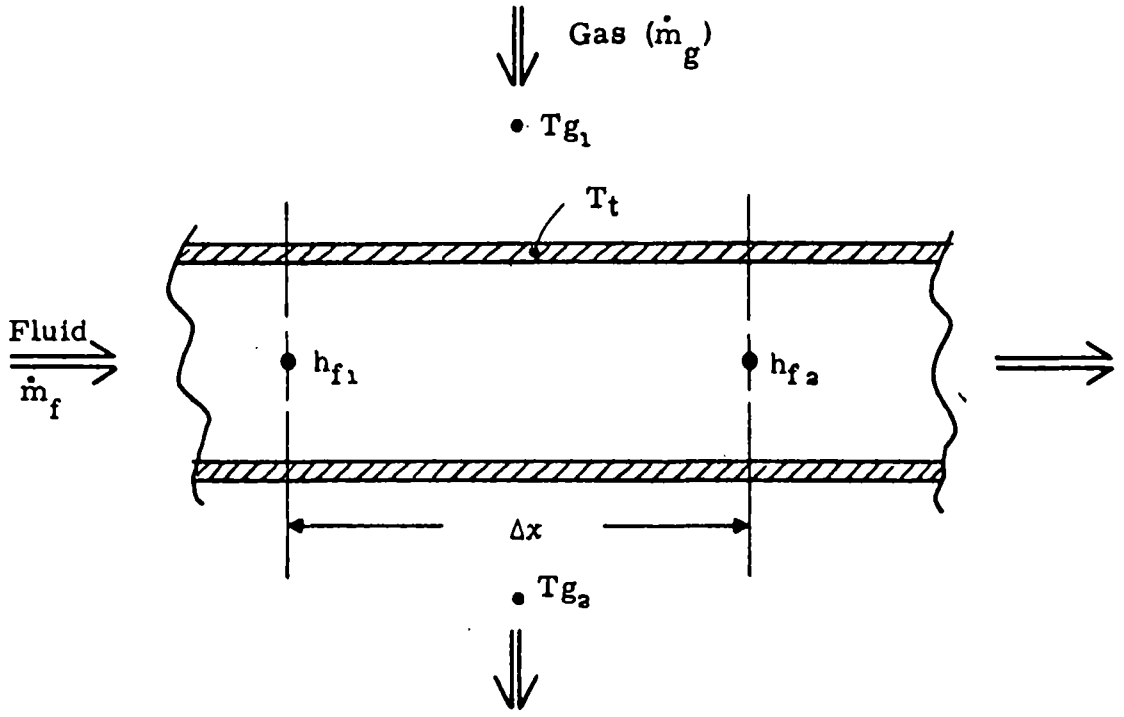

Figure 13. Node Pattern

Fluid. For the two-phase fluid, the fluid temperature $T_f = T_{sat}$, whereas for the subcooled or superheated condition, the fluid temperature is calculated from the equation-of-state relation corresponding to the bulk fluid enthalpy and pressure within a lump.

Thus from the definition,

$$h_f - h_r = c_{p_r} (T_f - T_r) \tag{68}$$

where h_r and T_r are fluid enthalpy and temperature respectively at a reference point, and c_{p_r} is the mean specific heat over the range. For subcooled fluid, c_p is almost constant; therefore the reference point is taken at the saturated liquid condition. However, in the superheat case, c_p varies significantly with pressure and enthalpy; therefore, the reference enthalpy varies for for each lump and is taken at a slightly lower value from the bulk fluid enthalpy for that lump.

For the transient case,

$$h_{f2}(t+\Delta t) = F_{f2f1} h_{f1}(t) + F_{f2f2} h_{f2}(t) + F_{f2t}(T_t - T_x) \tag{69}$$

and for the quasi-steady case,

$$h_{f2}(t+\Delta t) \equiv h_{f2}(t) = F_{f2f1}(t)\, h_{f1}(t) + F_{f2t} \cdot c_{p_r} (T_t - T_x) \tag{70}$$

where

$$\left.\begin{aligned} T_x &= T_{sat} && \text{for two-phase fluid} \\ T_x &= \left(T_r - \frac{h_r}{c_{p_r}}\right) && \text{for subcooled or superheated fluid} \end{aligned}\right\} \tag{71}$$

and the F coefficients are defined in Table 5. The quantities used in the table are

$$\left.\begin{aligned} H_{tf} &= h_{tf} \cdot A_{tf} \\ H_{gt} &= h_{gt} \cdot A_{gt} \end{aligned}\right\} \tag{72}$$

and $\dot{m}$ = fluid mass flow rate at the entrance of the lump.

Tube. Since the energy transmitted to the fluid side depends on the fluid temperature, the transient relation for tube material depends on the fluid phase. Thus, for subcooled or superheated fluid,

$$\begin{aligned} T_t(t+\Delta t) = {} & F_{tt}\, T_t(t) + F_{tg}\left(T_{g_1}(t) + T_{g_2}(t)\right) \\ & + F_{tf}\left(h_{f_1}(t) + h_{f_2}(t)\right) + F_{con} \end{aligned} \tag{73}$$

and for two-phase fluid,

$$T_t(t+\Delta t) = F_{tt}\, T_t(t) + F_{tg}\left(T_{g_1}(t) + T_{g_2}(t)\right) + F_{tf} \cdot T_{sat} \tag{74}$$

where the F coefficients are as given in Table 5. These relations are valid for both transient and quasi-steady situations, with proper values of F coefficients.

Gas. The energy relations are expressed here in terms of gas temperature rather than its enthalpy. Since the change-of-phase condition does not exist here, this choice is valid. Further, the quasi-steady assumption is accepted here, to avoid extremely small iteration time steps resulting from stability considerations. Thus,

$$T_{g_2}(t+\Delta t) = T_{g_2}(t) = F_{g_2g_1}\, T_{g_1}(t) + F_{g_2t}\, T_t(t) \tag{75}$$

The F coefficients are explained in Table 5.

Stability Criteria for Energy Equations. One important feature of the explicit method is the upper limits for the lump size, Δx, and the time step, Δt, necessary to avoid numerical instability. Both these limits apply to any transient equation, whereas only the lump size limit applies to the quasi-steady relations. These limits are obtained by requiring that all the F coefficients associated with transient terms be non-negative and less than unity (see Table 6).

Table 5

FINITE-DIFFERENCE RELATIONS

(I) Fluid: Transient Case

Fluid Phase	F_{f2f1}	F_{f2f2}	F_{f2t}
Subcooled or Superheat	$\frac{\Delta t}{\Delta x} \cdot \frac{E_f}{C_f}\left(1 - \frac{H_{tf}}{E_f} \cdot \frac{\Delta x}{2}\right)$	$1 - \frac{\Delta t}{\Delta x} \cdot \frac{E_f}{C_f}\left(1 + \frac{H_{tf}}{E_f} \cdot \frac{\Delta x}{2}\right)$	$\Delta t \cdot c_{p_r} \cdot \frac{H_{tf}}{C_f}$
2-phase	$\frac{\Delta t}{\Delta x} \cdot \frac{\dot{m}}{A\rho}$	$1 - \frac{\Delta t}{\Delta x} \frac{\dot{m}}{A\rho}$	$\Delta t \cdot \frac{H_{tf}}{A\rho}$

(II) Fluid: Quasi-steady

Subcooled or Superheat	$\frac{1 - B}{1 + B}$ where $B = \frac{\Delta x}{2\, c_{p_r}} \cdot \frac{H_{tf}}{\dot{m}}$	0	$\frac{2B}{1 + B}$ where $B = \frac{\Delta x}{2\, c_{p_r}} \cdot \frac{H_{tf}}{\dot{m}}$
2-phase	1	0	$\frac{H_{tf} \cdot \Delta x}{\dot{m}}$

(III) Tube: Transient

Fluid Phase	F_{tt}	F_{tg}	F_{tf}	F_{con}
Subcooled or Superheat	$1 - \frac{\Delta t}{C_t}(H_{tf} + H_{gt})$	$\frac{\Delta t}{2} \cdot \frac{H_{gt}}{C_t}$	$\frac{\Delta t}{2\, c_{p_r}} \cdot \frac{H_{tf}}{C_t}$	$\Delta t \cdot \frac{t_f}{C_t}\left(T_r - \frac{h_r}{c_{p_r}}\right)$
2-phase	$1 - \frac{\Delta t}{C_t}(H_{tf} + H_{gt})$	$\frac{\Delta t}{2} \cdot \frac{H_{gt}}{C_t}$	$\Delta t \cdot \frac{H_{tf}}{C_t}$	0

(IV) Tube: Quasi-steady

Fluid Phase	Ftt	F_{tg}	F_{tf}	F_{con}
Subcooled of Superheat	0	$\frac{H_{gt}}{2(H_{gt} + H_{tf})}$	$\frac{H_{tf}}{2\, c_{p_r}(H_{gt} + H_{tf})}$	$\frac{H_{tf}}{(H_{gt} + H_{tf})} \cdot \left(T_r - \frac{h_r}{c_{p_r}}\right)$
2-phase	0	$\frac{H_{gt}}{2(H_{gt} + H_{tf})}$	$\frac{H_{tf}}{(H_{gt} + H_{tf})}$	0

(V) Gas: Quasi-steady

$F_{g2g1} = \frac{1 - B}{1 + B}$
$F_{g2t} = 1 - F_{g2g1}$
where $B = \frac{H_{gt} \cdot \Delta x}{2\, \dot{m}_g\, c_{p_g}}$

Table 6

STABILITY LIMITS FOR ENERGY EQUATIONS

(I) Fluid	
Subcooled or Superheat	$\Delta x \leq \frac{2 E_f}{H_{tf}}$
	$\Delta t \leq \frac{2 C_f / H_{tf}}{\left[1 + \frac{2 E_f}{H_{tf}} \cdot \frac{1}{\Delta x}\right]}$
Two-phase	$\Delta t \leq \frac{A \cdot \rho}{\dot{m}} \Delta x$
(II) Tube	
For any fluid phase	$\Delta t \leq \frac{C_t}{(H_{gt} + H_{tf})}$
(III) Gas	
No. of iterations in gas flow direction	$N \geq \frac{H_{gt} \cdot \Delta x}{2 \dot{m}_g c_{pg}}$

Note: In the two-phase situation, enthalpy change occurs at constant temperature; hence, $E_f \rightarrow \infty$. Consequently there is no fluid stability limit on Δx, and an external limit should be specified for accuracy.

Note that the stability limit on the gas side cannot impose a limit on Δx; hence, the heat transfer area on the gas side should be subdivided to meet the stability limit. Thus, if

A_{st} = Surface area permitted by stability limit

N = Required number of iterations

then

$$B = \frac{h_{gt} A_{st} \Delta x}{2 \dot{m}_g c_{p_g}} \leq 1$$

that is

$$A_{st} \leq \frac{2\,\dot{m}_g\,c_{p_g}}{h_{gt}\,\Delta x} \tag{76}$$

But the total surface area on the gas side between the two gas nodes is A_{gt}. Hence,

$$N = \frac{A_{gt}}{A_{st}}$$

that is

$$N \geq \frac{h_{gt}\,A_{gt}\,\Delta x}{2\,\dot{m}_g\,c_{p_g}}$$

or

$$N \geq \frac{H_{gt}\,\Delta x}{2\,\dot{m}_g\,c_{p_g}} \tag{77}$$

Note that the quantities on the right-hand side of Equation 76 are not affected by by the subdivision of distance between two gas nodes. Hence, local iteration is permissible.

Finite-difference Approximation of Continuity Equation. In this section, the explicit finite-difference form for continuity relation for two-phase or superheat fluid, Equation 60, is developed. It is assumed that the fluid pressure, P, is uniform within a lump.

Writing Equation 60 in terms of density, ρ,

$$\dot{m}_2 - \dot{m}_1 = -A \cdot \Delta x \cdot \frac{\partial \rho}{\partial t}$$

But $\rho = f(h_f, P)$

that is

$$\frac{\partial \rho}{\partial t} = \frac{\partial \rho}{\partial h}\bigg|_P \frac{dh_f}{dt} + \frac{\partial \rho}{\partial P}\bigg|_{h_f} \frac{dP}{dt}$$

For simplicity, assume the pressure, P, as constant during the time interval Δt. Then

$$\dot{m}_2 - \dot{m}_1 = -A \left(\frac{\partial \rho}{\partial h}\right)_P \cdot \Delta x \cdot \frac{\Delta h_f}{\Delta t} \tag{78}$$

Equation 78 contains a time-derivative term for fluid enthalpy. To eliminate numerical error arising from the "high-gain" characteristics of the

derivative term, Equation 78 is combined with the corresponding energy equation for the fluid.

Thus, taking the lump size for the continuity equation the same as that for the energy equation,

$$\dot{m}_2 - \dot{m}_1 = -A \left(\frac{\partial e}{\partial h}\right)_P \cdot \Delta x \cdot \frac{h_f(x+\Delta x,\ t+\Delta t) - h_f(x+\Delta x,\ t)}{\Delta t} \tag{79}$$

Note that the enthalpy change, Δh_f, taken at the exit node, is consistent with the assumption used in the finite-difference approximation of the energy equation.

For Two-phase Flow

$$\Delta h_{f_2} = h_f\,(x+\Delta x,\ t+\Delta t) - h_f\,(x+\Delta x,\ t) \tag{80}$$

$$= \frac{\dot{m}_1}{A\rho}\,\frac{\Delta t}{\Delta x}\left(h_{f_1} - h_{f_2}\right) + \frac{H_{tf}}{A\rho} \cdot \Delta t\,(T_t - T_{sat}) \tag{81}$$

Substituting in Equation 79 and rearranging,

$$\dot{m}_2 = A_3 \dot{m}_1 + A_4 \tag{82}$$

where

$$A_3 = 1 - \left(\frac{\partial \rho}{\partial h}\right)_P \frac{(h_{f_1} - h_{f_2})}{\rho}$$

$$A_4 = -\left(\frac{\partial \rho}{\partial h}\right)_P \frac{H_{tf}\,\Delta x\,(T_t - T_{sat})}{\rho} \tag{83}$$

For Superheated Fluid. The corresponding energy relation can be used to derive similar mass flow relation for superheated fluid. Thus,

$$\dot{m}_2 = A_5\ \dot{m}_1 + A_6 \tag{84}$$

where

$$A_5 = 1 - \left(\frac{\partial \rho}{\partial h}\right)_P \frac{(h_{f_1} - h_{f_2})}{\rho} \tag{85}$$

$$A_6 = \left(\frac{\partial \rho}{\partial h}\right)_P \cdot \frac{H_{tf}\,\Delta x}{\rho\ c_{p_r}} \left[\frac{h_{f_2} + h_{f_1}}{2} - c_{p_r}(T_t - T_x)\right] \tag{86}$$

$$T_x = T_r - \left(h_r / c_{p_r}\right) \tag{87}$$

Finite-difference Approximation of Momentum Equation. In the present approach, the spatial pressure distribution due to momentum relation has been neglected during the transient calculations. This assumption would be acceptable if the momentum pressure drop is not a very significant portion of the system operating pressure level. The simplifications offered by this assumption are significant; the major advantage is the absence of additional restrictions on time and lump step sizes.

Hellman and others (Ref. 24) have treated the problem of finite-difference analysis as applied to the momentum equation. In a special case of a horizontal tube with natural and forced convection, the stability criterion for the time step is shown to be

$$\Delta t < \frac{2}{\frac{Ag}{\Delta x}(k_1 + 3k_2\dot{m})} \tag{88}$$

where g = acceleration, and k_1 and k_2 are associated with the friction-drop relations as

$$\Delta p = f(\dot{m}) = k_1|\dot{m}| + k_2\dot{m}^2 \tag{89}$$

It can be seen that this limitation is nonexistent under the assumptions of this problem.

Pressure Transient -- Lumped-parameter Model. Earlier, explicit finite-difference relations were developed for the enthalpy (or temperature) and flow distribution for various flow subsystems. It was assumed in the derivation that the fluid pressure remained constant during the integration time interval, Δt. The difference between the inlet and exit mass flows would exist during the dynamic operation; a difference would also exist between energy available from the hot gases and that removed or absorbed by the fluid. The net result would be a fluid pressure variation.

Transient thermodynamics will be used to derive the relations for the fluid pressure. The analysis will be based on a lumped parameter model (this is acceptable because spatial variation of pressure (due to momentum effects) has been ruled out during the transient operation). The derivation is based on the extension of Brown's pioneering work in transient thermodynamics (Ref. 25).

The total vapor generator volume is taken as a single unit; it is divided into several hypothetical sections bounded by the interphases representing the fluid change-of-phase (Figure 14). For each section, the interphases and the system, the conservation equations are written which yield the pressure variation information. Note that all the mass flow directions into the vapor generator are assumed positive. The sign for the exit flow in actual computation should be watched.

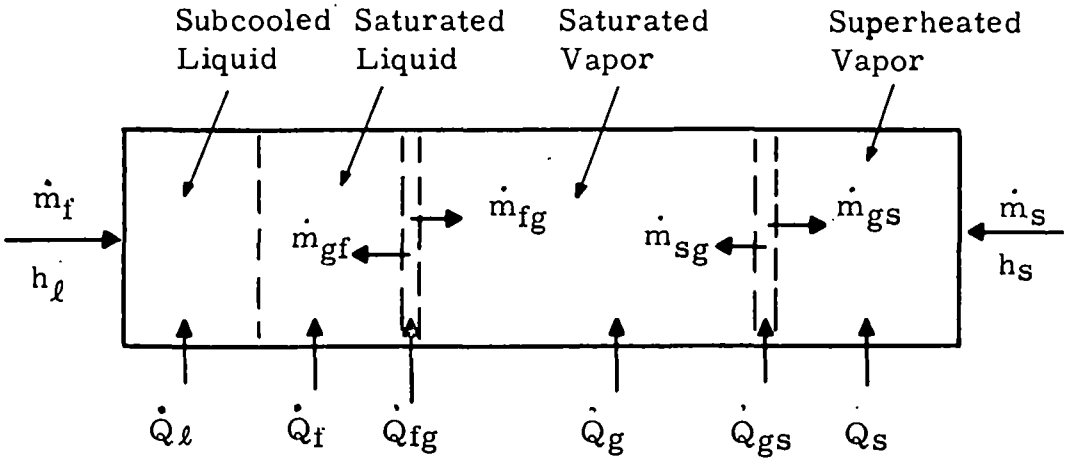

Figure 14. Schematic of Phases and Interphases

Mass Balance. Assume the liquid is incompressible.

$$\left.\begin{aligned} &\text{Superheated vapor:} && \dot{M}_s &&= \dot{m}_{gs} + \dot{m}_s \\ &\text{Saturated vapor:} && \dot{M}_g &&= \dot{m}_{fg} + \dot{m}_{sg} \end{aligned}\right\} \quad (90)$$

$$\left.\begin{aligned} &\text{Saturated liquid:} && \dot{M}_f &&= \dot{m}_f + \dot{m}_{gf} \\ &\text{Subcooled liquid:} && 0 &&= \dot{m}_f - \dot{m}_f \\ &\text{Liquid interphase:} && 0 &&= \dot{m}_{gf} + \dot{m}_{fg} \\ &\text{Vapor interphase:} && 0 &&= \dot{m}_{gs} + \dot{m}_{sg} \\ &\text{System:} && \dot{M}_g + \dot{M}_f + \dot{M}_s &&= \dot{m}_f + \dot{m}_s \end{aligned}\right\} \quad (91)$$

Volume Balance. Assume 1) the change of subcooled liquid volume is zero, and 2) the interphases have no volume.

Superheated Vapor:

$$\left.\begin{aligned} \dot{\overline{M_s v_s}} &= \dot{M}_s v_s + M_s \frac{dv_s}{dt} \\ \text{But } v_s &= f(P, h_s) \\ \text{that is,} \quad \frac{dv_s}{dt} &= \frac{\partial v_s}{\partial p}\Big|_{h_s} \frac{dP}{dt} + \frac{\partial v_s}{\partial h_s}\Big|_{p} \frac{dh_s}{dt} \\ &= B_1 \dot{P} + B_2 \dot{h}_s \\ \text{Hence,} \quad \dot{\overline{M_s v_s}} &= \dot{M}_s v_s + M_s [B_1 \dot{P} + B_2 \dot{h}_s] \end{aligned}\right\} \quad (92\text{-Cont'd})$$

Saturated Vapor:

$$\dot{\overline{M_g v_g}} = \dot{M}_g v_g + M_g \frac{dv_g}{dp} \cdot \dot{P}$$

Saturated liquid:

$$\dot{\overline{M_f v_f}} = \dot{M}_f v_f + M_f \frac{dv_f}{dp} \cdot \dot{P}$$

System:

$$\dot{V} = 0 = \left(\dot{\overline{M_g v_g}}\right) + \left(\dot{\overline{M_s v_s}}\right) + \left(\dot{\overline{M_f v_f}}\right) \qquad (92)$$

It should be noted that in each case the system equation, obtained directly, agrees with the result obtained from combining all section relations together.

Now, combining mass and volume balance relations,

$$(\dot{m}_{fg} - \dot{m}_{gs}) v_g + (\dot{m}_{gs} + \dot{m}_s) v_s + (\dot{m}_1 - \dot{m}_{fg}) v_f$$

$$+ \left(M_g \frac{dv_g}{dp} + B_1 M_s + M_f \frac{dv_f}{dp} \right) \dot{P} + B_2 M_s \frac{dh_s}{dt} = 0$$

After rearranging, the equation becomes

$$- \left(M_g \frac{dv_g}{dp} + M_s \frac{\partial v_s}{\partial p}\Big|_{h_s} + M_f \frac{dv_f}{dp} \right) \dot{P}$$

$$= (\dot{m}_f + \dot{m}_s) v_f + \dot{m}_s (v_s - v_f) + v_{fg} \left(\dot{m}_{fg} + \frac{v_s - v_g}{v_{fg}} \dot{m}_{gs} \right)$$

$$+ M_s \frac{\partial v_s}{\partial h_s}\Big|_p \frac{dh_s}{dt} \qquad (93)$$

This equation can be used to calculate pressure transients if the terms $\dot{m}_{fg}$ and $\dot{m}_{gs}$ can be eliminated. This will be done by using energy relations.

Energy Balance. Assume that the change of energy stored in subcooled fluid can be neglected because of its small order of magnitude.

Superheated vapor:

$$\dot{Q}_s + h_s \dot{m}_{gs} + h_s \dot{m}_s = \left(\dot{\overline{M_s h_s}}\right) - M_s v_s \dot{P}/J$$

$$= M_s \frac{dh_s}{dt} + h_s \dot{M}_s - M_s v_s \dot{P}/J$$

Combining with the corresponding mass balance relation,

$$\dot{Q}_s = M_s \left(\frac{dh_s}{dt} - \frac{v_s}{J} \dot{P} \right) \tag{94}$$

Saturated vapor:

$$\dot{Q}_g + h_g \dot{m}_{fg} + h_g \dot{m}_{sg} = \overline{\dot{M}_g h_g} - M_g v_g \dot{P}/J$$

That is,

$$\dot{Q}_g = M_g \left(\frac{dh_g}{dp} - \frac{v_g}{J} \right) \dot{P} \tag{95}$$

Saturated liquid:

$$\dot{Q}_f + h_f \dot{m}_f + h_f \dot{m}_{gf} = \overline{\dot{M}_f h_f} - M_f v_f \dot{P}/J$$

That is,

$$\dot{Q}_f = M_f \left(\frac{dh_f}{dp} - \frac{v_f}{J} \right) \dot{P} \tag{96}$$

Subcooled liquid:

$$\dot{Q}_\ell + h_\ell \dot{m}_f - h_f \dot{m}_f = \overline{\dot{M}_\ell h_\ell} - M_\ell v_\ell \dot{P}/J$$

That is,

$$\dot{Q}_\ell = \dot{m}_f (h_f - h_\ell) - M_\ell \frac{v_\ell}{J} \dot{P} \tag{97}$$

Interphases:

$$\dot{Q}_{fg} + h_f \dot{m}_{fg} + h_g \dot{m}_{gf} = 0$$

and

$$\dot{Q}_{gs} + h_g \dot{m}_{gs} + h_s \dot{m}_{sg} = 0$$

That is,

$$\dot{Q}_{fg} = \dot{m}_{fg} h_{fg}$$

$$\dot{Q}_{gs} = \dot{m}_{gs} (h_s - h_g) \tag{98}$$

System:

$$\Sigma \dot{Q} + h_\ell \dot{m}_f + h_s \dot{m}_s = \overline{\dot{M}_f h_f} + \overline{\dot{M}_g h_g} + \overline{\dot{M}_s h_s} - \frac{V}{J} \dot{P}$$

That is,

$$\Sigma \dot{Q} - \dot{m}_f (h_f - h_\ell) - h_{fg} \left(\dot{m}_{fg} + \frac{h_s - h_g}{h_{fg}} \dot{m}_{gs} \right)$$

$$= M_s \frac{dh_s}{dt} + \left[M_g \frac{dh_g}{dp} + M_f \frac{dh_f}{dp} - \frac{V}{J} \right] \dot{P} \tag{99}$$

Equations 93 and 99 should now be combined to derive an explicit relation for dP/dt. For simplicity, assume

$$\frac{v_s - v_g}{v_{fg}} \approx \frac{h_s - h_g}{h_{fg}} \tag{100}$$

Note that both of the terms above have the same signs. Though the actual agreement between the two quantities depends on the fluid and the operating point in superheat zone, the error for CP-34 fluid is in the range of 10 to 30% (Figure 15). This approximation can be relaxed as in Reference 25.

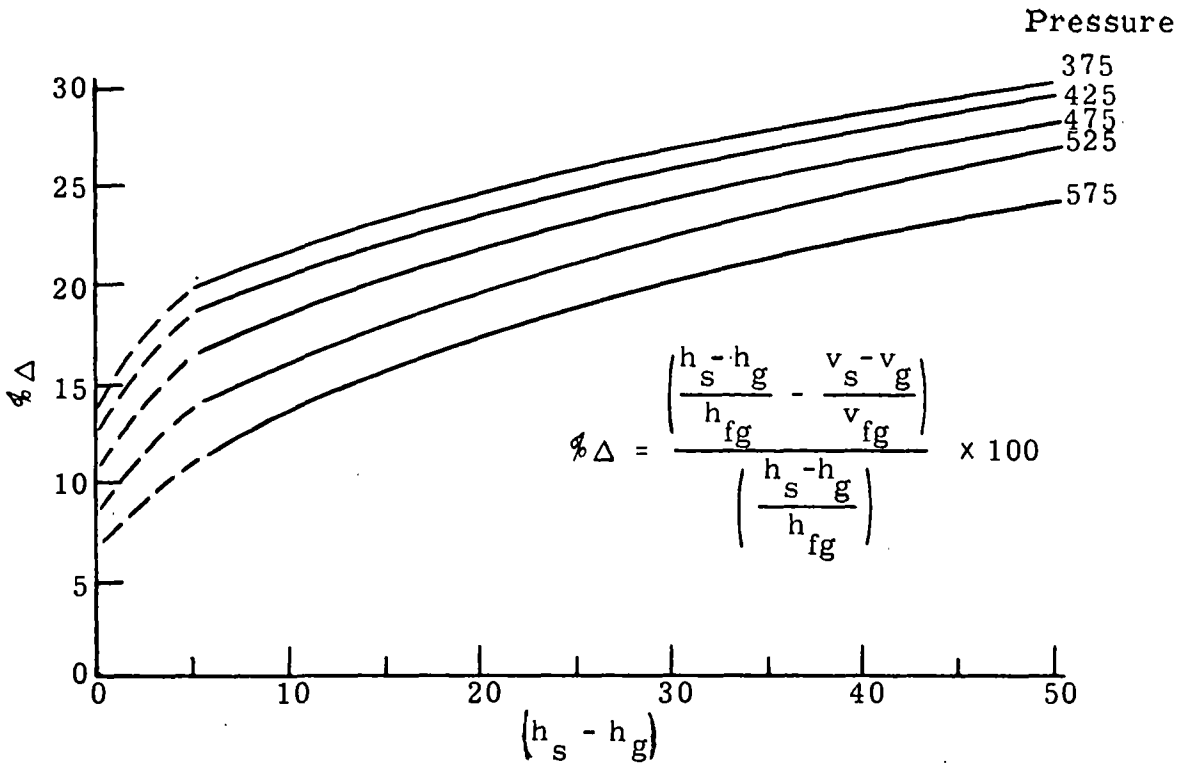

Figure 15. Error in Approximation $(v_s - v_g)/v_{fg} = (h_s - h_g)/h_{fg}$ for CP-34

Combining Equations 93, 99, and 100 and using the proper sign convention for $\dot{m}_s$,

$$\frac{dP}{dt} = \frac{(\dot{m}_f - \dot{m}_s)v_f + M_s\left[\left(\frac{\partial v_s}{\partial h}\Big|_p - \frac{v_{fg}}{h_{fg}}\right)\frac{\bar{dh}_s}{dt} + \frac{v_{fg}}{h_{fg}}\left[\Sigma \dot{Q} - \dot{m}_f(h_f - h_\ell) - \dot{m}_s(h_s - h_f)\right]\right]}{\frac{v_{fg}}{h_{fg}}\left[M_g\frac{dh_g}{dp} + M_f\frac{dh_f}{dp} - \frac{V}{J}\right] - \left[M_f\frac{dv_f}{dp} + M_g\frac{dv_g}{dp} + M_s\frac{\partial v_s}{\partial p}\Big|_h\right]} \tag{101}$$

Analytic Procedure

For economic reasons, it might be necessary to use a quasi-steady representation for some of the energy-storage components of a heat exchanger unit. This is usually done at the price of eliminating some fast transients, but it does not affect the model accuracy. The decision as to whether a quasi-steady or a dynamic model is necessary for a particular component is not arbitrary; it is related to the geometry, the thermal properties, and the energy-storage capacity of surrounding streams. The selection for the particular vapor generator considered here (TECO design for CP-34 fluid, Ref. 1) is given in Table 7.

An example of the interpretation of Table 7 would be the case of working fluid in the boiling phase. The corresponding modes of energy equations to be used are: quasi-steady relations for combustion gas and tube metal, and dynamic relation for the fluid itself.

Table 7

SELECTION OF ENERGY EQUATION MODELS

Working Fluid Phase	Combustion Gas	Tube	Fluid
Subcooled	Quasi-steady	Dynamic	Dynamic
Boiling	Quasi-steady	Quasi-steady	Dynamic
Superheated	Quasi-steady	Dynamic	Quasi-steady

The computation procedure for the case of fluid is now explained to illustrate the basis of the computer model. At any given time, (t), the fluid enthalpy and tube temperature distribution are known. The mass flow, $\dot{m}$, is taken at the entrance node. From this and other known geometric and operating parameters, the dynamic parameters E_f, C_f, H_{tf}, etc., are computed for the given lump sizes at time t. On the basis of the average fluid conditions within the lump, its phase is determined. The proper stability criterion is then applied to obtain Δx. Similarly, Δx corresponding to other energy-subsystems (tube, gas if it is counter or parallel flow) should be calculated, and the minimum of these limiting lengths should be selected as the final lump size. If the selected lump size is different from the original lump size the parameter H_{tf} is obtained for a new node pattern by linear interpolation.

The allowable time step Δt is calculated next. It is taken as the minimum of those dictated by the stability limits for each energy subsystem. The energy relation is then used to obtain the fluid enthalpy at the exit node at time $(t + \Delta t)$.

For each lump, the continuity equation is then used to obtain mass flow rate at exit node. Since the fluid transients propagate very fast compared to

thermal transients, the mass flow relation is considered an instantaneous process, and the calculated exit flow value is used in the energy calculation for the next lump.

The exit conditions of the previous lump are set as the inlet conditions for the next lump, and the calculations are repeated until the vapor generator exit node is reached.

The fluid pressure change is next calculated by the use of Equation 101. This completes the transient solution, giving the fluid-state distribution at time $(t + \Delta t)$.

For the next iteration, the distribution at $(t + \Delta t)$ is now reset as the distribution at (t), and the process is repeated to obtain the transient distribution at the next time.

At any time, the momentum relations can be used to obtain axial fluid pressure distribution.

Computer Model

The vapor generator model is entitled VAPORG, and is listed in Volume II, the Users Manual. The important features of this computer program are described here. The program is designed to require minimal geometric and design data. To summarize, it first calculates a steady-state distribution of fluid enthalpy, gas temperature, and tube-wall temperature; it then continues to calculate transient behavior for a specified time period as a result of the specified disturbance at the boundary. The details are given below.

One important convention used in the program should be stressed. Each heat exchanger unit is subdivided into various fluid passes. Each fluid pass has uniform geometry and is subjected to uniform flow conditions. The fluid passes are consecutively numbered in the direction of fluid flowing through the tube. Figure 16 illustrates various situations.

Using the basic geometric data, the program first calculates all the quantities of interest (e.g., hydraulic diameter, flow cross-section area, etc. for each fluid pass). Since such quantities are time-independent, this calculation section is bypassed during subsequent calculation loops.

To start the program, initial distribution of the fluid enthalpy and gas temperature is required. The program is designed to accept estimated values of these quantities at the inlet and exit of each fluid pass; a linear interpolation is used for distribution within a fluid pass. Initially, each fluid pass has only one lump. For each lump, a first guess on the tube temperature is obtained. (From this point on, the discussion is not limited to one lump per coil, since the calculation would restart here for each iteration step.)

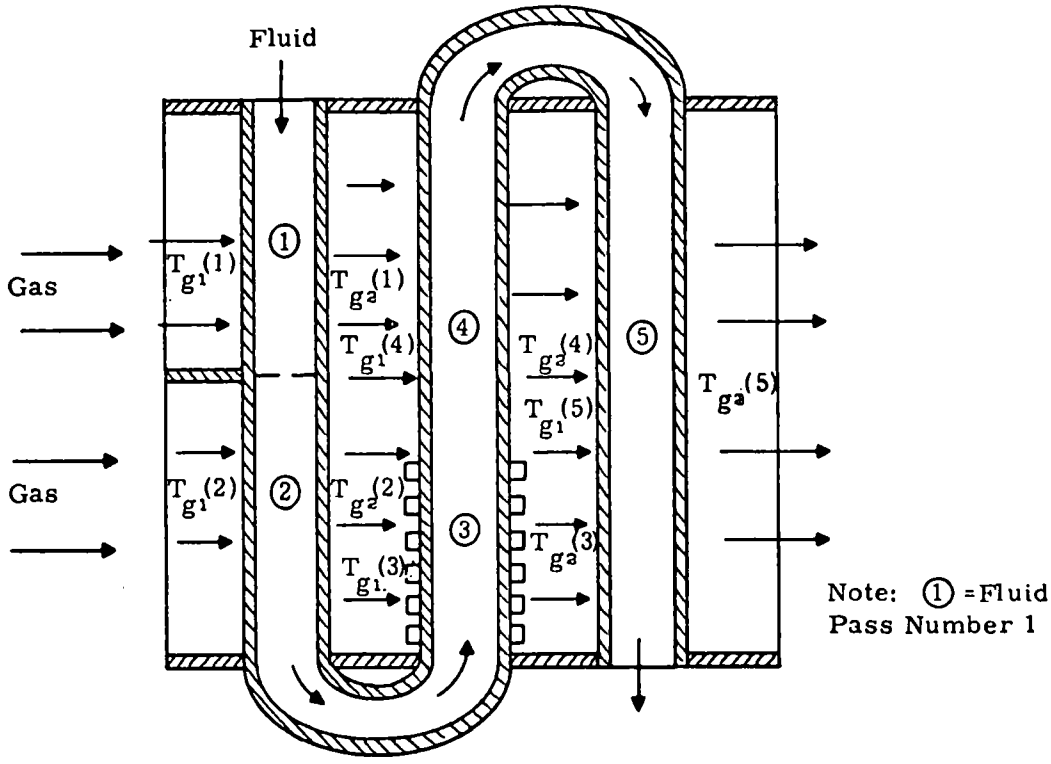

Fluid Pass Numbering for a Cross-flow Heat Exchanger

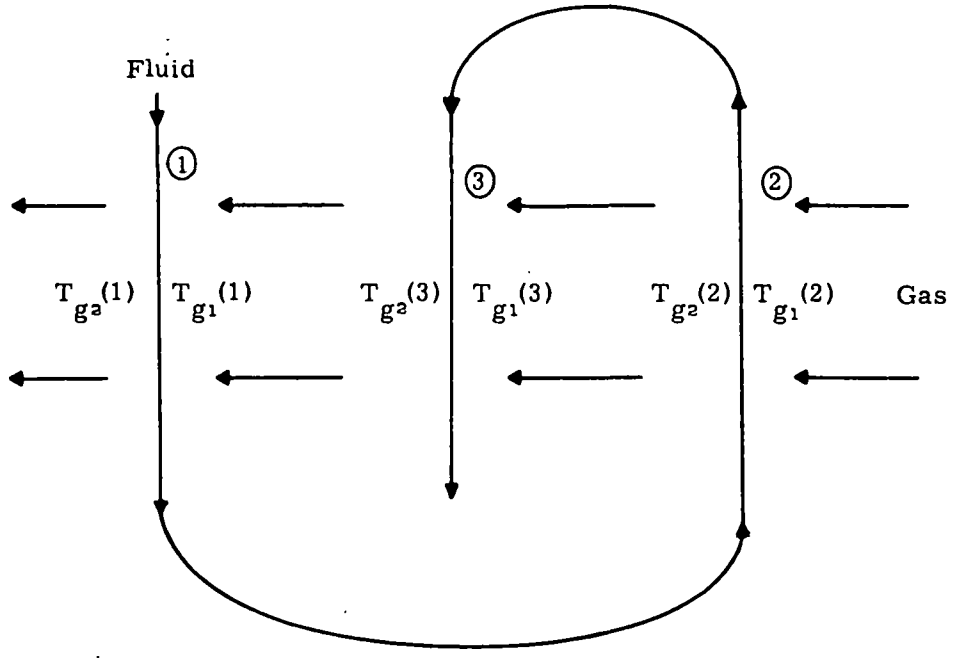

Fluid Pass Numbering for a Cross-flow Heat Exchanger with a Different Fluid Flow Path

Figure 16. Fluid Pass Numbering Process

For each lump, the average conditions are used to calculate the fluid- and gas-side heat transfer coefficients and, hence, transient parameters H_{tf}, H_{gt}, C_t, C_f. From the stability criterion, the allowable lump size, and hence required number of lumps for the fluid path, are obtained. The process is repeated until all the lumps at time t for the fluid pass are covered. The maximum of all the lumps calculated from the stability criterion for each lump is taken for time $(t + \Delta t)$. If the new value of the number of lumps at $(t + \Delta t)$ is different from that at (t), the present enthalpy distribution and other transient parameters are evaluated, through linear interpolation, to obtain all the parameters at the new node pattern. The fluid phase for each lump is also reestablished.

If the transient condition is imposed on an initial steady state of the component, the steady-state distribution of all dynamic parameters should be obtained at a desired operating condition. This can be done by using quasi-steady relations for all energy streams and solving the simultaneous equations through iteration until the convergence within a specified limit is obtained. The mass flows and pressures are held constant during the iteration process

During the transient operation, a time step Δt is computed from the stability criterion. Note that the selected time step should satisfy the stability criteria for all of the energy streams for all fluid passes. The fluid enthalpy, gas temperature, tube temperature, and fluid mass-flow distributions at time $(t + \Delta t)$ are obtained by the method outlined earlier. It is assumed that perfect mixing of gases occurs; therefore temperature variation of inlet gas is neglected.

At the end of each time step, the following quantities are available for each fluid pass:

- Fluid enthalpy distribution at the entrance and exit nodes of each lump
- Gas temperature distribution at the entrance and exit of gas nodes at the middle of each lump
- Tube temperature at the midlump node
- Fluid mass flow rate at each fluid node

This information from the preceding lump is appropriately transmitted to the next lump, and the computation is repeated until the exit end is reached.

With the values of parameters at the boundary known, the pressure at the time $(t + \Delta t)$ is calculated, using the lumped parameter pressure model. The dynamic parameter values at $(t+ \Delta t)$ are now reset as the 'present' values, and the computation sequence is repeated to obtain the solution after Δt. The sequence is repeated until the external time step limit is reached. Then the axial pressure distribution is computed from the friction and mo-

mentum pressure drop relations, and the exit pressure and enthalpy are calculated. In a system model, this information at the exit plane is transmitted to the next component to affect its input fluid properties.

Details of TECO Vapor Generator

The program VAPORG is presently set up for the Thermo Electron Corporation vapor generator design for the CP-34 system (Ref. 1). Figure 17 is a pictorial view of the unit. The combustion gases from the combustion chambers at the top enter the central cavity of the vapor generator and flow radially outward. The working fluid, CP-34, passes through a series of concentric coils; it enters the outer coil in subcooled state, then passes to the inner coil and finally through the middle coil, from which it exits. Some important details of the flow paths are given in Table 8.

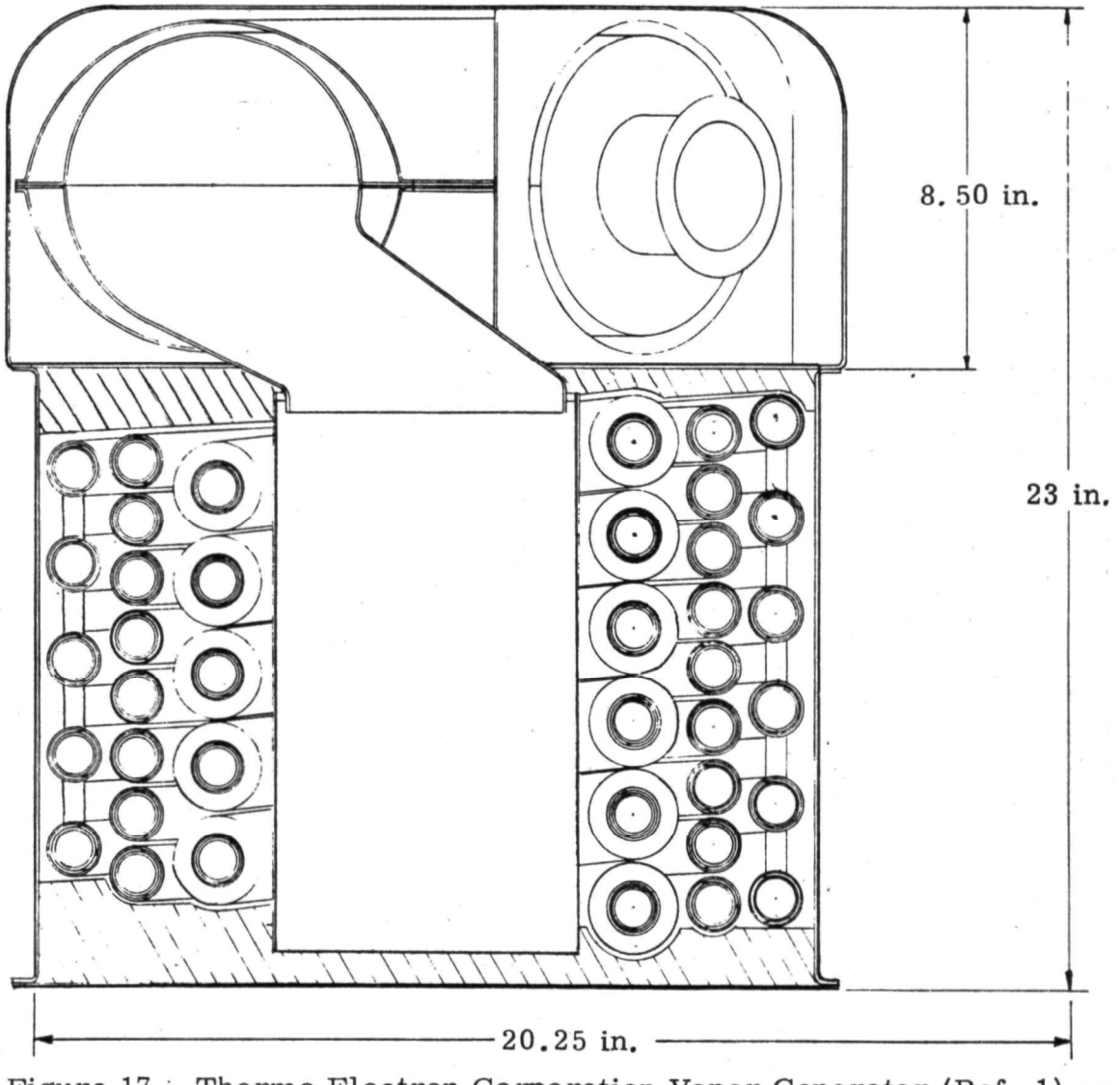

Figure 17. Thermo Electron Corporation Vapor Generator (Ref. 1) -- Cross Section Through Burner-boiler, Short Axis

Table 8

DETAILS OF FLOW PATHS FOR THE TECO VAPOR GENERATOR

Coil No.	Inner Tube Inside Diameter	Inner Tube Outside Diameter	Outer Tube Inside Diameter	Outer Tube Outside Diameter	Length (ft)	Inner Tube Surface	Outer Tube Surface
1	0.930	1.000	1.125	1.315	26	Bare	Ball-matrix
2	0.930	1.000	1.125	1.315	17	Longitudinal fins	Circumferential fins
3	0.930	1.000	1.125	1.315	35	Bare	Bare

Note that the actual tube construction is made up of two concentric tubes separated by a water wall. The purpose of the water wall is to limit the inner tube-wall temperature so that the organic working fluid does not thermally decompose. In the model the thermal resistance of the water wall was neglected and the energy-storage capacity was lumped with the tube-wall capacities.

Important heat transfer and pressure drop relations used in the program are given in Appendix III, "Heat Transfer and Pressure Drop Relations," of this volume.

Results

The VAPORG program was run with the design data of the Thermo Electron Vapor Generator. The results are summarized below.

Steady-state Run. Before the transient behavior can be studied, a steady-state distribution of fluid, gas, and tube-wall temperatures at desired operating levels is required. This can be done by:

1. Using the transient program, with boundary values and fluid pressure held constant.
2. Solving steady-state conservation equations simultaneously.

A combination of the two methods was used here to derive the steady-state distribution. An approximation of the steady-state condition was obtained by an iterative solution of the steady-state equations. The approximation was then input into the transient model, which was run with the boundary values held constant to obtain the final steady-state condition. This technique is much faster and more economical than driving the transient model to steady-state from arbitrary initial conditions.

Further discussion of the manner in which steady-state distributions are obtained is given later in this subsection under the heading "Regenerator."

The results for the vapor generator are summarized in Figures 18 through 21. The steady-state fluid-enthalpy distribution obtained from the program is shown in Figure 18. The enthalpy change across the vapor generator agrees within 6% with the steady-state results calculated by Thermo Electron (Ref. 1).

The fluid temperature distribution is shown in Figure 19. The results in the subcooled region compare well. The boiling section predicted by the model is much shorter than that calculated by TECO. As a consequence, the superheat zones differ significantly in their size. Resolution of this difference is important because the size of the superheat region has a significant effect on the dynamic behavior. The slope of the temperature profile in the superheat region predicted by the model compares well with the TECO calculated slope. Therefore it seems that the boiling region is the only area in which differences exist.

Figure 20 indicates the difference in steady-state wall temperature distribution. As can be seen, the model predicts different wall temperature from that obtained by Thermo Electron.

The reason for this difference is believed to be that the water-jacket resistance between the inner and outer tube walls has been neglected, and the vapor generator was treated as a single-wall device with equivalent heat capacity.

The Thermo Electron design, which includes the water jacket, results in lower inner-wall temperature in the two-phase flow region, a lower heat transfer rate to the working fluid, and hence a longer two-phase flow region.

The model can be easily modified and a water-jacket resistance included so that the steady-state temperature distributions match. However, the actual heat transfer mechanism in the 1/10-inch water jacket between the two walls is not well known. In the Thermo Electron analysis it was assumed that boiling occurs on the inner surface of the outer wall and condensation on the outer surface of the inner wall. Whether this is true or not should be established experimentally. By using the transient vapor generator model, however, the water-jacket resistance can be varied parametrically in order to determine the sensitivity of steady-state and dynamic performance to the value of this parameter.

Figure 21 presents the steady-state gas temperature distribution.

Transient Results. After the model was brought to steady state, it was subjected to several transients. The vapor generator model was run open-loop with different exit boundary conditions. Figure 22 shows the vapor-generator transient response to a 17.6% step increase in inlet fluid flow. The combustion gas flow was held constant and the exit fluid flow varied in proportion to $\sqrt{p - 50}$.

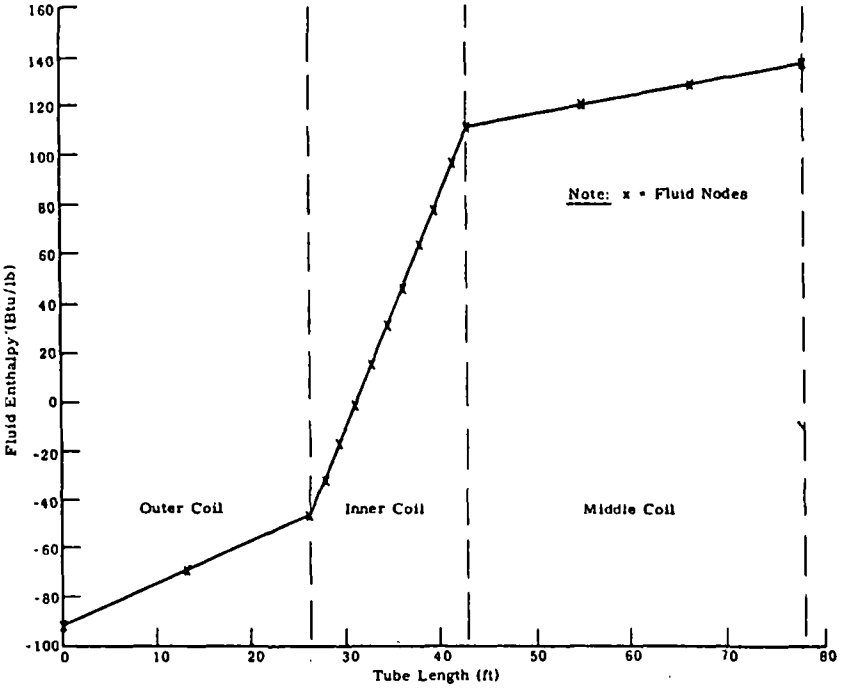

Figure 18. Vapor Generator -- Steady-state Enthalpy Distribution of Working Fluid. Vapor Generator Design as for TECO System (Ref. 1)

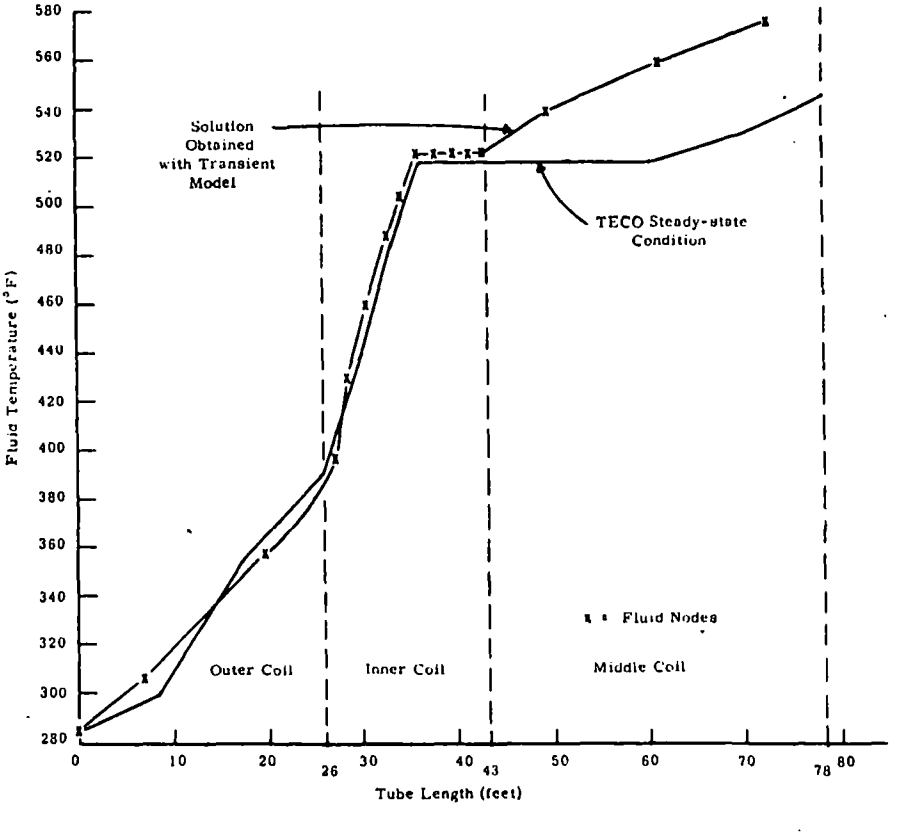

Figure 19. Comparison of Steady-state Temperature Distribution for Working Fluid in Vapor Generator

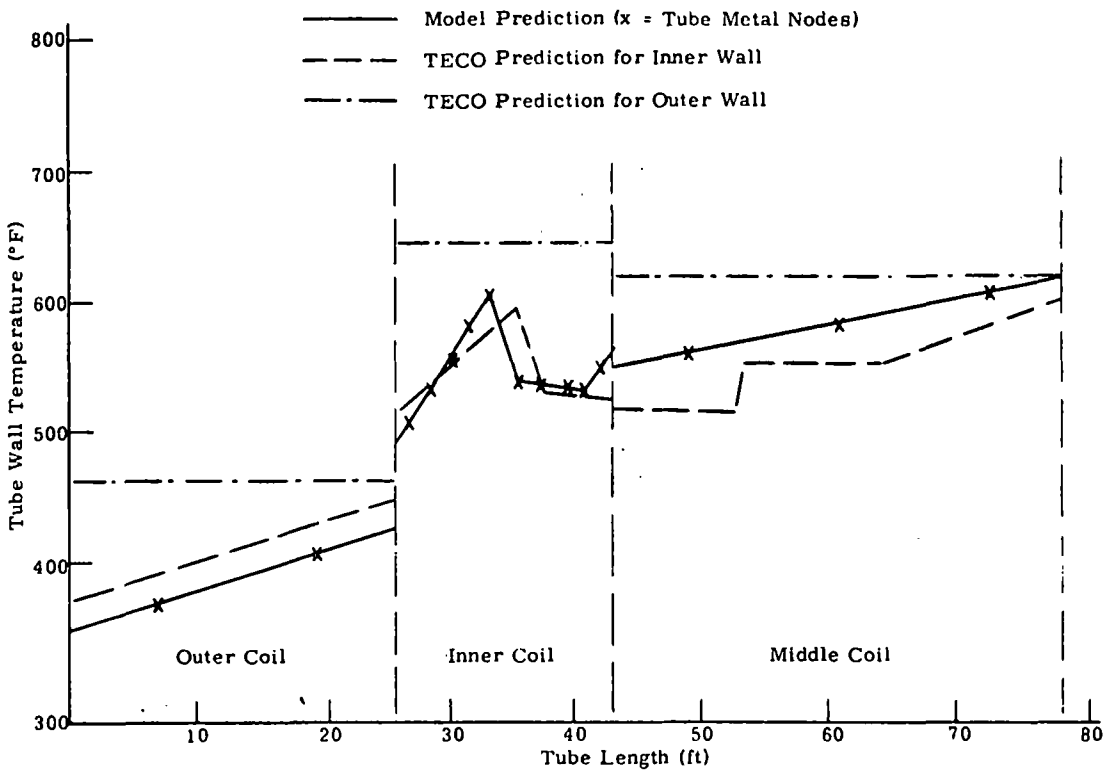

Figure 20. Vapor Generator -- Steady-state Tube Wall Temperature Distribution. Vapor Generator Design as for TECO System (Ref. 1)

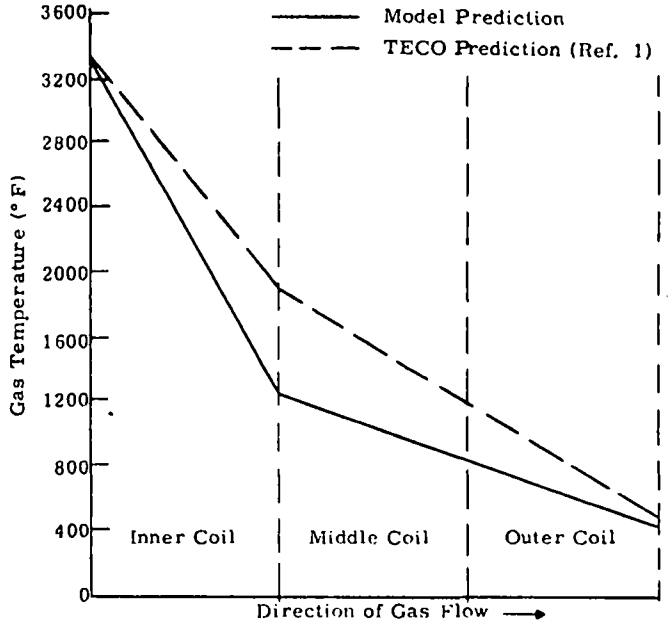

Figure 21. Vapor Generator -- Steady-state Combustion-gas Temperature Distribution

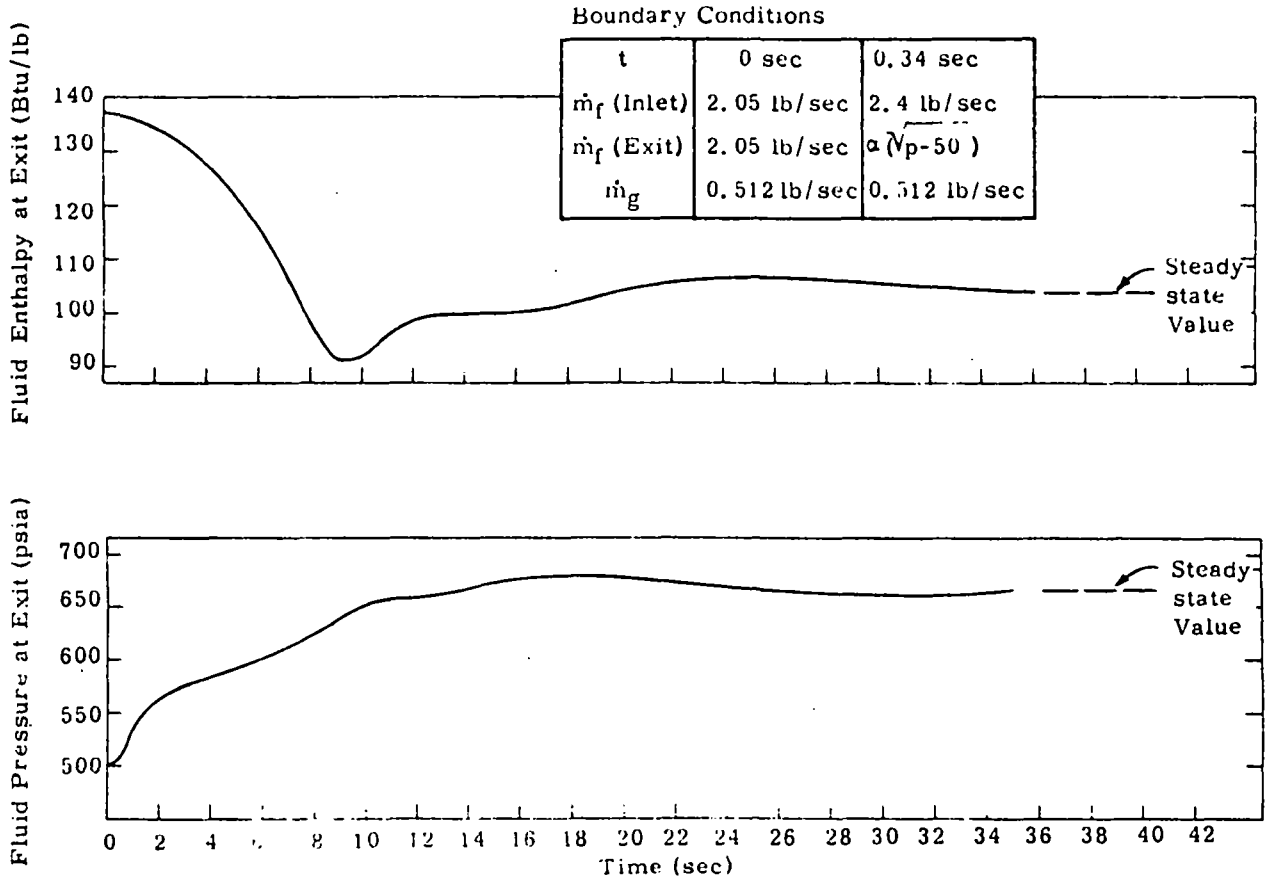

Figure 22. Vapor-generator Transient Response to a Change in Inlet Fluid Flow

The steady state that must be reached at the end of the transient can be calculated as:

$$p_f(\text{at exit}) = 670 \text{ psia}$$

$$h_f(\text{at exit}) = 104 \text{ Btu/lb}$$

where the enthalpy value is calculated assuming the heat rate remains constant.

As can be seen from Figure 22, the pressure and enthalpy both tend to level out at these steady-state values. Ninety percent of the pressure change occurs in about 10 seconds.

A certain "noise," due to the forward finite difference method employed, is always present in the computer solution, irrespective of the size of the lump and the time step. The noise is greatest (about 5% noise on the enthalpy trace) during the early parts of the transient and dies out as the heat exchanger approaches steady state. The results shown in Figure 22 are the mean curves plotted through the noise.

Figure 23 shows the vapor-generator transient response to a 10% step decrease in combustion-gas flow rate. The inlet fluid flow was held constant and the exit flow rate varied proportionally to $p/\sqrt{T}$.

The steady state after the transient can be approximated as:

$$p_f(\text{at exit}) = 496 \text{ psia}$$

$$h_f(\text{at exit}) = 118 \text{ Btu/lb}$$

where in calculating the enthalpy value the heat rate at 30 seconds is employed. As can be seen in Figure 23, the exit pressure remains fairly constant while the exit enthalpy drops slowly, with ninety percent of the enthalpy change occurring in about 25 seconds. The noise on this set of traces was negligible.

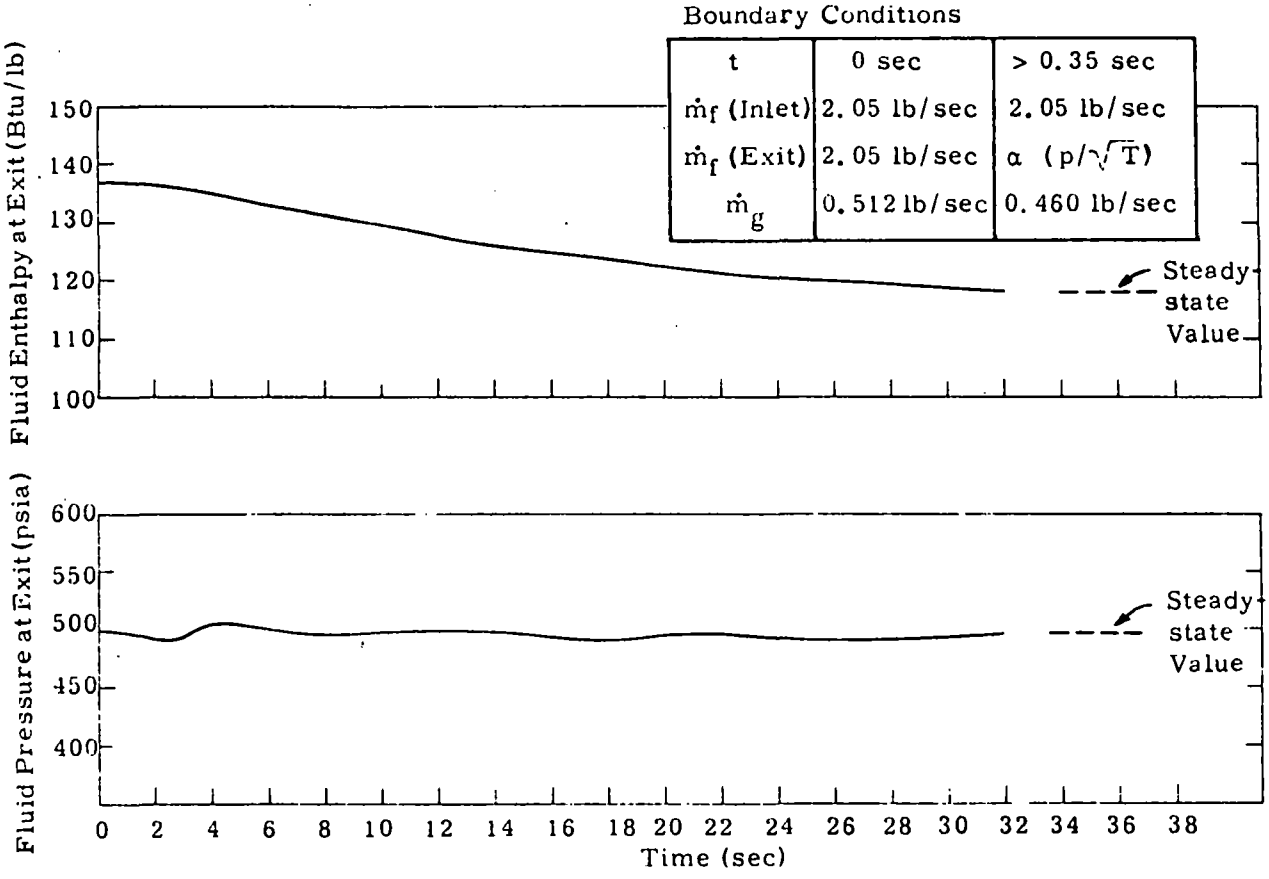

Figure 23. Vapor-generator Transient Response to a Change in Combustion-gas Flow Rate

CONDENSER

The automotive condensers are usually of the cross-flow type, with the working fluid flowing inside the tube and cooling air outside. The fluid enters the unit in a slightly superheated state and leaves in a subcooled condition.

From the simulation standpoint, the condenser model is closely similar to the vapor generator model, except for the direction of fluid enthalpy change. Hence, the relations derived earlier for the vapor generator are directly applicable here and will not be repeated.

General Description of Model

The condenser usually has multiple fluid passes, arranged in a series fashion. Each fluid pass consists of a number of parallel fluid paths, with headers at both ends. If it is assumed that the only effect of parallel fluid paths is to divide the air and fluid flows appropriately, consideration of one fluid path is representative. Since the serial fluid passes resemble the once-through vapor generator arrangement, the comments concerning the once-through unit given in the "Vapor Generator" subsection are directly applicable here.

Transient Analysis and Analytic Procedure

The conservation equations, their finite-difference approximations, and corresponding stability criteria given for the once-through vapor generator are also directly applicable here.

The selection of the nature of transient relation for the particular condenser considered is given in Table 9. For example, in the superheated working fluid region, the air energy equations are quasi-steady, the tube equations are dynamic, and the working fluid equations are quasi-steady.

Table 9

SELECTION OF ENERGY RELATIONS FOR CONDENSER

Fluid Phase	Air	Tube	Fluid
Superheated	Quasi-steady	Dynamic	Quasi-steady
Condensing	Quasi-steady	Quasi-steady	Dynamic
Subcooled	Quasi-steady	Dynamic	Dynamic

Computer Model and Results

The condenser model is entitled CONDENS, and is listed in Volume II. The structure and the data requirement of this program are identical to those for the vapor generator.

The Thermo Electron condenser design, on which CONDENS is based, is represented in Figure 24 (Ref. 1). Briefly, it has three fluid passes, with 30 parallel flow paths in each. Each tube has louvered fins on the outside. The flow area is not identical for all fluid passes.

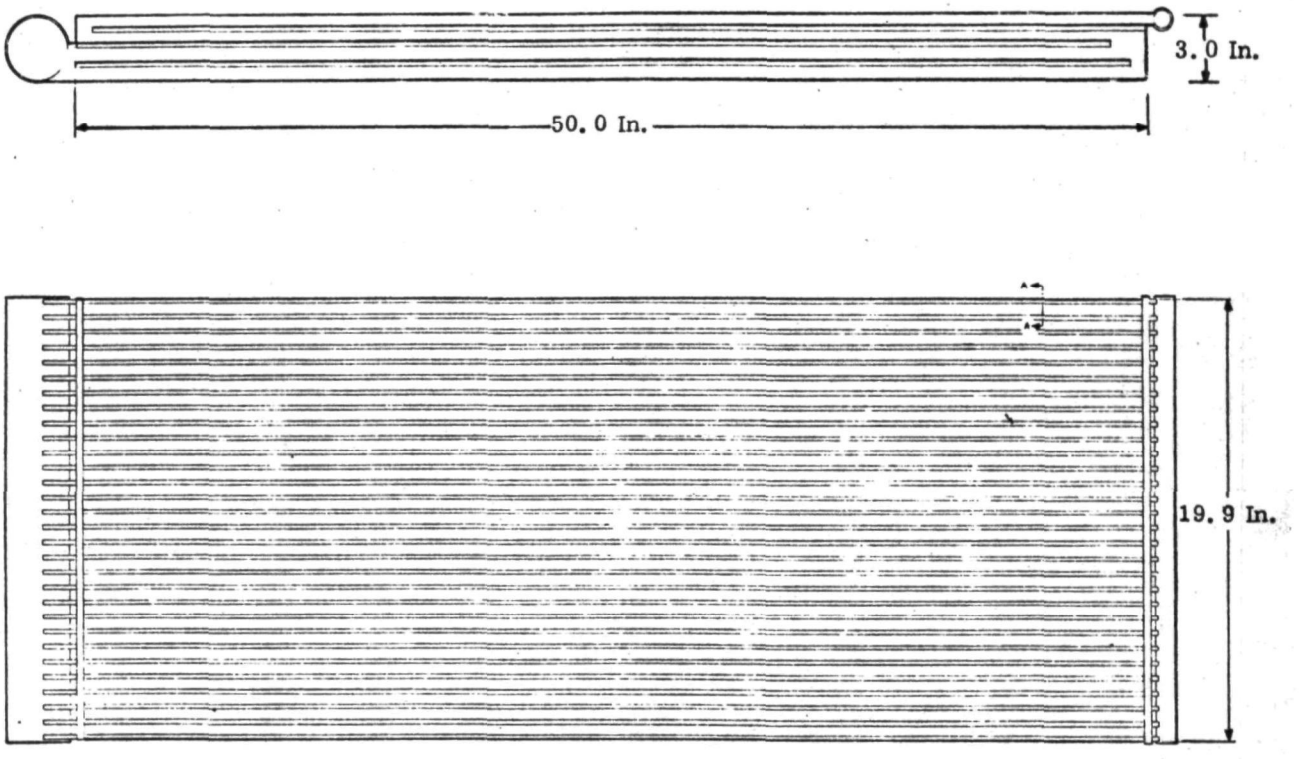

Figure 24. Condenser Design (Ref. 1)

The pressure drop and heat transfer correlations used here are mostly similar to those given in Appendix III for the vapor generator.

The CONDENS program was run with the design data of the Thermo Electron condenser. The steady-state temperature distribution was obtained in a manner similar to that for the vapor generator. The results shown on Figure 25 compare with the Thermo Electron calculations within two percent at the end points (TECO did not calculate the enthalpy distribution throughout the condenser).

After the condenser model was brought to steady state, it was subjected to a 10% step decrease in inlet fluid flow. The airflow rate was held constant and the exit fluid flow was proportional to $\sqrt{p - 10}$. The results are shown in Figure 26. The initial exit pressure and enthalpy are:

$$p_f(\text{at exit}) = 24.55 \text{ psia}$$

$$h_f(\text{at exit}) = -131.12 \text{ Btu/lb}$$

At the end of the transient the steady-state values that should be reached are:

$$p_f(\text{at exit}) = 21.7 \text{ psia}$$

$$h_f(\text{at exit}) = -134.01 \text{ Btu/lb}$$

These values were obtained by solving the steady-state conservation equations at the new fluid mass-flow rate. Therefore, at the end of the transient,

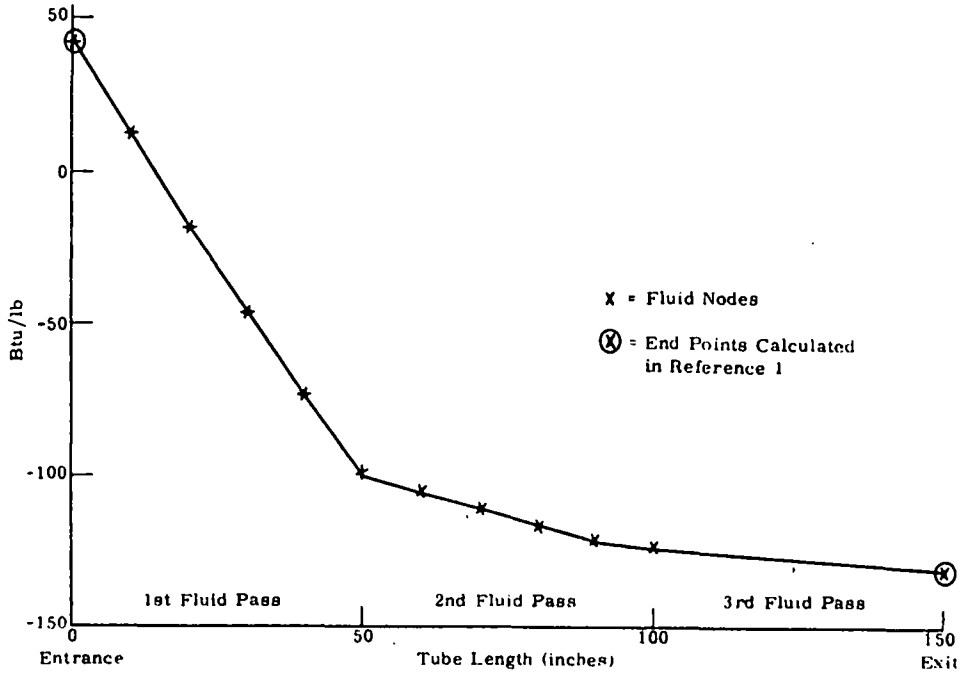

Figure 25. Condenser -- Steady-state Enthalpy Distribution Liquid Side -- as Calculated by Transient Model

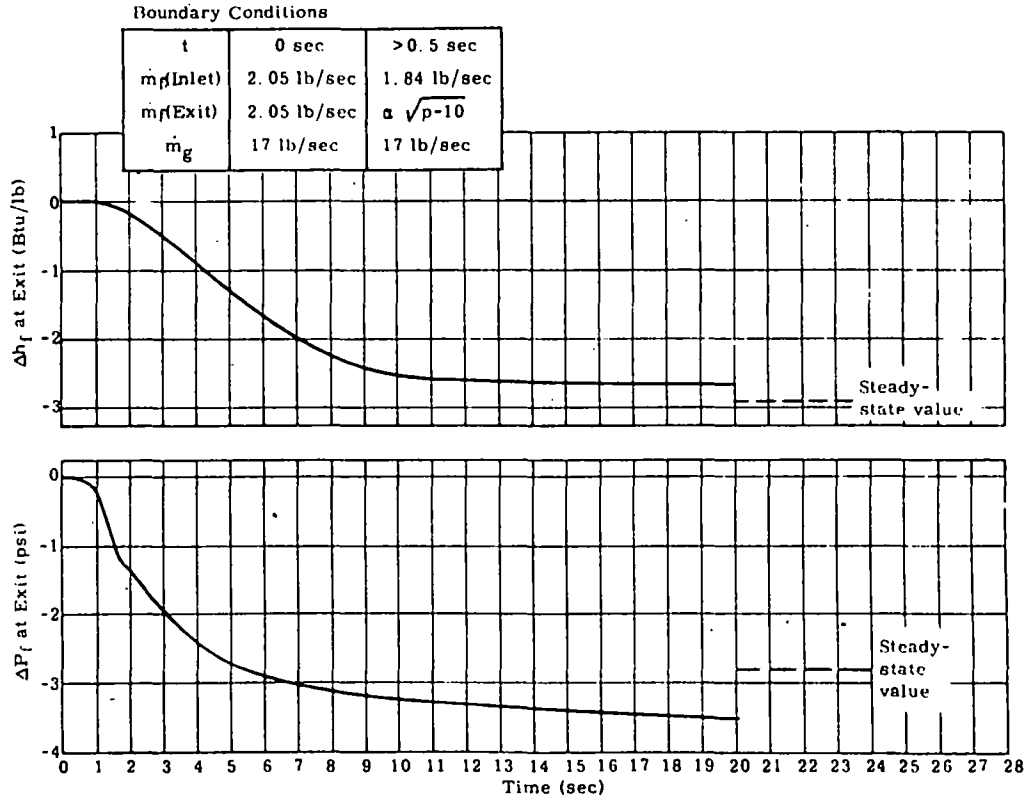

Figure 26. Condenser Transient Response to a Change in Inlet Fluid Flow

$$\Delta p_f \text{(at exit)} = -2.85 \text{ psi}$$

$$\Delta h_f \text{(at exit)} = -2.89 \text{ Btu/lb}$$

These values are also plotted on Figure 26.

After 20 seconds the pressure is within 3% of its final value; the enthalpy is within 0.3%.

An interesting point to note is that for a 10% decrease in inlet fluid flow, the enthalpy change across the condenser increases by less than 2%. Therefore, the heat rate of the condenser is not the same before and after the transient (remember, for a similar transient for the vapor generator, the heat rate remained constant; the enthalpy change increase balanced the mass flow decrease). For the condenser the decrease in fluid flow rate causes a decrease in interior heat-transfer coefficient; hence, the enthalpy increase is less than it would be if the heat rate remained constant. This illustrates the importance of the heat transfer mechanism in determining the transient behavior of the condenser.

REGENERATOR

The regenerator is a heat exchanger in which the thermal energy of the superheated vapor is transferred to the subcooled fluid circulated by the feed-pump. Ideally, the regenerator should be so sized that the vapor leaving the regenerator still has some degree of superheat; that is, no change of phase exists for either fluid. Generally, the subcooled fluid flows through the tube and the vapor outside it. The particular design studied here has a cross-flow configuration with all these features. The mathematical model of the regenerator is again similar to that of the vapor generator, with one major simplification arising from the absence of phase change: the dynamic fluid pressure variation need not be considered. Since the models are similar, the relations derived earlier are applicable here and will not be repeated.

General Description of Model

The regenerator usually has multiple fluid passes, arranged in series, the fluid traveling through several tube lengths in each pass. If it is assumed that perfect mixing exists on the vapor side, the cross-counterflow arrangement can be safely approximated as a cross-flow arrangement. Since the subcooled liquid usually will not change phase, the dynamic relations for the regenerator are similar to those for the vapor-generator subcooled phase.

Transient Analysis and Analytic Procedure

The conservation equations, their finite-difference approximations, and corresponding stability criteria given for the once-through vapor generator are directly applicable here. The vapor-side relations are quasi-steady, whereas the tube and the fluid-side relations are dynamic representations.

Computer Model and Results

The regenerator model is entitled REGEN and is listed in Volume II. The structure and the data requirements of this program are identical with those for the vapor generator.

The TECO regenerator design, on which the REGEN model is based, is represented in Figure 27 (Ref. 1). Briefly, the vapor flow to the regenerator is divided into four sections; it enters the regenerator from the sides, flows axially inward, and exits from the center through a common exit section. Likewise, the fluid-flow to the regenerator is divided into four sections. It enters at the top of the inner tube row near the centerline, then moves through the entire tube length and proceeds to the next tube in the same vertical fluid pass until it

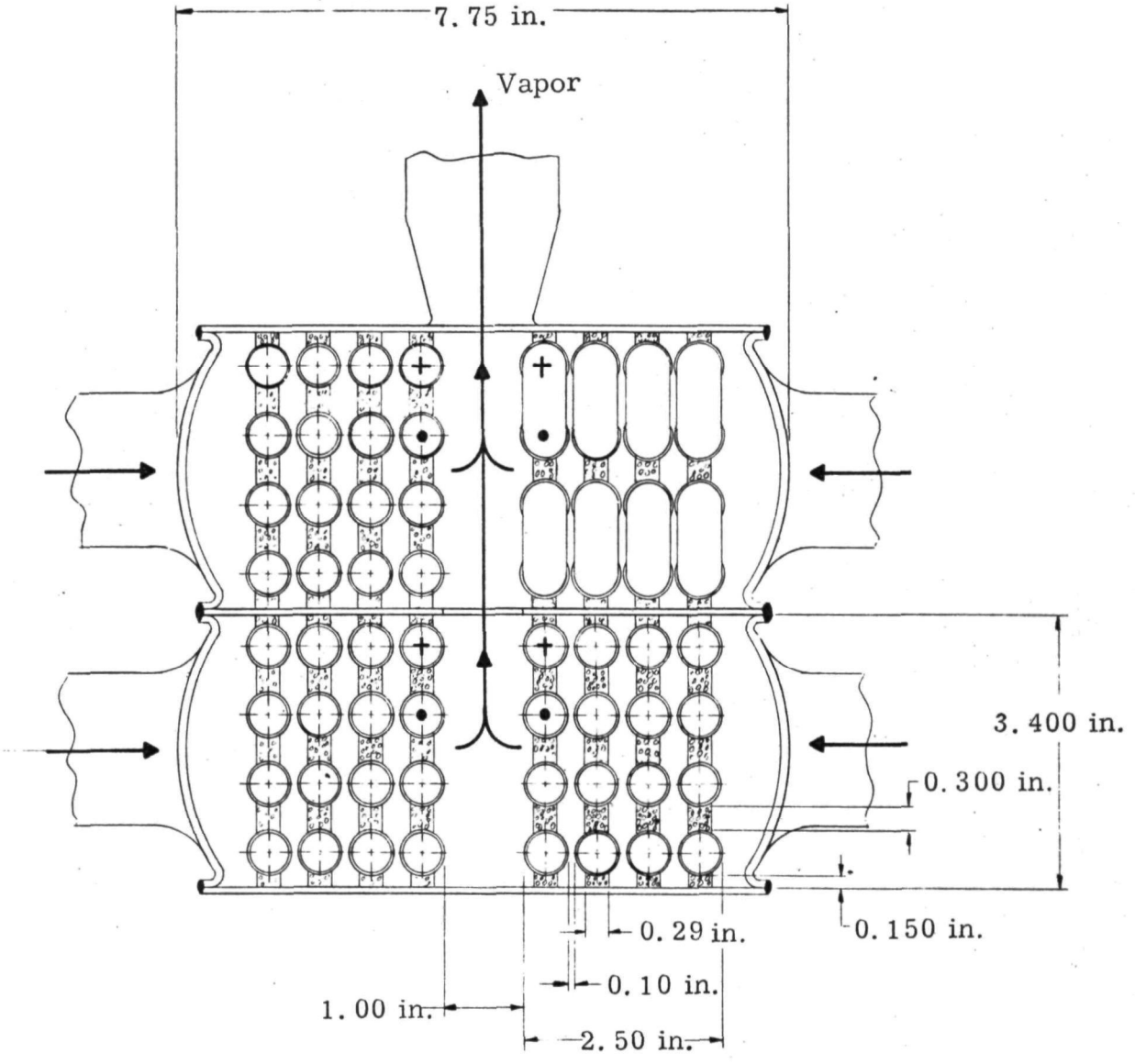

Figure 27. Regenerator Design (Ref. 1)

completes the fourth tube; it then moves to the bottom tube of the next fluid pass, and so on, until it travels through all of the four fluid passes. Note that the fluid exits at the same plane where the vapor enters; hence, a counterflow effect. The tube has a ball-matrix extended surface on its outside.

The pressure-drop and heat transfer correlations applicable here are largely similar to those given in Appendix III for the vapor generator.

The regenerator program was run with the design data of the Thermo Electron Corporation regenerator.

Steady-state Runs. Since the regenerator model is simpler and more economical to run than the condenser and vapor generator (absence of two-phase flow) it was decided to try to obtain the steady-state solution directly. It should be recalled that for the vapor generator and condenser this solution was approximated by iterating the steady state conservation equations before employing the model. For the regenerator, arbitrary liquid, gas, and tube temperature distributions were assumed and the transient model driven to steady state, with the inlet conditions held constant. Figure 28 gives the variation in spatial liquid-enthalpy distribution as a function of time. The curve marked 1 represents the initial guess, and the curve marked 105 is the distribution at steady state. The fact that there is a wide variation in liquid-enthalpy distribution between the two times is due to the initial tube temperature estimation (marked 1), which is significantly different from that at the steady state (marked 105), as shown in Figure 29. Similarly, Figure 30 gives the vapor-temperature spatial distribution as a function of time during this process of deriving the steady-state condition.

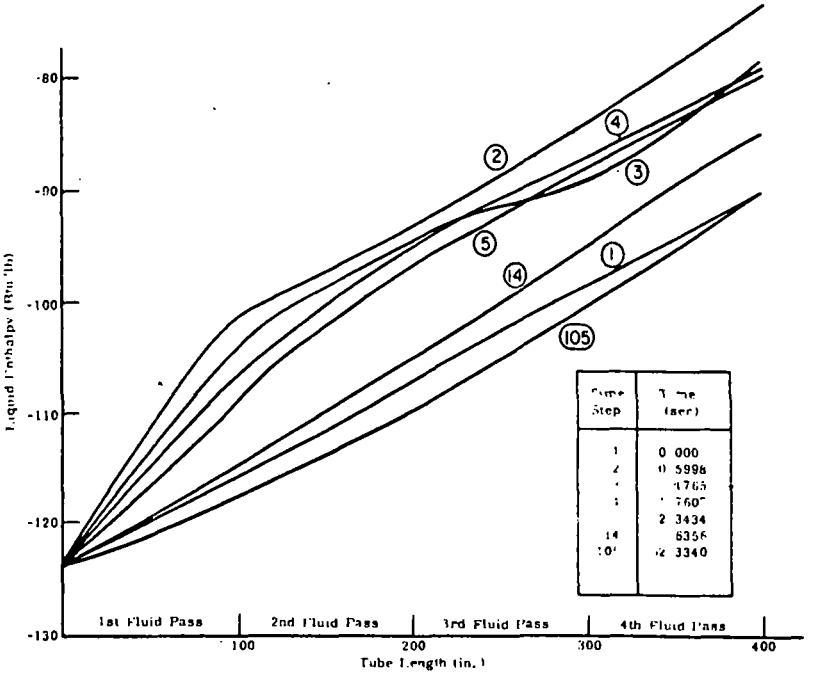

Figure 28. Regenerator Liquid Enthalpy -- Derivation of Steady-state Solution Employing Transient Model

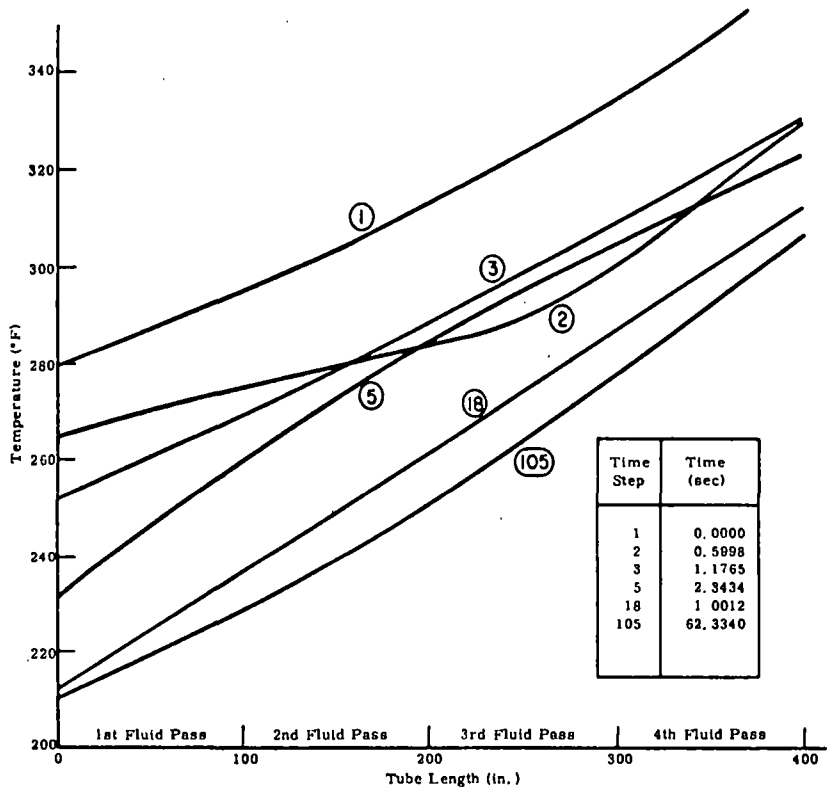

Figure 29. Regenerator Tube-wall Temperature -- Derivation of Steady-state Solution Employing Transient Model

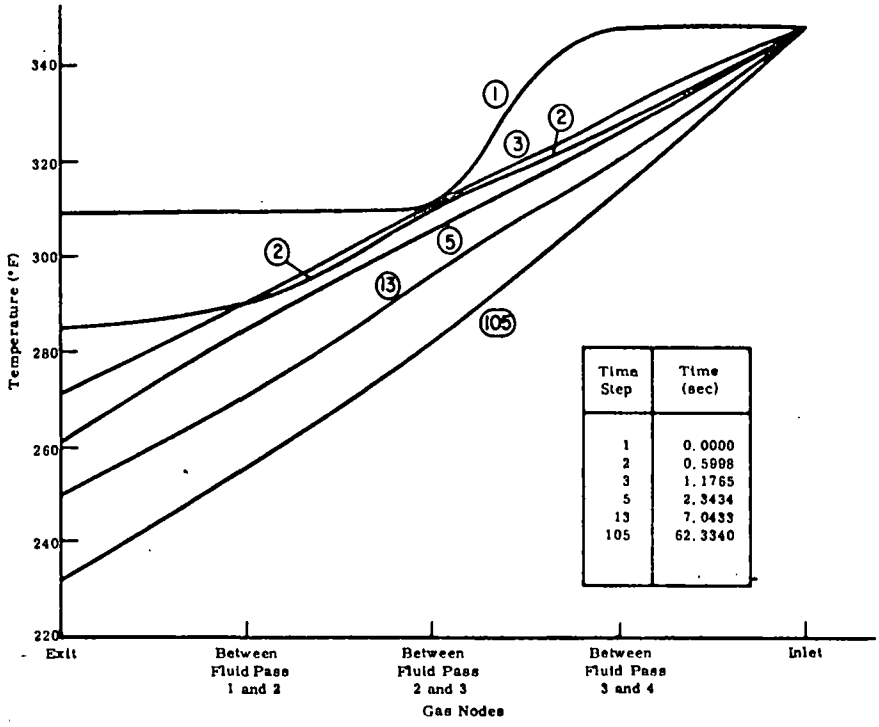

Figure 30. Regenerator Gas Temperature -- Derivation of Steady-state Solution Employing Transient Model

Transient Results. The steady-state distribution for the regenerator was supplied as the initial distribution, and the model was subjected to 20% drop in fluid enthalpy at the entrance. Figure 31 gives the corresponding variation in fluid enthalpy and vapor temperature at the exit as a function of time. The vapor temperature shows an immediate effect of the input enthalpy disturbance; this is due to the counterflow arrangement for the two fluid streams. The fluid enthalpy at exit lags the input disturbance by approximately one transport delay, which is expected. The final steady-state values also agree with a simple energy balance.

Figure 32 shows the effect on fluid temperature distribution as a function of time. Again the delay due to fluid transport mechanism can be noted. Figure 33 presents the tube temperature variation, and Figure 34 the vapor temperature variation.

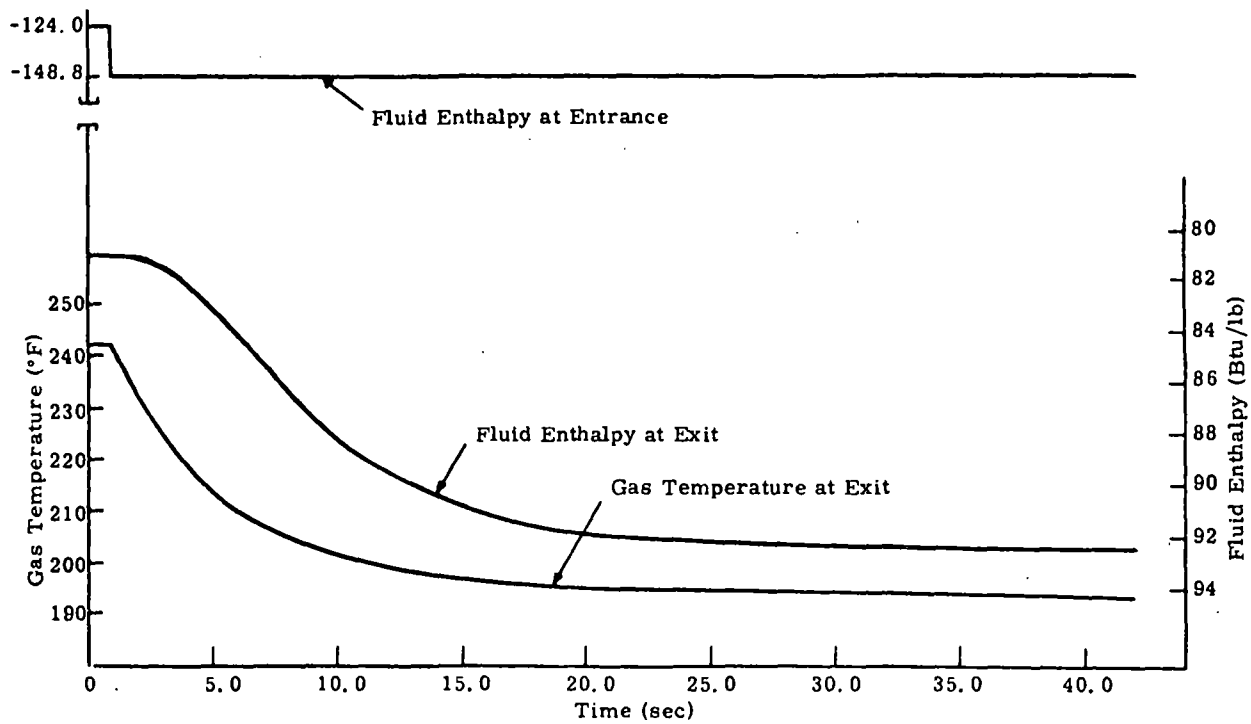

Figure 31. Regenerator Transient

COMBUSTOR

The combustor model was developed as three submodels dealing with

- Flame temperature
- Thermal transients
- Emissions

Each submodel will be derived separately below. At the end of this section, linking of the submodels to form the total combustor model will be discussed.

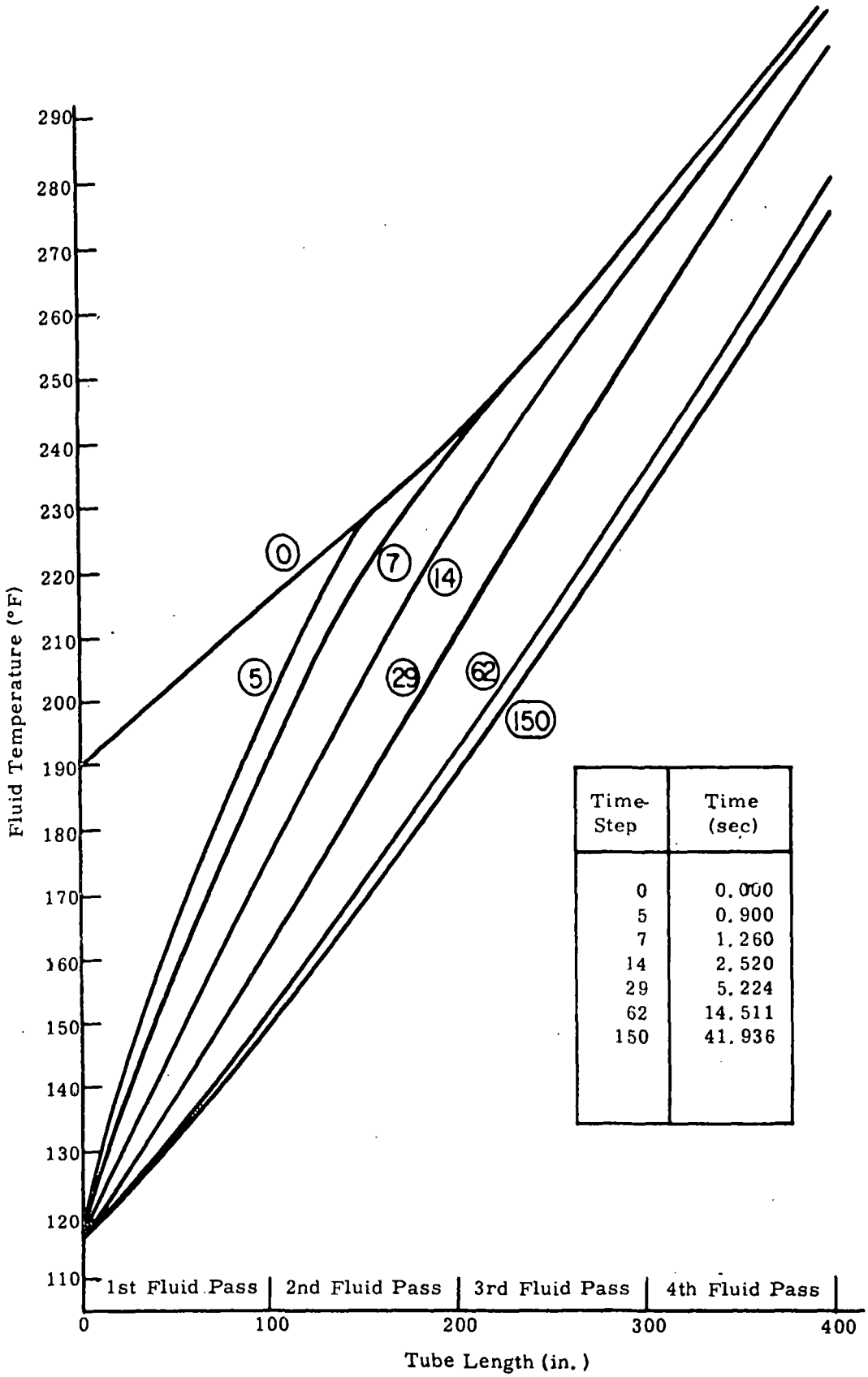

Figure 32. Regenerator Transient -- Fluid Temperature

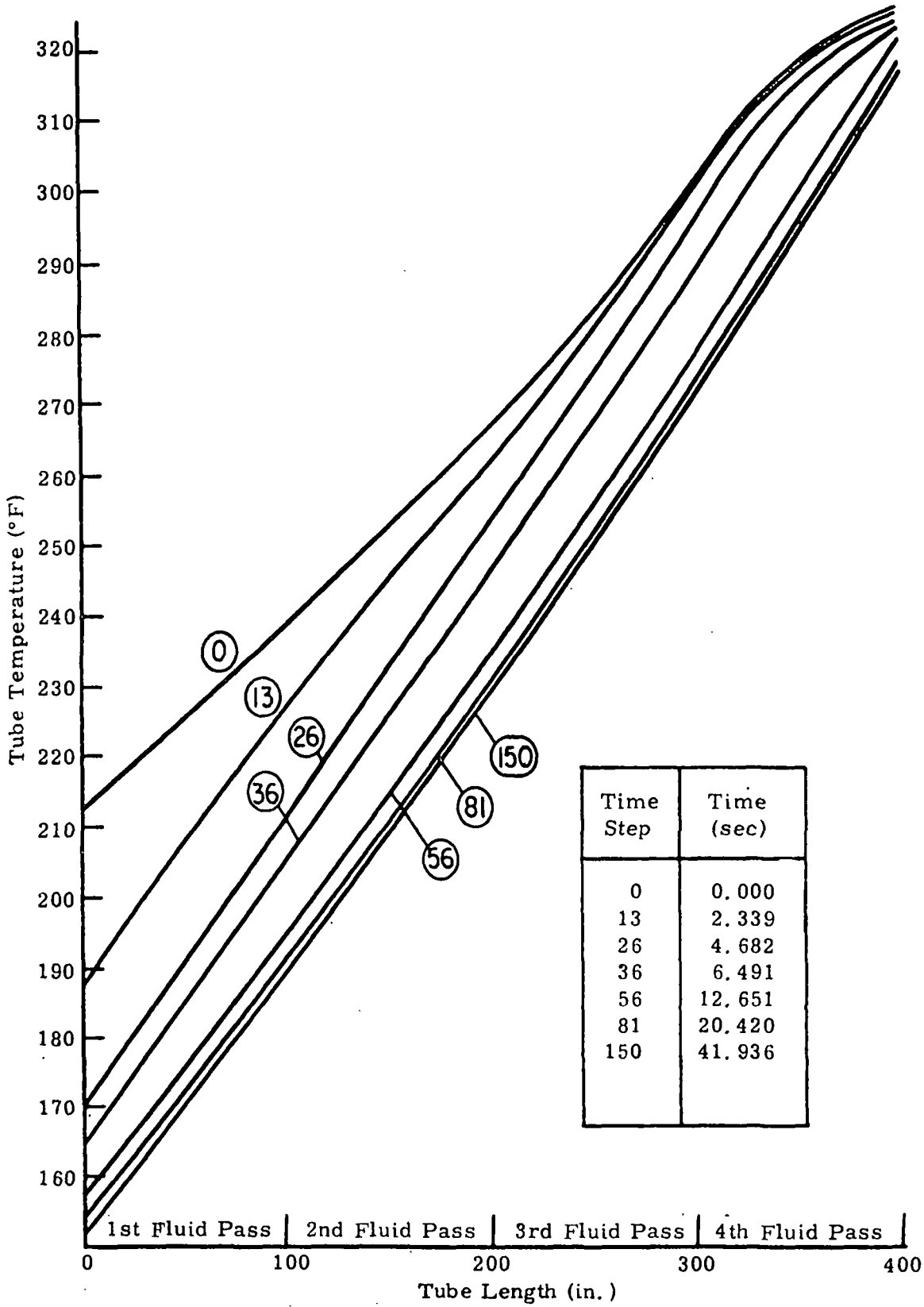

Figure 33. Regenerator Transient -- Tube-wall Temperature

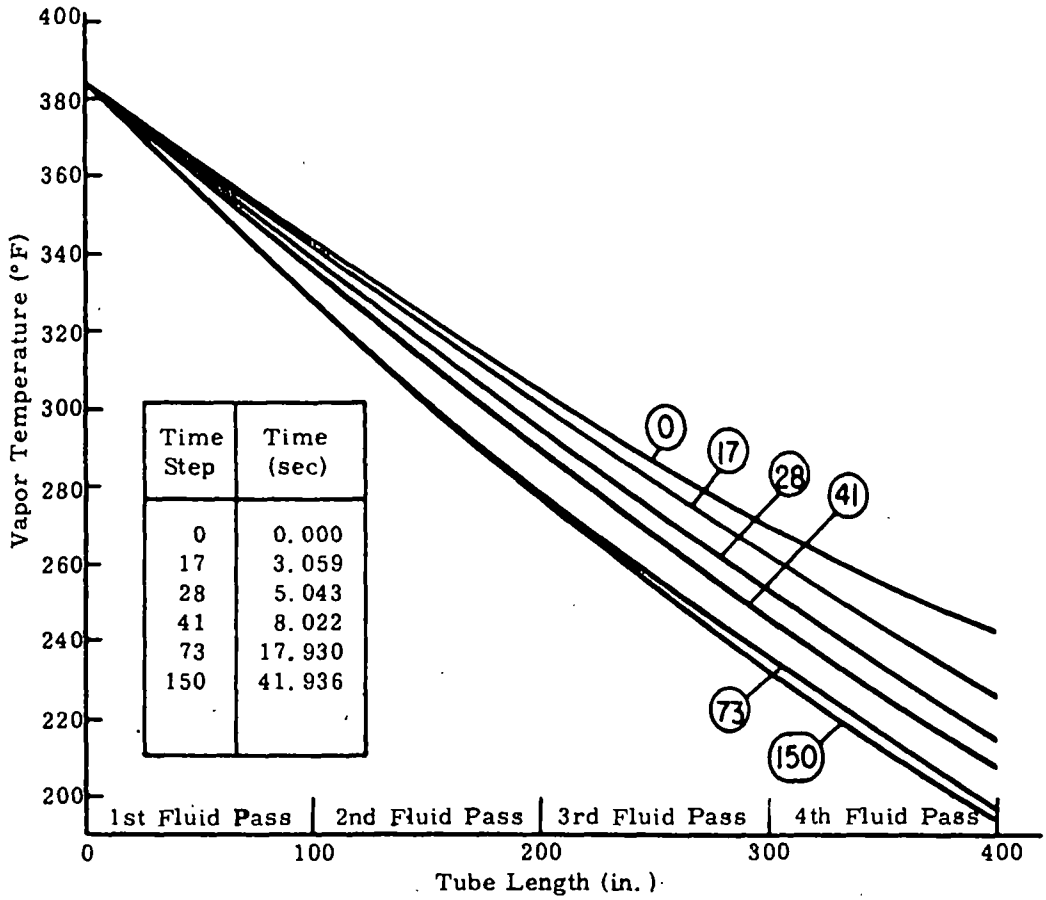

Figure 34. Regenerator Transient -- Vapor Temperature

NOMENCLATURE

Alphabetical Symbols	
b	Number of hydrogen moles in reaction
c	Percent of carbon by weight in fuel
Cp_a	Specific heat of air
Cp_g	Specific heat of gas
Cp_s	Specific heat of shell
Cp_t	Specific heat of tube
D_{cs}	Hydraulic diameter shell - tube flow passage
D_{ct}	Hydraulic diameter tube flow passage
e	Equivalence ratio

Alphabetical Symbols (Cont'd)

f	Fuel air ratio
f_{max}	Fuel air ratio maximum limit
f_{min}	Fuel air ratio minimum limit
f_s	Stoichiometric fuel air ratio
h_{sa}	Heat transfer coefficient between shell and air
h_{ta}	Heat transfer coefficient between tube and air
h_{tg}	Heat transfer coefficient between gas and tube
$h(T)$	Enthalpy at temperature T
L_{cs}	Shell length
L_{ct}	Tube length
LHV	Lower heating value of fuel
M_c	Molecular weight of carbon
M_h	Molecular weight of hydrogen
$\dot{m}_a$	Air mass flow rate
$\dot{m}_f$	Fuel mass flow rate
$\dot{m}_g$	Mass flow rate of combustion gas
N_{ba}	Equivalent turbulent friction length due to bends in air flow path
N_{bg}	Equivalent turbulent friction length due to bends in gas flow path
p_e	Pressure of gas at combustor exhaust
p_o	Pressure of air at combustor inlet
S_{sa}	Shell wetted area
S_{ta}	Tube - air wetted area
S_{tg}	Tube - gas wetted area

Alphabetical Symbols (Cont'd)

t	Time
T_a	Air temperature
T_f	Flame temperature
T_g	Gas temperature
T_o	Ambient temperature
T_s	Shell temperature
T_t	Tube temperature
W_s	Shell weight
W_t	Tube weight
x	Distance

Greek Symbols

Δt	Time step
Δt_e	External time step
Δt_s	Stability time step

FLAME TEMPERATURE SUBMODEL

Derivation of Basic Equations

Consider a reaction for the combustion of a hydrocarbon fuel containing a fraction (c) of carbon (by weight), and a fraction (1 - c) of hydrogen. The stoichiometric reaction in air is

$$CH_b + (1+\frac{b}{4})\, O_2 + 4(1+\frac{b}{4})\, N_2 \rightarrow \frac{b}{2} H_2O + CO_2 + 4(1+\frac{b}{4})\, N_2 \qquad (102)$$

where

$$b = 12\, \frac{(1-c)}{c} \qquad (102a)$$

and the fuel air ratio is

$$f_s = (12 + b) / \left[32(1+\frac{b}{4}) + (28)\, 4\, (1+\frac{b}{4})\right] \qquad (103)$$

For a reaction off stoichiometric conditions with a fuel air ratio (f), the equation for a lean mixture is

$$CH_b + \left(\frac{1}{e}\right)\left(1+\frac{b}{4}\right) O_2 + \left(\frac{1}{e}\right) 4\left(1+\frac{b}{4}\right) N_2 \rightarrow \frac{b}{2} H_2O + CO_2$$

$$+ \left(\frac{1}{e} - 1\right) \left(1+\frac{b}{4}\right) O_2 + \left(\frac{1}{e}\right) 4\left(1+\frac{b}{4}\right) N_2 \qquad (104)$$

For a rich mixture, the reaction is

$$CH_b + \left(\frac{1}{e}\right)\left(1+\frac{b}{4}\right) O_2 + \frac{1}{e} 4\left(1+\frac{b}{4}\right) N_2 \rightarrow \left[\frac{b}{2} - \left(1-\frac{1}{e}\right)\left(1+\frac{b}{4}\right)\right] H_2O$$

$$+ \left[1 - \left(1-\frac{1}{e}\right)\left(\frac{1}{2}+\frac{b}{8}\right)\right] CO_2 + \frac{4}{e}\left(1+\frac{b}{4}\right) N_2 + \left(1-\frac{1}{e}\right)\left(\frac{1}{2}+\frac{b}{8}\right) C$$

$$+ 2\left(1-\frac{1}{e}\right)\left(1+\frac{b}{4}\right) H \qquad (105)$$

where

$$e = \frac{f}{f_s} \qquad (105a)$$

By employing the coefficients in the above equations, the flame temperature can be calculated. The basic equation employed is

$$h(T_f) = h(T_a) + (12 + b)\, LHV \qquad (106)$$

where $h(T_f)$ is the enthalpy of the products of reaction at the flame temperature, $h(T_a)$ is the enthalpy of the products at the combustion air temperature and LHV is the lower heating value of the fuel.

The enthalpy of the products H_2O, CO_2, N_2, and O_2 are tabulated as a function of temperature in Reference 26. These are on a per-unit weight basis and must be multiplied by the appropriate coefficients from Equations 104 and 105 in order to be used in Equation 106.

Model Development

The flame temperature submodel has the following input:

$$T_a,\ \dot{m}_f,\ \text{and}\ \dot{m}_a.$$

The following data must be supplied:

$$c \text{ and } LHV,\ f_{max},\ f_{min}$$

The enthalpy of the products of combustion are curve-fit as a function of temperature. Therefore, an iterative procedure is required to find T_f by using Equation 106.

The outputs of the model are T_f, e, and b. T_f is employed by the thermal transient submodel; e and b are employed by the emission submodel. The flame temperature submodel is entitled COMB1 and is listed in Volume II, the Users Manual.

THERMAL TRANSIENT SUBMODEL

Derivation of Basic Equations

The schematic combustor configuration assumed for the thermal transient submodel is shown in Figure 35. Ambient air at temperature T_o passes between the combustor shell and the tube and is preheated to temperature T_a. Fuel is then mixed with the air, combustion takes place, and the products of combustion reach flame temperature T_f. The combustion gas then flows through the combustion tube, its temperature dropping to T_g as a result of heat transfer to the tube wall. The gas at T_g then flows over the vapor generator coils.

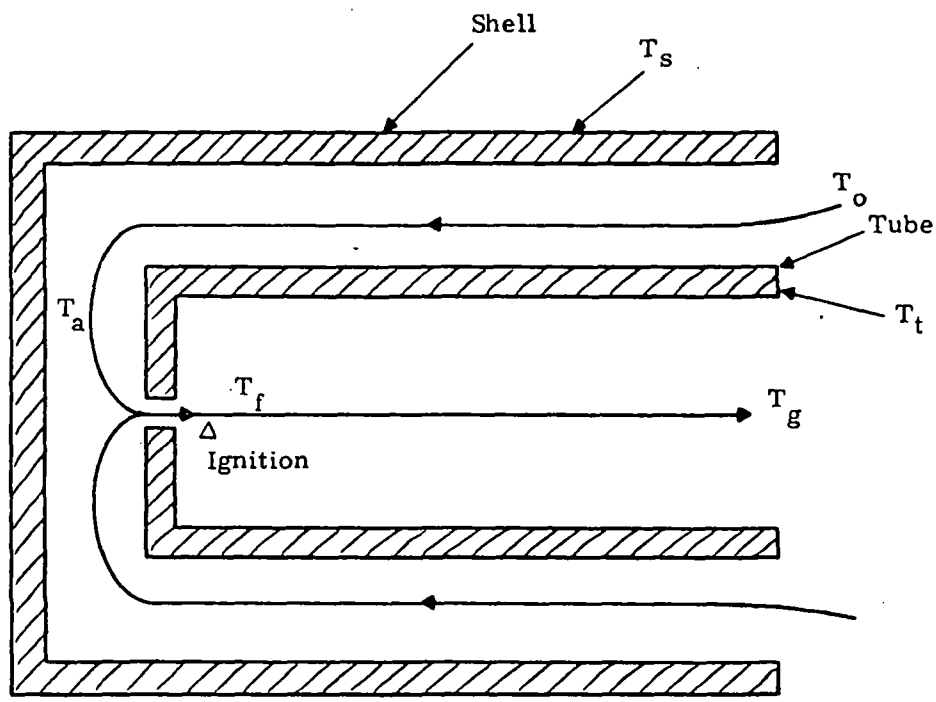

Figure 35. Combustor Schematic

The basic equations which describe the transient thermal process are:

Shell: (treated in lumped manner)

$$C_s \frac{dT_s}{dt} + H_{sa} (T_s - T_a) = 0 \qquad (107)$$

where

$$C_s = W_s Cp_s \qquad (107a)$$

$$H_{sa} = h_{sa} S_{sa} \tag{107b}$$

Air: (assuming quasi-steady)

$$E_a \frac{dT_a}{dx} \Delta x + H_{sa} (T_a - T_s) + H_{ta} (T_a - T_t) = 0 \tag{108}$$

where:

$$E_a = \dot{m}_a Cp_a \tag{108a}$$

$$H_{ta} = h_{ta} S_{ta} \tag{108b}$$

Tube: (treated in lumped manner)

$$C_t \frac{dT_t}{dt} + H_{ta} (T_t - T_a) + H_{tg} (T_t - T_g) = 0 \tag{109}$$

where:

$$C_t = W_t Cp_t \tag{109a}$$

$$H_{tg} = h_{tg} S_{tg} \tag{109b}$$

Gas: (assuming quasi-steady)

$$E_g \frac{dT_g}{dx} \Delta x + H_{tg} (T_g - T_t) = 0 \tag{110}$$

where:

$$E_g = \dot{m}_g Cp_g \tag{110a}$$

$$\dot{m}_g = \dot{m}_a + \dot{m}_f \tag{110b}$$

The combustor is treated as a lumped model and the following finite-difference approximations are made:

$$\frac{dT_s}{dt} = \frac{T_s(t+\Delta t) - T_s(t)}{\Delta t} \tag{111}$$

$$\frac{dT_a}{dx} = \frac{T_a - T_o}{\Delta x} \tag{112}$$

$$\frac{dT_t}{dt} = \frac{T_t(t+\Delta t) - T_t(t)}{\Delta t} \tag{113}$$

$$\frac{dT_g}{dx} = \frac{T_g - T_f}{\Delta x} \tag{114}$$

These approximations are substituted into the differential equations, and the results are:

Shell:

$$T_s\,(t+\Delta t) = F_{sa}\,T_a(t) + F_{ss}\,T_s(t) \tag{115}$$

where:

$$F_{sa} = \frac{H_{sa}\,\Delta t}{C_s} \tag{115a}$$

$$F_{ss} = 1 - \frac{H_{sa}\,\Delta t}{C_s} \tag{115b}$$

Air:

$$T_a\,(t+\Delta t) = F_{as}\,T_s(t) + F_{at}\,T_t(t) + F_{ao}\,T_o \tag{116}$$

where:

$$F_{as} = H_{sa} / (E_a + H_{sa} + H_{ta}) \tag{116a}$$

$$F_{at} = H_{ta} / (E_a + H_{sa} + H_{ta}) \tag{116b}$$

$$F_{ao} = E_a / (E_a + H_{sa} + H_{ta}) \tag{116c}$$

Tube:

$$T_t\,(t+\Delta t) = F_{ta}\,T_a(t) + F_{tg}\,T_g(t) + F_{tt}\,T_t(t). \tag{117}$$

where:

$$F_{ta} = H_{ta}\,\Delta t / C_t \tag{117a}$$

$$F_{tg} = H_{tg}\,\Delta t / C_t \tag{117b}$$

$$F_{tt} = 1 - \frac{H_{ta} + H_{tg}}{C_t}\,\Delta t \tag{117c}$$

Gas:

$$T_g\,(t+\Delta t) = F_{gt}\,T_t(t) + F_{gf}\,T_f(t) \tag{118}$$

where:

$$F_{gt} = H_{tg} / (E_g + H_{tg}) \tag{118a}$$

$$F_{gf} = E_g / (E_g + H_{tg}) \tag{118b}$$

The stability criterion requires that the coefficients F be positive. Therefore,

$$\Delta t_s \leq \text{Min} \left[\frac{C_s}{H_{sa}} , \frac{C_t}{H_{ta} + H_{tg}} \right] \qquad (119)$$

This sets the time-step size for the integration.

Model Development

The input to the transient thermal combustor submodel is

$$T_o,\ T_s(t),\ T_a(t),\ T_t(t),\ T_g(t),\ T_f(t+\Delta t_e), \text{ and } \Delta t_e$$

The following dimensional and geometric data must be provided:

$$W_s,\ W_t,\ S_{sa},\ S_{ta},\ S_{tg}$$

The outputs are

$$T_s(t+\Delta t_e),\ T_a(t+\Delta t_e),\ T_t(t+\Delta t_e), \text{ and } T_g(t+\Delta t_e).$$

If the integration is to be stable, the integration time step Δt must be less than the value (Δt_s), defined in Equation 119. Therefore, if Δt is less than Δt_e, the integration is carried out for several time steps Δt until the elapsed time is Δt_e. The pressure drop through the combustor due to friction and flow turn losses is calculated after each time interval Δt_e.

The transient thermal combustor model is entitled COMB2 and is listed in Volume II.

EMISSIONS SUBMODEL DEVELOPMENT

Accurate theoretical prediction of the emissions from an external combustor operating off-design and during transients is an impossible task. Therefore, experimental data were employed to derive the emissions submodel. When this model was formulated, however, experimental data for off-design and transient emissions were very scarce. Complete data describing emissions as a function of equivalence ratio, inlet air temperature, turndown ratio, and residence time were not available.

The model was based on data supplied by the Office of Air Programs, Environmental Protective Agency. Plotted in Figures 36 to 39, are design-point data for several different combustors operating at different equivalence ratios and inlet temperatures. More comprehensive data have recently been generated (Ref. 27 and 28) and should be used to obtain a more realistic model of combustor emissions.

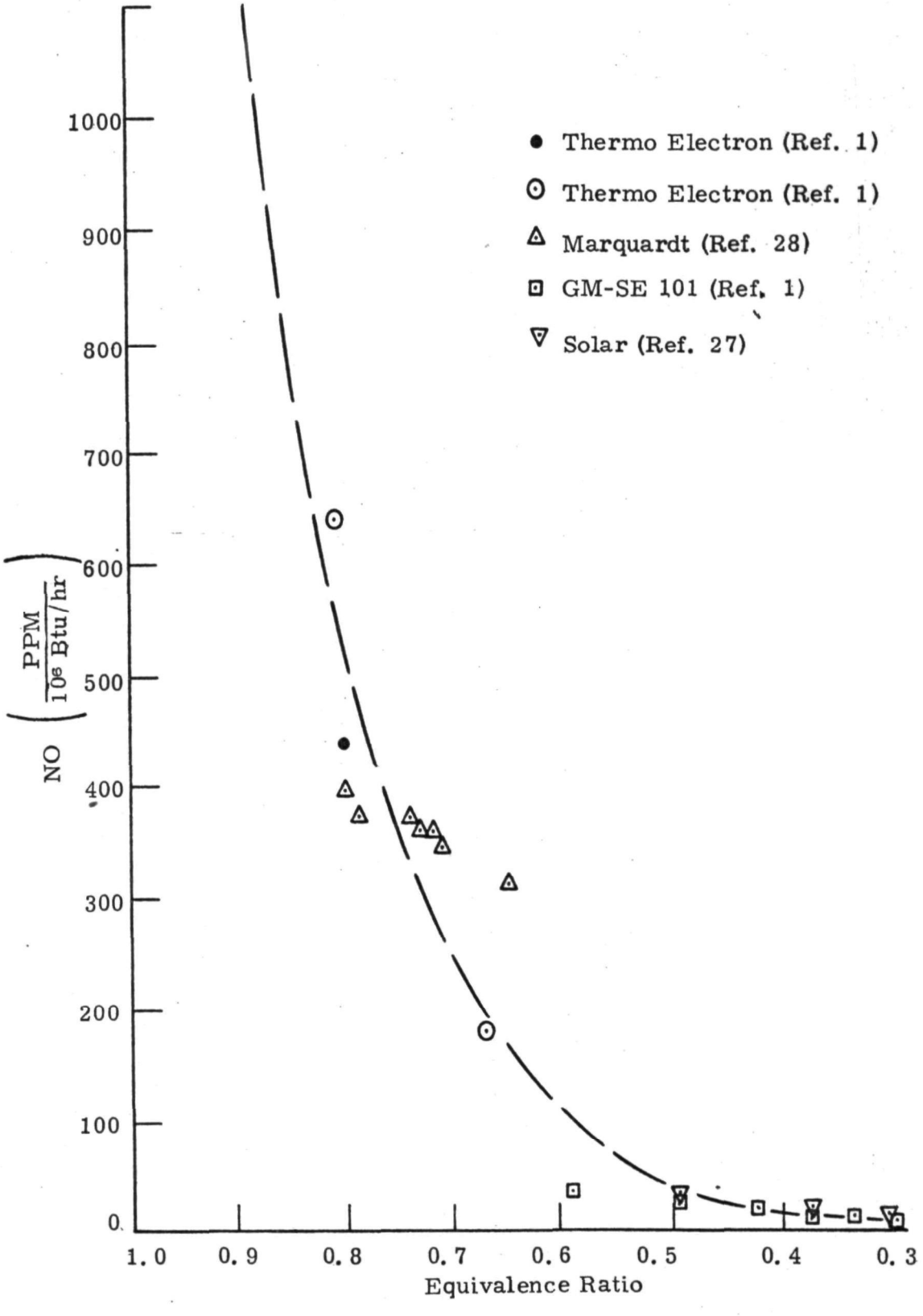

Figure 36. Nitrogen Oxide. Measured Exhaust Concentrations

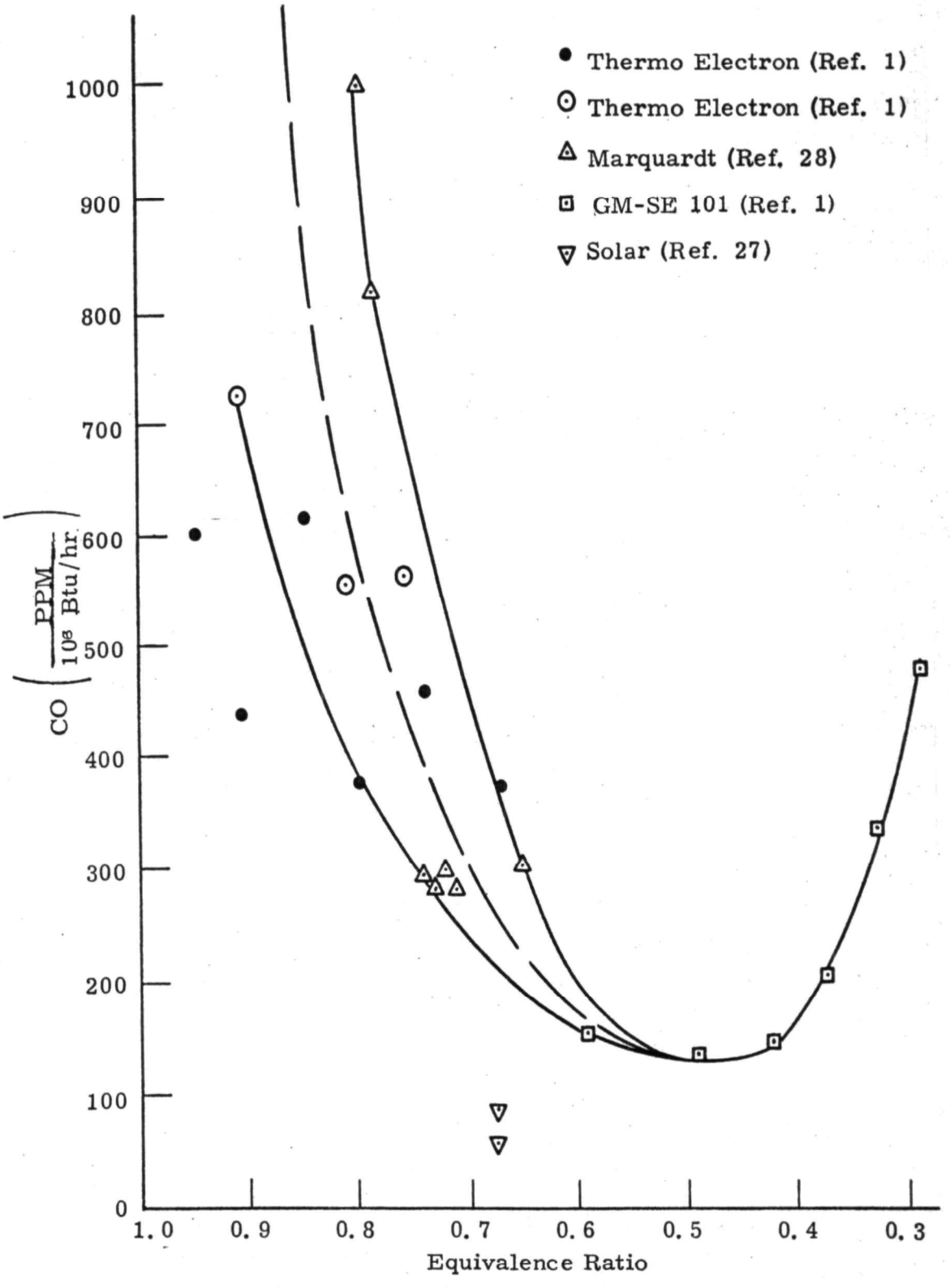

Figure 37. Carbon Monoxide. Measured Exhaust Concentrations

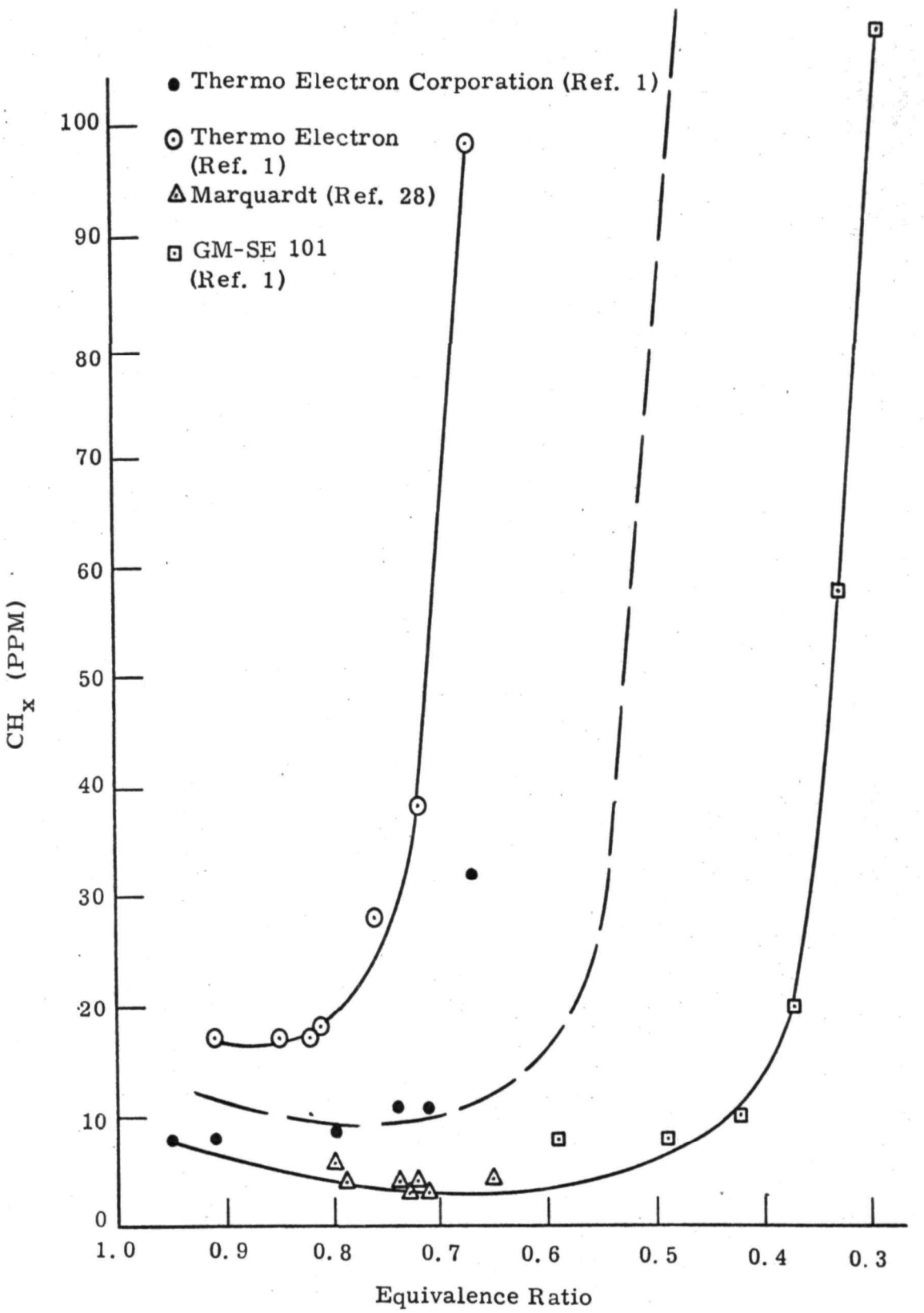

Figure 38. Unburned Hydrocarbons. Measured Exhaust Concentrations

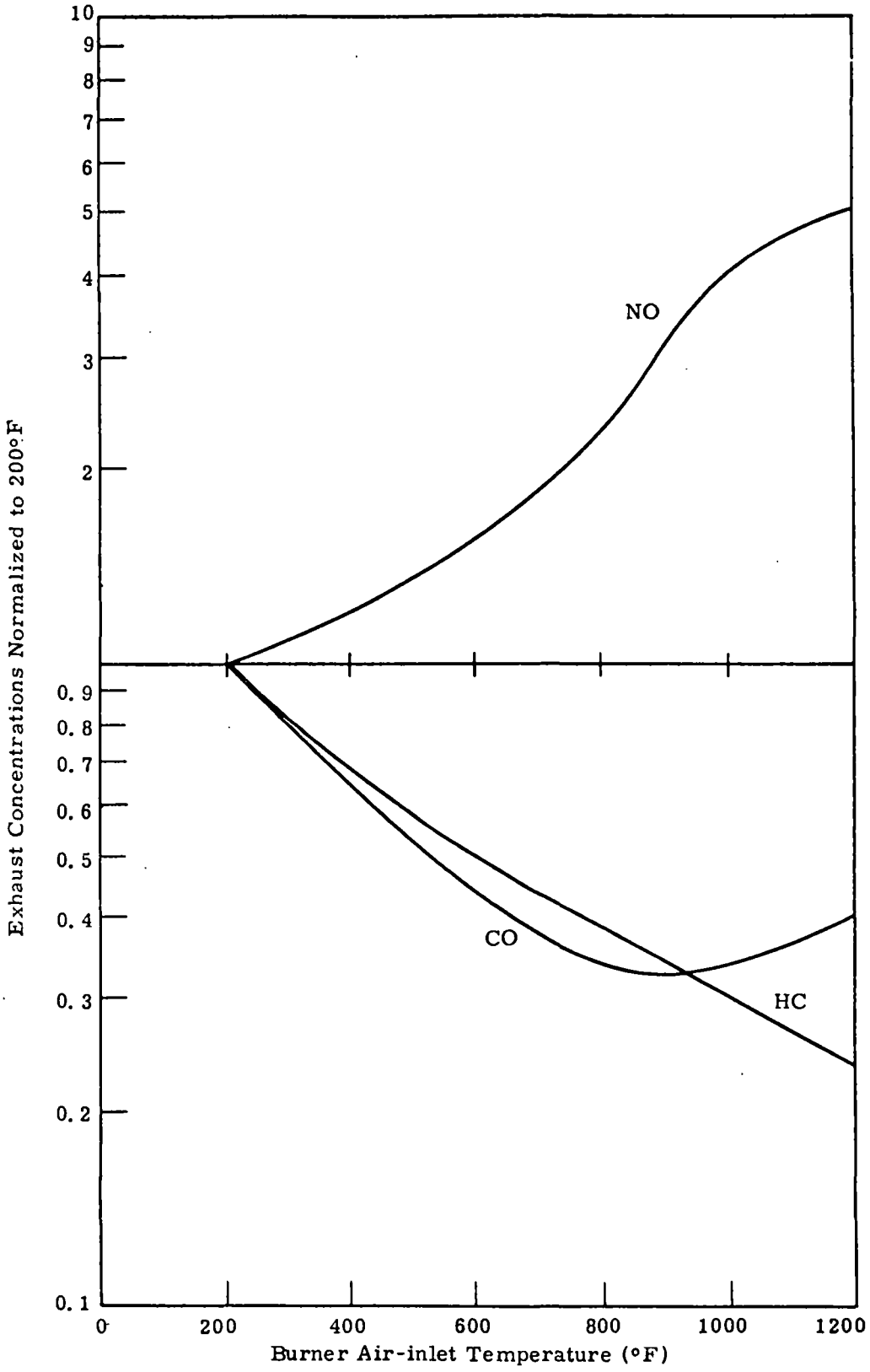

Figure 39. Characteristic Normalized Exhaust Concentrations (e = 0.59)

The information in Figures 36 to 39 has been curve-fit with polynomial functions which are used directly in the emissions submodel. The inputs to the model are:

T_a, e, and Δt.

The emissions are calculated (PPM/10^6 Btu/hr). This value is then multiplied by the design heat rate of the combustor to obtain the emissions in parts per million. The coefficients of the reaction equation determined in the flame temperature submodel are transmitted to the emission model and the emissions are calculated in two forms: 1) grams per gram fuel, and 2) the total grams in time interval Δt.

The emissions submodel is entitled COMB3 and is listed in Volume II.

TOTAL COMBUSTOR MODEL

Figure 40 shows the linking of the three combustor submodels to form the total combustor model. The inputs are:

p_o, T_o, $\dot{m}_f$, $\dot{m}_a$, and Δt_e

The outputs are:

p_e, T_t, T_s, T_a, T_g, T_f, and the emissions after an elapsed time of Δt_e

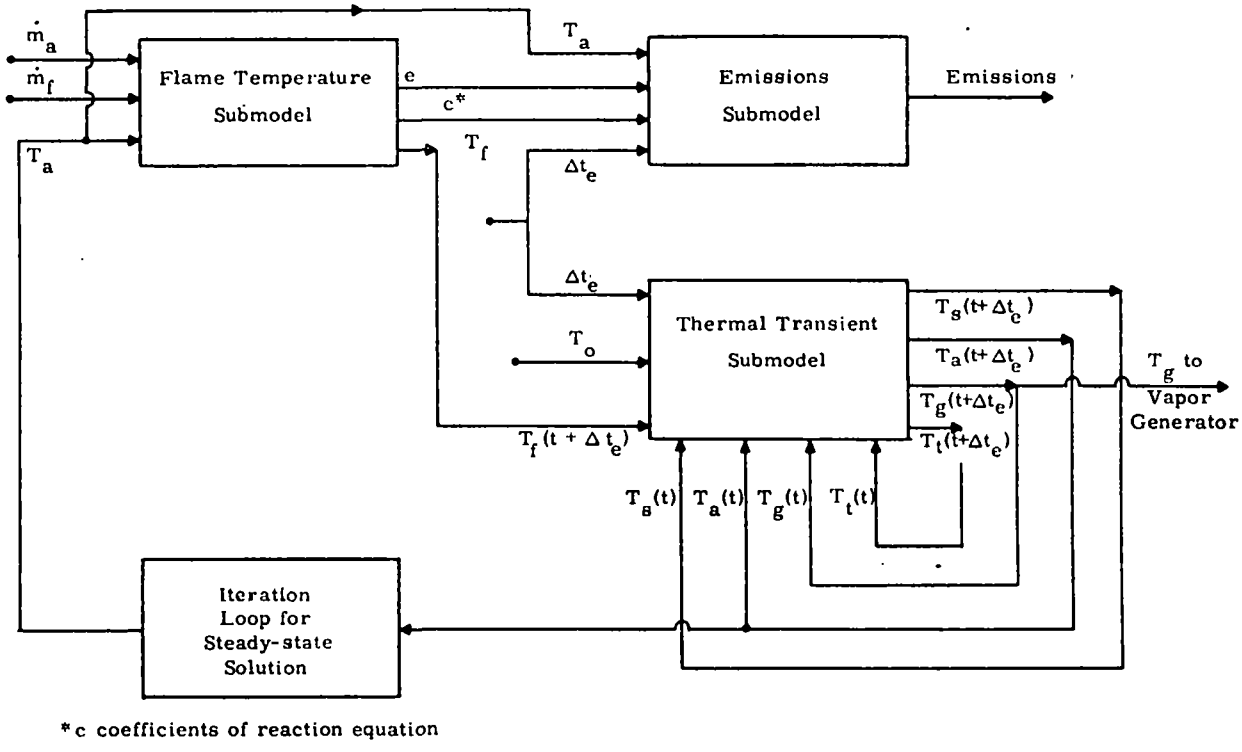

Figure 40. Combustor Model -- Linking of Combustor Submodels

An iterative procedure is required to derive the steady-state conditions, since the flame temperature submodel requires a value of T_a which is determined by the thermal transient submodel. Therefore, the following procedure is employed:

1. Initially, $T_a = T_o$ and the flame temperature submodel is used to find T_f.
2. The thermal transient model is run with T_f, $\dot{m}_f$, and $\dot{m}_a$ held constant until the transients die out and the steady-state solution is obtained for T_s, T_g, T_c, and T_a.
3. The new value of T_a is used in the flame temperature submodel, and the calculations are iterated until convergence.

Once the steady-state solution is obtained, transient cases can be run using the value of $T_a(t)$ to find the value of $T_f(t+\Delta t_e)$ in the flame temperature subroutine, which is, in turn, used in the thermal transient subroutine to determine

$$T_s(t+\Delta t_e),\ T_t(t+\Delta t_e),\ T_g(t+\Delta t_e),\ \text{and}\ T_a(t+\Delta t_e)$$

The total combustor model is entitled COMBST and is listed in Volume II, the Users Manual.

RESULTS

The combustor model was run to derive the steady-state solution at:

p_o = 14.7 psi

T_o = 85°F

$\dot{m}_f$ = 0.0123 lb/sec

$\dot{m}_a$ = 0.2435 lb/sec

LHV = 20180 Btu/lb

c = 0.85

W_s = 6.8 lb

W_t = 3.15 lb

S_{sa} = 454 in.^{2}

S_{ta} = 374 in.^{2}

S_{tg} = 374 in.^{2}

D_{cs} = 4 in.

D_{ct} = 7 in.

L_{cs} = 0.708 ft

L_{ct} = 1.415 ft

N_{ba} = 75

N_{bg} = 30

The above values approximately represent a single branch of the combustor in Reference 1 at the design condition. The following results are obtained:

T_a = 129°F

T_f = 3325°F

T_s = 125°F

T_t = 260°F

T_g = 3293°F

NO = $1.01\ 10^{-2}$ grams/gram of fuel

CO = 1.0510^{-2} grams/gram of fuel

HC = $7.32\ 10^{-5}$ grams/gram of fuel

p_e = 14.699 psi

If a fuel economy of 10 miles per gallon is assumed, the emissions in grams per mile are

NO = 3.24 grams/mile

CO = 3.37 grams/mile

HC = 0.0235 grams/mile

The Environment Protection Agency's emission-level goals are (Ref. 29):

NO = 0.4 grams/mile

CO = 4.7 grams/mile

HC = 0.14 grams/mile

The results obtained from the model meet the goals for hydrocarbon and carbon monoxide emissions but are higher than the goal for nitrogen oxide. Figure 41 shows that the nitrogen oxide goals can be achieved by decreasing the equivalence ratio to about 0.5. However, this is accompanied by an increase in hydrocarbon emissions and a decrease in combustion gas temperature. This figure illustrates the sensitivity of emissions to fuel/air ratio and indicates the trade-offs possible between emission levels and system efficiency.

The pressure drop calculated by the combustor model is very small and compares to the results obtained in Reference 1. The steady-state condition having been obtained, a fuel-air transient was run.

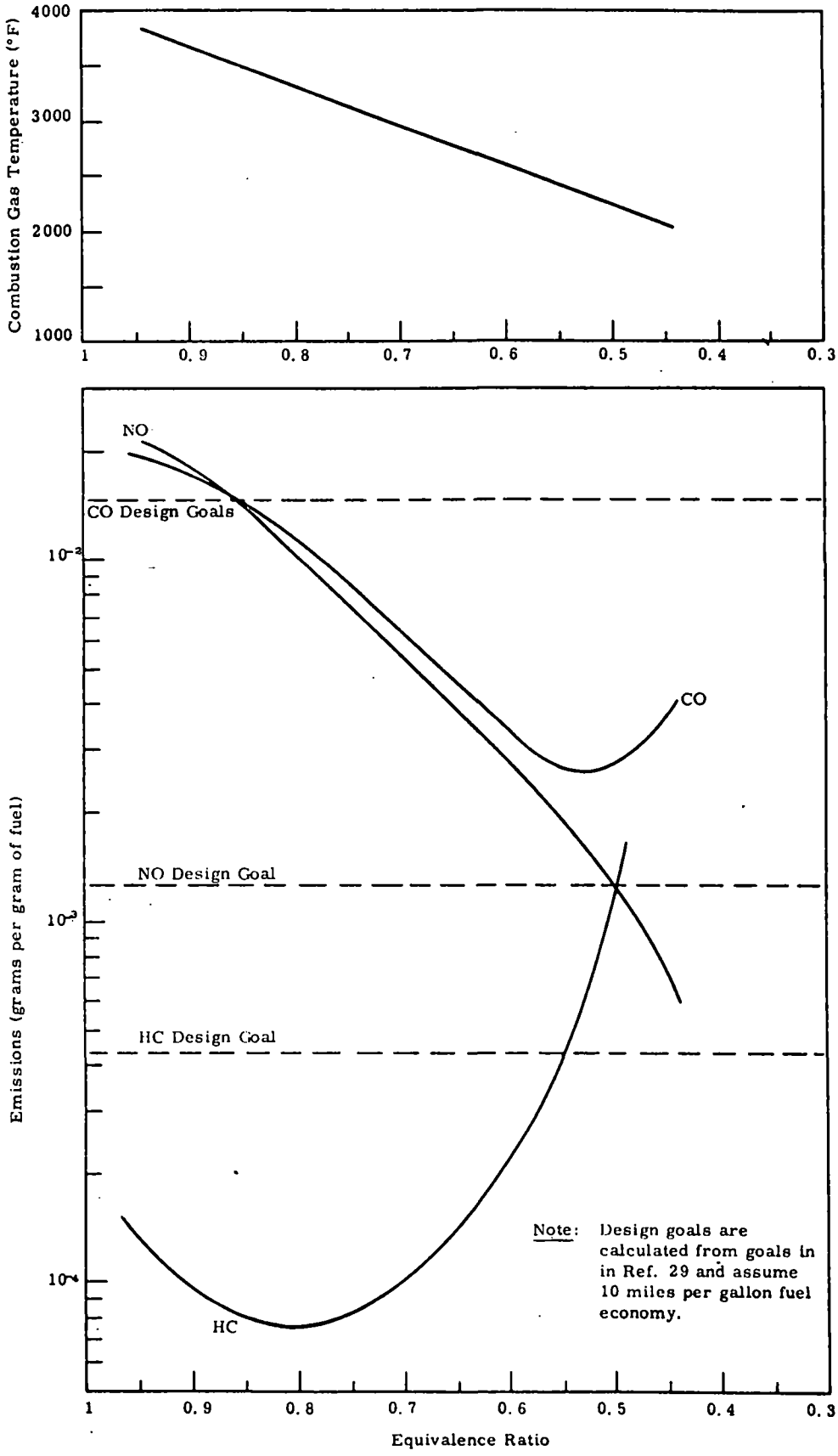

Figure 41. Combustor Model Results

Fuel Air Ratio Transient: A 10% step decrease in fuel/air ratio is applied, with the total flow rate held constant. The results are shown below.

$t = 0^-$	$t = 0^+$	$t = 60$
$\dot{m}_f = 0.0123$ lb/sec	$\dot{m}_f = 0.0111$ lb/sec	$\dot{m}_f = 0.01115$ lb/sec
$\dot{m}_a = 0.2435$ lb/sec	$\dot{m}_a = 0.245$ lb/sec	$\dot{m}_a = 0.245$ lb/sec
$\dot{m}_f/\dot{m}_a = 0.0505$	$\dot{m}_f/\dot{m}_a = 0.0455$	$\dot{m}_f/\dot{m}_a = 0.0455$
$\dot{m}_f + \dot{m}_a = 0.2558$ lb/sec	$\dot{m}_f + \dot{m}_a = 0.2561$ lb/sec	$\dot{m}_f + \dot{m}_a = 0.2561$ lb/sec
$T_o = 85°F$	$T_o = 85°F$	$T_o = 85°F$
$T_a = 129°F$	$T_a = 130°F$	$T_a = 107°F$
$T_f = 3325°F$	$T_f = 3061°F$	$T_f = 3061°F$
$T_s = 125°F$	$T_s = 125°F$	$T_s = 123°F$
$T_t = 260°F$	$T_t = 260°F$	$T_t = 273°F$
$T_g = 3293°F$	$T_g = 3031°F$	$T_g = 3039°F$

The step change in the fuel/air ratio produces an initial instantaneous step change in both flame temperature and inlet air temperature. The air temperature change is instantaneous because of the quasi-steady approximation which neglects the air heat capacity. This is followed by a slow-transient change in T_x, T_t, T_a, T_f, and T_g, as indicated. As can be seen from these results, the change in gas temperature in the 60-second interval is negligible and the dominant effect is caused by the initial step change in flame temperature.

CONTROLS

The controls analyzed here for a reciprocating engine and organic working fluid are the basic configuration defined in the Thermo Electron Corporation report (Reference 1). It is recognized that TECO has significantly changed its control philosophy since this original report; before further analysis, therefore, these changes should be considered in the model. At this stage of the program, no attempt was made to optimize or alter the design, and this phase of the modeling study is concerned strictly with the instantaneous control equations. Later phases are to consider dynamics of the control components.

NOMENCLATURE

Alphabetical Symbols	
A_1 through A_9	Fuel valve diaphragm and bellows effective areas (see Figure 43) $in.^2$
AO	Normalized accelerator pedal position

Alphabetical Symbols (Cont'd)	
C_5	Air/fuel ratio
IR	Cut-off, or intake ratio
K_b	Gain of temperature trim on fuel flow, lb/hr °F
K_E	Engine flow constant, lb/hr rpm
K_P	Pump displacement factor at full stroke lb/hr rpm
Q	Boiler (vapor generator) flow, lb/hr
Q_A	Air flow, lb/hr
Q_E	Engine vapor flow
Q_F	Fuel flow, lb/hr
RPM	Engine speed, rpm
S_P	Normalized pump stroke
T	Boiler (vapor generator) outlet temperature, °F
η_v	Pump volumetric efficiency

CONTROL DEFINITION

Figure 42 is a simplified overall schematic diagram of the control system. Basically, it breaks down into two distinct areas. First is the burner fuel/air control, which serves to control the vapor generator outlet temperature and maintain the fuel/air ratio. The second area comprises the cut-off and feedpump controls. The cut-off control is directly controlled by the driver and sets the power output of the engine. The feedpump control is linked to the cut-off control to provide anticipation and serves to maintain vapor generator output pressure by modulating the feedpump stroke. A third control, not shown in Figure 42, is the condenser fan control, which varies the ratio of the fan drive as a function of engine speed. A more detailed discussion of the control loops accompanies the derivations of the instantaneous equations. (Appendix I of this volume presents the instantaneous control equations for an alternative engine, with a reciprocating expander and steam as the working fluid.)

BURNER CONTROL

The TECO burner control consists of an airflow control and a fuel-flow control valve. The form analyzed here uses a pressure drop across an orifice

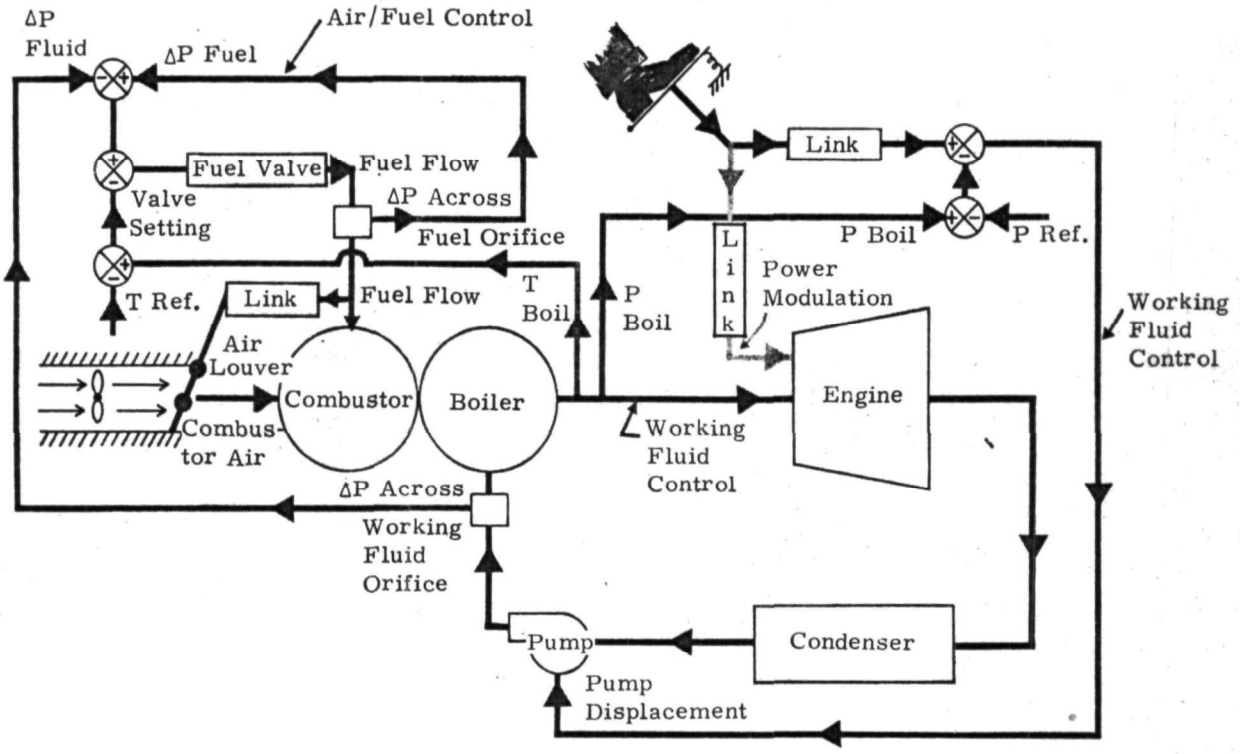

Figure 42. Schematic of Power, Working Fluid, and Air/Fuel Control

in the organic flow line (from the regenerator) to serve as a reference for the fuel valve (see Figure 42). This sets a fuel valve metering area so that fuel flow is roughly proportional to organic flow rate; a quick-acting signal is provided which anticipates the need for a change in fuel flow to compensate for changes in organic flow rate.

Pressure from a temperature sensing bulb in the vaporizer outlet line serves as a slow-acting reset on fuel valve position so that, in effect, the fuel valve maintains a fuel flow rate to hold boiler outlet temperature constant. Figure 43 is a schematic diagram of the fuel valve itself; a separate regulator maintains a relatively constant fuel supply pressure to the valve.

The fuel passing from the fuel valve goes to the fuel nozzle. The back pressure of the fuel nozzle serves as a measure of fuel flow and is the reference for the air valve. Air valve position is maintained as a function of fuel nozzle back pressure in the 1970 TECO design by means of a spring-loaded piston actuator and linkage, as shown in Figure 44. The result is theoretically that airflow is maintained as a direct ratio of fuel flow. This relationship is highly dependent on constant combustor air-blower characteristics and on low friction in the actuator. Recognizing these limitations, TECO has altered the design. The analysis below is based on the original design, but since it implies perfect components with instantaneous response, should yield results similar to an analysis of the more recent system with the same assumptions.

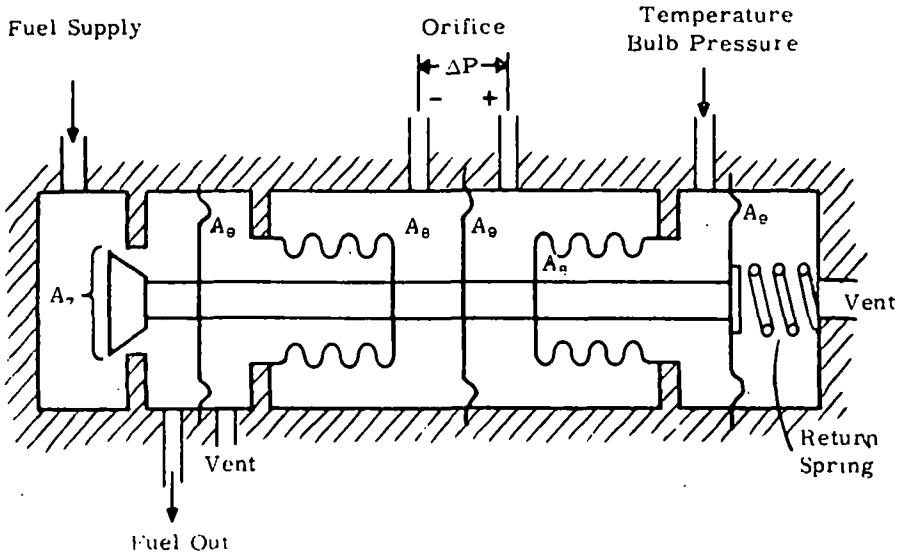

$A_1 = A_2 = A_3 - A_4$

$A_5 = A_3 - A_6$

Figure 43. Fuel Valve -- Simplified Schematic

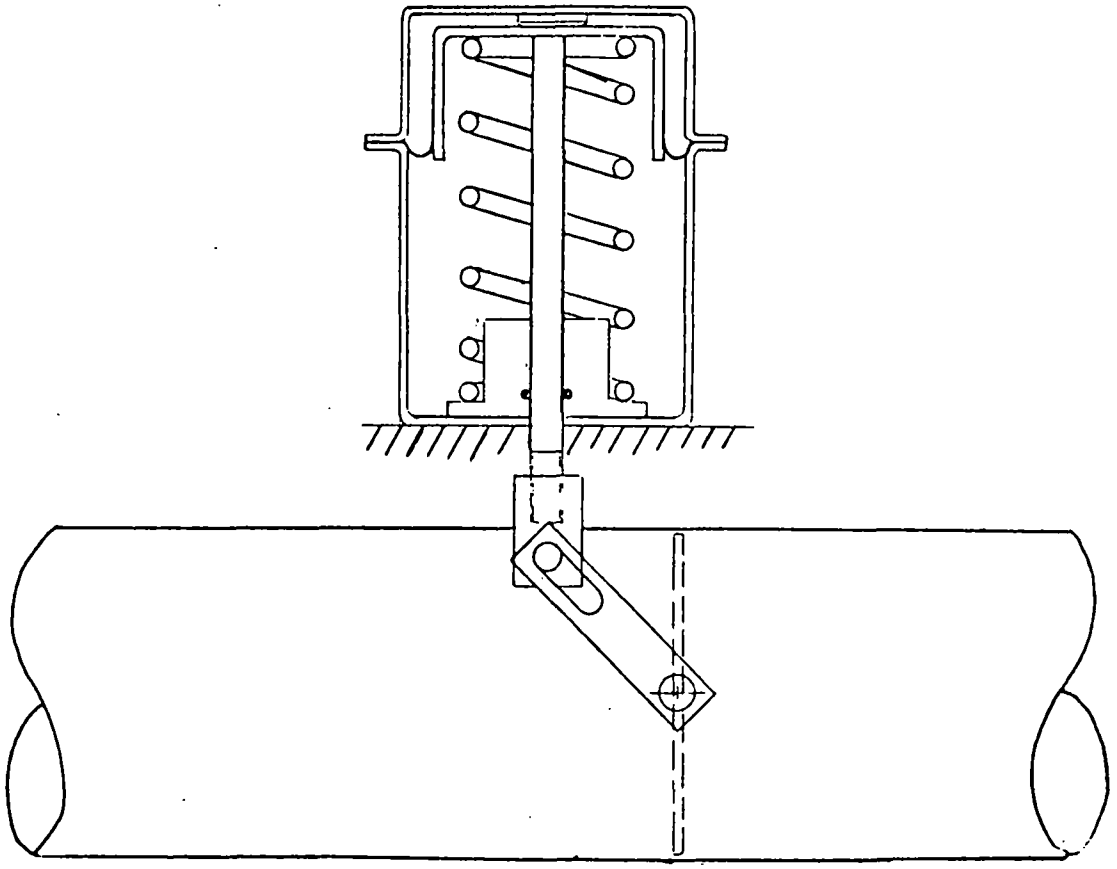

Figure 44. Original Thermo Electron Air Valve

Air Valve

As described above, the air valve is moved as a function of fuel nozzle back pressure by means of a spring-loaded actuator and compensating linkage. The net effect, assuming no friction, constant blower characteristics, and instantaneous response, is to maintain a constant air/fuel ratio, or

$$Q_A = C\,Q_f \tag{120}$$

where $C = 19.8$.

Fuel Valve

The fuel-valve instantaneous equations depend on inputs from the organic-flow sensing orifice, the temperature sensing bulb, the fuel supply pressure, and the fuel nozzle back pressure. Figure 43 shows the fuel valve configuration; Figure 45 is the interacting block diagram showing the instantaneous relationship of the fuel valve position to the above parameters.

The relationship implies negligible mass and damping of the moving parts and neglects inertance and compressibility of the fuel and the organic fluid. It also assumes a negligible time constant of the temperature sensing bulb. These dynamic terms must, of course, be accounted for in the next phase of the analysis but are neglected at this point.

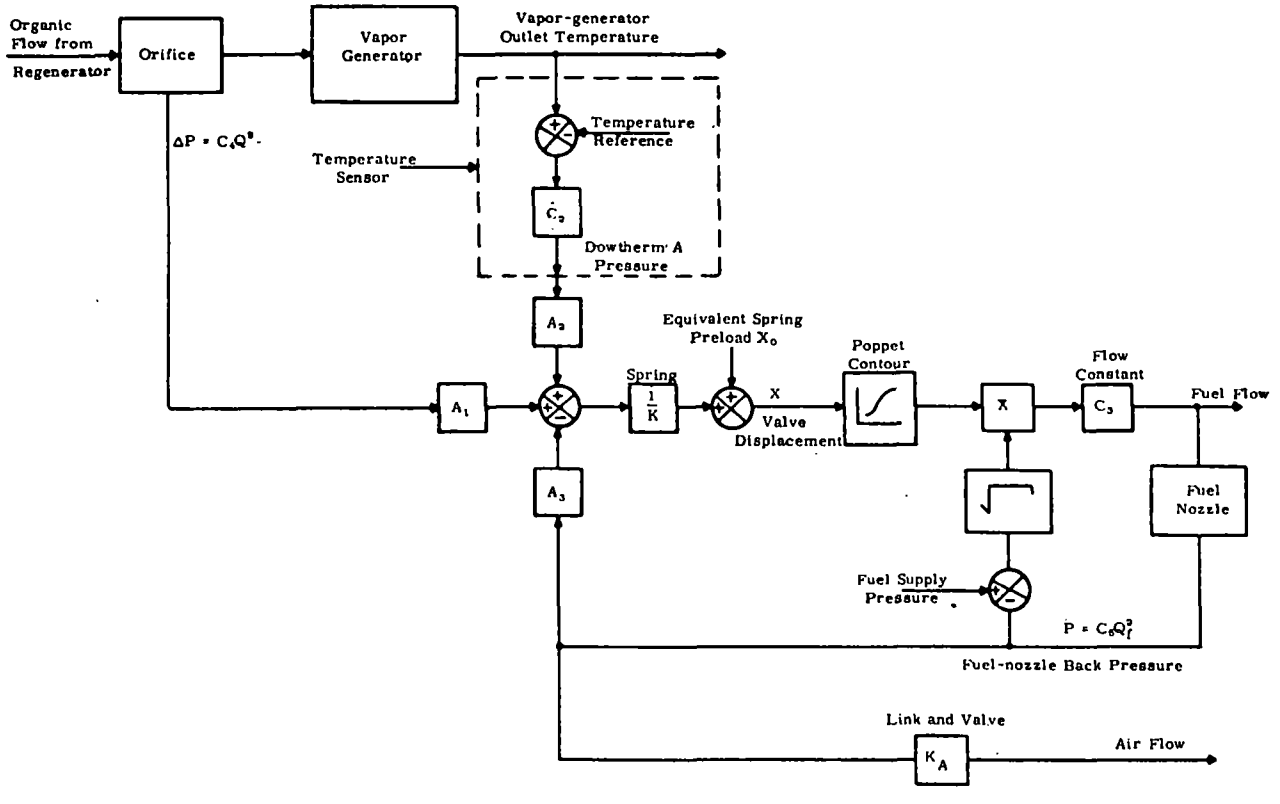

Figure 45. Burner Control -- Block Diagram

Thermo Electron has made provision for a contoured metering poppet in the fuel valve in order to linearize the relationship between fuel flow and organic flow. The relationships of Figure 45 were solved by an iterative computer solution to determine the fuel flow as a function of vapor temperature and organic flow rate. Areas used were supplied by the Thermo Electron Corporation, and the characteristics of Dowtherm A® fluid were used in establishing the temperature bulb pressure. The result is shown in Figure 46, where the valve characteristic of fuel flow versus organic flow is indeed linear at the outlet temperature of 550°F for the design vapor generator. As the temperature deviates from 500°F, the characteristic loses its linearity.

A model incorporating an exact solution must continuously solve the equations represented by the block diagram of Figure 45. This will be expensive in terms of computer time, since it will involve algebraic loops. For this first cut at the analysis, it was decided to develop a simpler model, which approximates the characteristics of Figure 46. This was done by considering that the normal operation will be at 550°F organic temperature and that deviations from this temperature will not be overly large. With that assumption, the fuel flow could be characterized by the equation

$$Q_F = 0.01208\, Q + K_b\, [T - 550] \qquad (121)$$

where, by inspection of Figure 46, it can be seen that K_b, the sensitivity of flow to vapor generator temperature, will vary as a function of vapor-generator flow rate.

K_b was determined by first cross-plotting the curves of Figure 46 into the format of Figure 47 and finding the slope of the resulting Q_f versus T lines at the 550°F point. The resulting values of K_b are plotted in Figure 48 as a function of organic flow rate Q. A curve fit of Figure 48 shows that it can be characterized to better than 2% accuracy by the equation

$$K_b = -8.1344 + 3.5389 \times 10^{-3}\, Q - 7.7945 \times 10^{-7}\, Q^2 + 8.6304 \times 10^{-11}\, Q^3 - 3.7709 \times 10^{-15}\, Q^4 \qquad (122)$$

Q_F = Fuel flow, lb/hr

Q = Organic flow, lb/hr

T = Vapor-generator outlet temperature, °F

In addition, the following absolute limits are provided by the control

$$\text{MAX } Q_F = 47.02 \text{ lb/hr} \qquad (123)$$

$$\text{MIN } Q_F = 4.851 \text{ lb/hr} \qquad (124)$$

®Registered trademark of the Dow Chemical Company

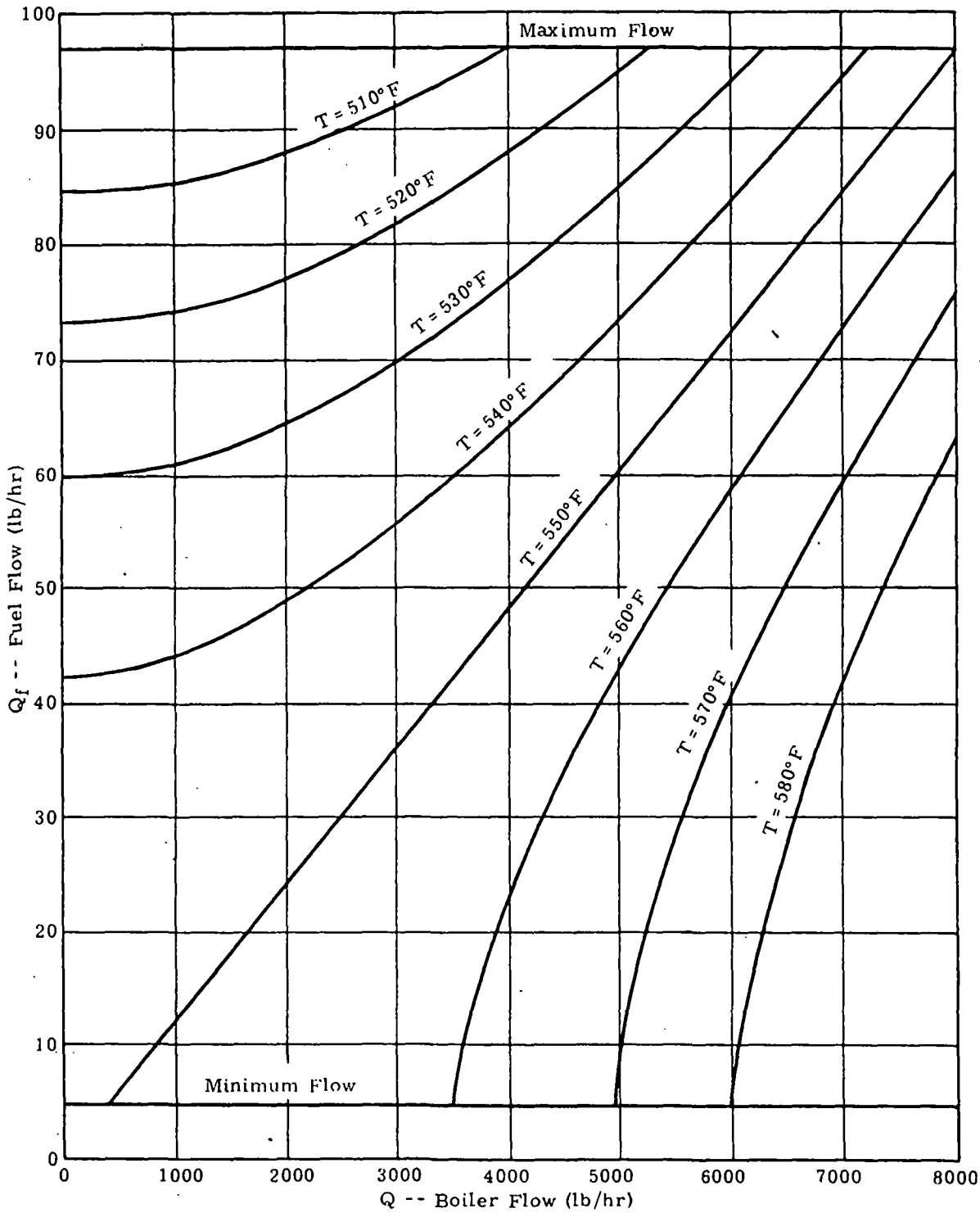

Figure 46. Fuel Flow Versus Boiler Flow -- CP-34 System; Contoured Poppet

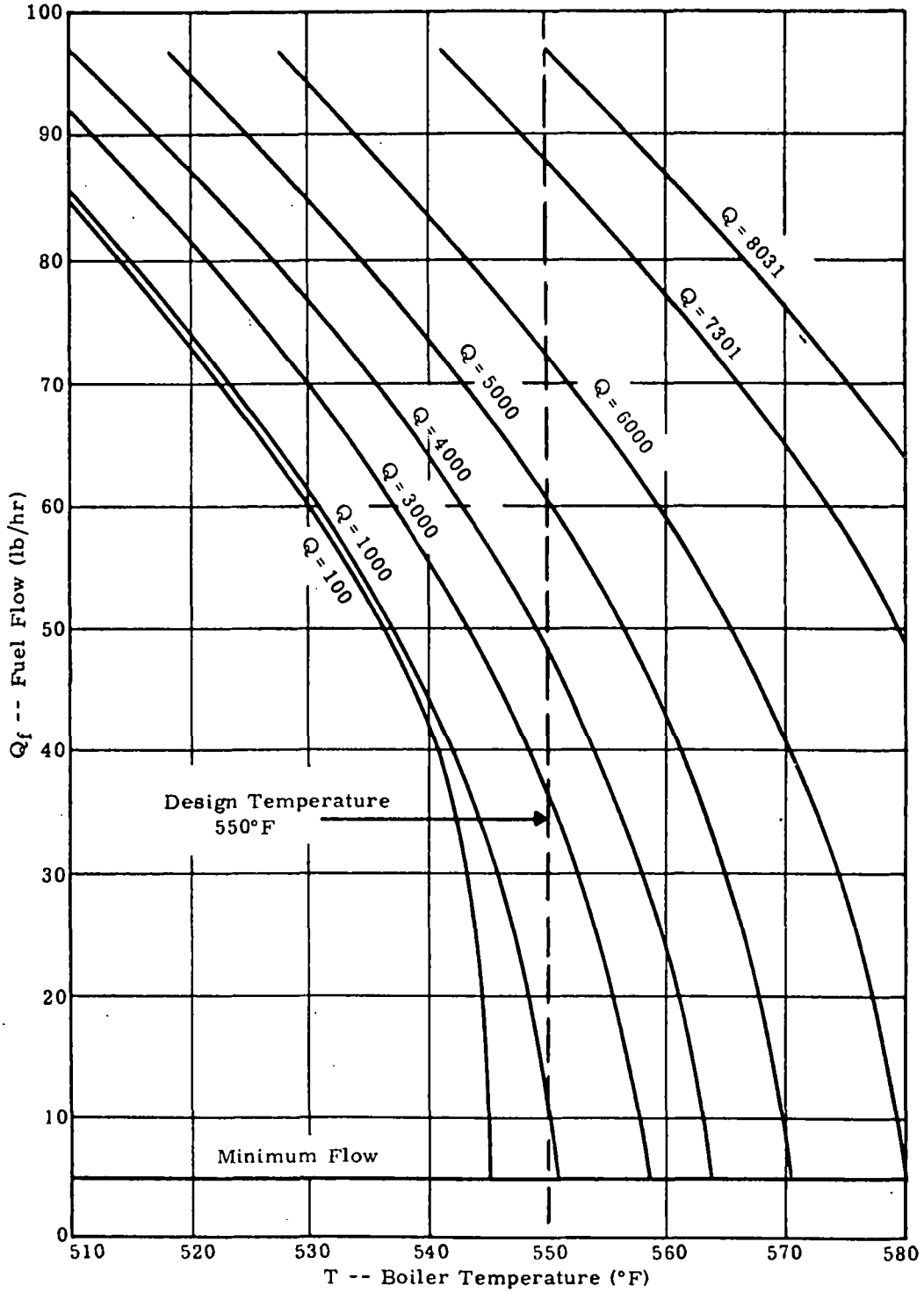

Figure 47. Fuel Flow Versus Boiler Temperature -- CP-34 System; Contoured Poppet

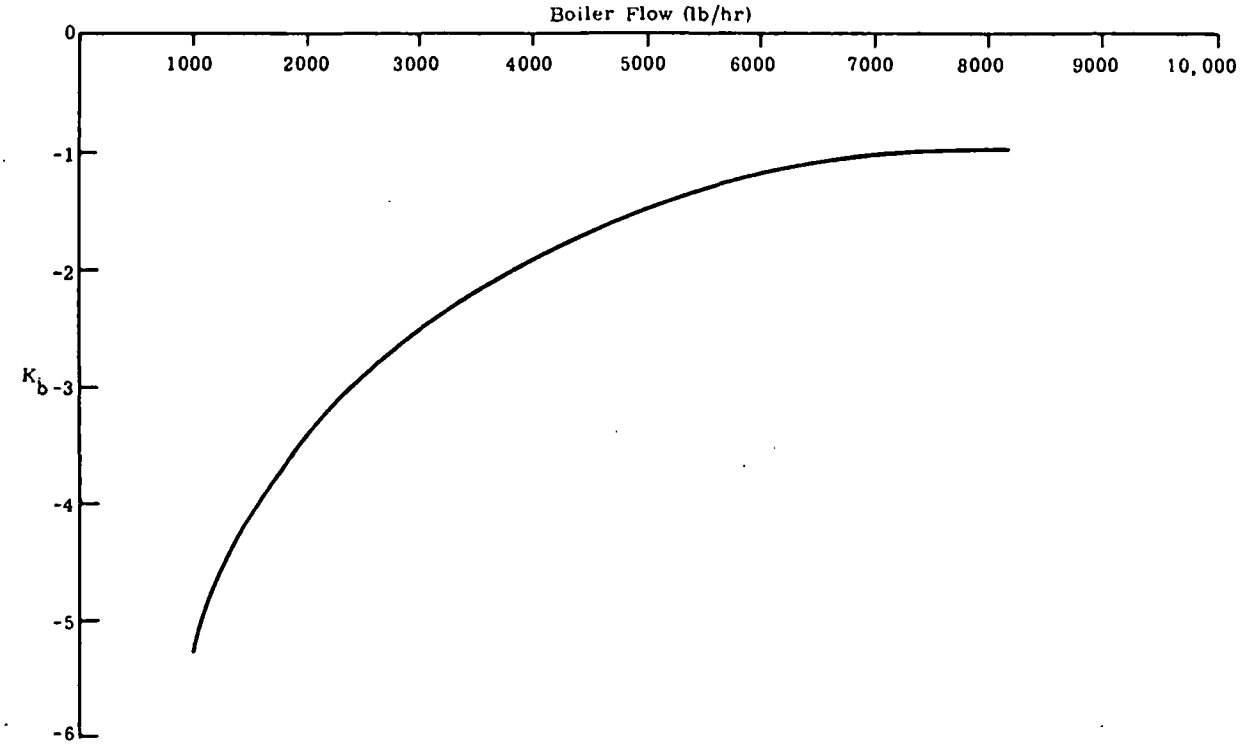

Figure 48. Slope of Q_f Versus Temperature Curve at Design Temperature (550°F) -- CP-34 System; Contoured Poppet

CUT-OFF AND FEEDPUMP CONTROL

The cut-off will be varied directly as a function of driver demand, with provision for a minimum cut-off limit to maintain idle speed under variable accessory load and a maximum cut-off to assure that flow demand does not exceed boiler capacity. The feedpump is a variable-stroke positive-displacement pump running at a fixed ratio to engine speed in normal operation and is linked directly to the valve cut-off, as will be explained below. A pressure bias is applied on the feedpump stroke control so that the feedpump control basically maintains boiler pressure. The simplified block diagram for the cut-off and feedpump control is given in Figure 49.

Cut-off Control

TECO limits the maximum intake ratio, or cut-off, to 0.29 for several reasons, feedpump size limits being probably the most overriding. For this reason, a fixed maximum of 0.29 is set; it is presumed this will occur when the driver input (accelerator pedal position) is at full scale (AO = 1). Therefore,

$$IR = 0.29\,(AO) \tag{125}$$

However, it is necessary to place a maximum limit on engine flow demand in order that it not normally exceed boiler capacity. The design flow of the

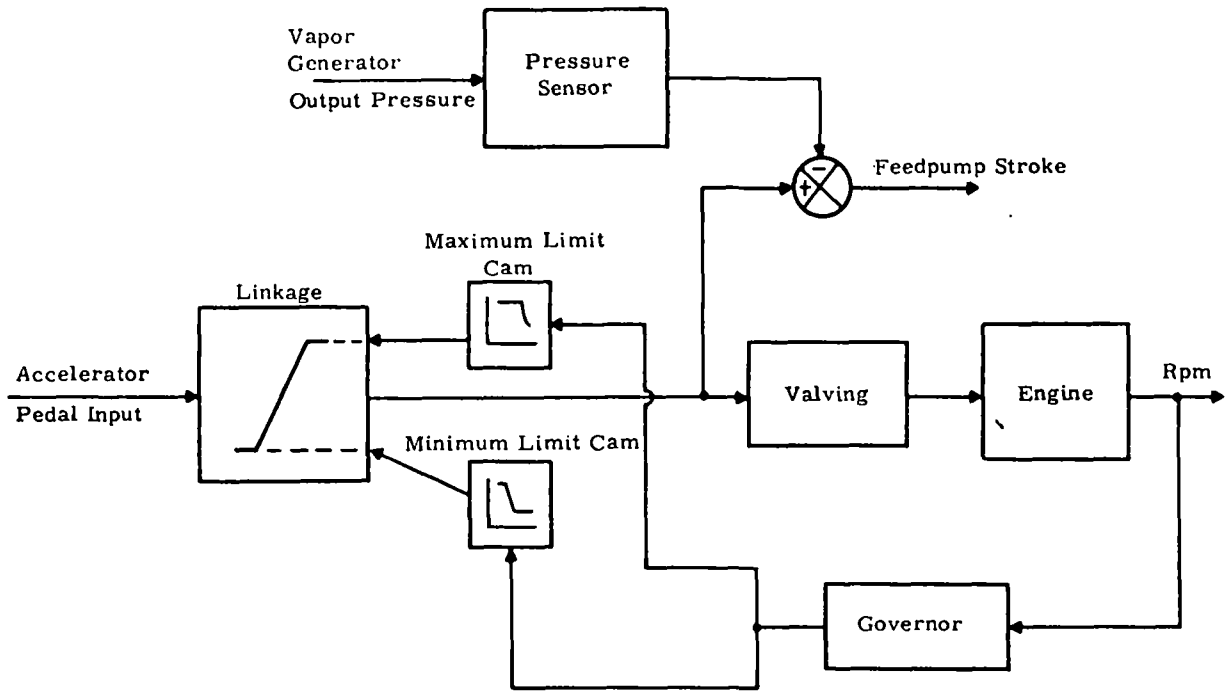

Figure 49. Engine Power Level and Vapor Generator Feedpump Control -- Functional Block Diagram

boiler is 7301 pounds per hour, this flow occurring at a cut-off of 0.137 and 2000 rpm engine speed. Since engine flow is approximately

$$Q_E \approx K_E \cdot RPM \cdot IR \tag{126}$$

it follows that K_E = 26.647 lb/hr rpm and, to maintain maximum engine flow constant,

$$IR_{MAX} = \frac{Q_{E\ design}}{K_E \cdot RPM} = \frac{274}{RPM} \tag{127}$$

It can be seen that IR of Equation 120 reaches the maximum level of 0.29 at 944.83 rpm. The maximum cut-off limit can thus be defined as

$$MAX\ IR = 0.29 \text{ for } RPM \leq 944.83 \tag{128}$$

$$= \frac{274}{RPM} \text{ for } RPM > 944.83 \tag{129}$$

The minimum cut-off must be maintained to hold an idle speed high enough to drive accessories under a wide range of accessory loads. The nominal idle speed will be 300 rpm, and it will be assumed that a 5% droop control will be maintained. In other words, a 5% drop in speed below 300 rpm would be enough to increase cut-off from zero to the maximum limit of 0.29. In equation form this works out to

$$\text{MIN IR} = 0.29 \text{ for RPM} < 285 \tag{130}$$

$$= 0.01933\,(300\text{-RPM}) \text{ for } 285 < \text{RPM} < 300 \tag{131}$$

$$= 0 \text{ for RPM} > 300 \tag{132}$$

The minimum limit of zero for speeds above 300 rpm may be modified in later models, since system requirements may demand at least a very small minimum flow under most conditions.

Pump Stroke Control

The pump stroke is varied in order to maintain vapor generator output pressure in the TECO design. This is done by two inputs. The first input is from the cut-off control and roughly holds pump flow equal to engine demand flow.

This can best be understood by comparing the engine and pump flow equations. The pump flow can be described as

$$Q_P = K_P \cdot \text{RPM} \cdot S_P \cdot \eta_v \tag{133}$$

where

K_P = Pump displacement factor at full stroke, based on engine speed, lb/hr-rpm

RPM = Engine speed in revolutions per minute

S_P = Pump stroke (unitless) where $S_P = 1$ = full displacement

η_v = Volumetric efficiency

Referring back to Equation 126,

$$Q_E \approx K_E \cdot \text{RPM} \cdot \text{IR} \tag{126}$$

To maintain pressure equilibrium, the pump flow must equal the engine flow. Equating flows of Equations 126 and 133,

$$K_E \cdot \text{RPM} \cdot \text{IR} \approx K_P \cdot \text{RPM} \cdot S_P \eta_v$$

and, solving for pump stroke,

$$S_P \approx \frac{K_E}{K_P \eta_v} \cdot \text{IR} \approx \text{Constant} \cdot \text{IR} \tag{134}$$

Volumetric efficiency decreases with pump speed. This implies that the ratio $K_E/K_P \eta_v$ must be determined for the most demanding condition on the pump from the standpoint of speed and stroke. The pump will be at full stroke when cut-off is maximum, the highest speed at maximum cut-off being 944.83 rpm. The constant relating cut-off to pump stroke is 3.448.

The pressure trim on the pump stroke assures a pressure control and compensates for variations in pump and engine efficiencies which are not accounted for in Equation 134. Here a 5% pressure droop control will be used. A decrease of 5% from set point pressure of 500 psi will cause the pump to go from zero to full stroke. To maintain a 500-psig vapor generator output pressure at design point flow and pump speed will require a pressure set point of 501.25 psi, based on a volumetric efficiency of

$$\eta_v = 1 - 0.05 \left| \frac{RPM}{600} \right| \tag{135}$$

The resulting instantaneous pump stroke equation is

$$S_P = 3.448\ (IR) - \left| \frac{P_b - 501.25}{25} \right| \tag{136}$$

CONDENSER FAN EQUATIONS

The condenser fan will be engine-driven and clutched between different speed ratios as a function of engine speed in order to provide sufficient cooling air at minimum power penalty. Equations supplied by TECO are

$$N_f = 3 \times RPM \text{ for } 0 < RPM < 800 \tag{137}$$

$$N_f = 2 \times RPM \text{ for } 800 < RPM < 1400 \tag{138}$$

$$N_f = 1 \times RPM \text{ for } RPM > 1400 \tag{139}$$

where

N_f = Fan speed, rpm

RPM = Engine speed, rpm

DISCUSSION AND RECOMMENDATIONS

The control modeling reported here is almost the simplest possible, in that it totally neglects the dynamics of the control elements. Yet, considering the fact that most of the control elements will react in fractions of a second compared to many seconds response time for most of the systems elements, this assumption is not unreasonable for a first cut at system modeling.

Modeling of the entire system using the instantaneous control model will give a valuable insight into overall system response and will immediately point up deficiencies in both control mode and component sizing. In fact, the one significant lag to be expected in the control as it now stands is the time lag of the freon-filled temperature sensing bulb used to sense boiler outlet temperature. These bulbs frequently have equivalent time constants of several seconds, and this lag should be incorporated into the model as soon as tests or analyses can be performed to determine its magnitude.

As the system model is run through transients, the need for additional compensating dynamics in the control system may become apparent. One area of concern involves the dynamic effects in the vapor generator during transients. It is entirely possible that an initial increase in flow could conceivably produce an initial decrease in pressure and a longer-term increase. A simple pressure control could be driven into instability (either sustained oscillations or a "hard over" condition) by such a situation.

In the event that the feedpump control were to react in this manner on the system model, two possible cures immediately come to mind. The first would be to provide limited authority to the pressure trim. The implications of this on system safety would, of course, have to be considered at the same time. The second approach would be to consider dynamic compensation (dashpot, etc.) of the pressure trim, or else provision for dynamic compensation in the link between the cut-off valve and the feedpump stroke. The point to be observed here is that the present system model is complete enough to show up such potential problems and will allow realistic testing of the possible cures.

A useful tool in synthesizing controls will also be parametric models of the system components. These will be simplified models whose dynamics will be empirically matched to those of the more complete model. The parametric models will undoubtedly have to be altered for different operating points, but will offer the advantage of reductions in computer time plus the capability of closed-form analytical representation where possible. The latter will be valuable in providing analytical insight into the control problems and will help to avoid the "cut and try" approach.

Using parametric models, the detailed control dynamics can be investigated at reasonable cost. Here the individual loops can be checked out analytically first, for stability and then response. Following that, the complete system can be checked for interaction effects due to control dynamics, using the parametric models. A subsequent check of the controls with dynamics on the complete detailed model would then be desirable.

The scope of this program did not permit consideration of alternate controls or different mechanization of the TECO control system. However, the general TECO control concept appears attractive in that it attempts to maintain quasi-steady-state conditions during transients, thereby avoiding major unbalances and upsets. Linking the feedpump stroke to valve cut-off is a form of feed-forward that should make a much tighter pressure loop than a straight pressure feedback control. Tying fuel flow to organic flow is also desirable because of the long time constants to be expected in the temperature sensing bulb.

The air/fuel mixture control will require additional design to assure adequate control over expected operating and ambient ranges. It might be desirable to control the air rather than the fuel and link the fuel flow to the

air flow. Since the control of the combustor is crucial to emissions of the engine, future modeling should be focused on this area to assure low emissions during both steady-state and transient operation.

Section 4

VEHICLE SYSTEM

In order to simulate propulsion system dynamics during transients that occur in realistic driving situations the following vehicle-system models were prepared.

- Transmission
- Vehicle
- Route
- Driver

Figure 50 shows the linkage of these models with the expander model. In summary, the expander torque is conveyed through the transmission to the vehicle wheels, where it acts to overcome motion resistance and accelerate the vehicle. The speed change is conveyed back through the transmission to the expander. The driver model senses the vehicle speed, location, and acceleration, compares them to reference values provided by the route-mission profile, and makes an appropriate correction to the accelerator pedal setting. This correction is transmitted through the controls to the propulsion system. This section describes the vehicle system models.

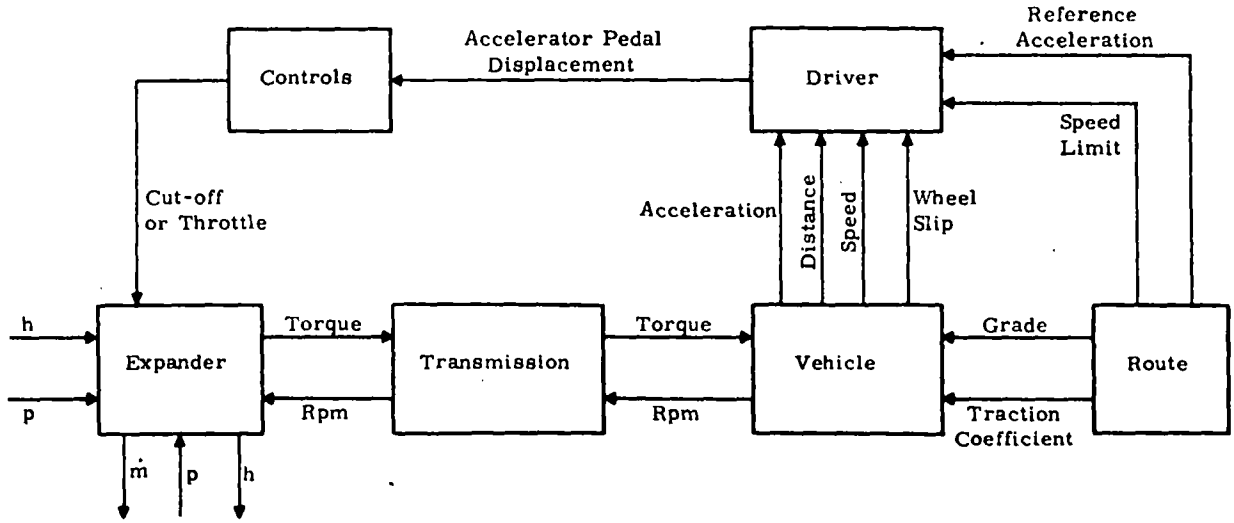

Figure 50. Engine Information Signal Loop

TRANSMISSION

NOMENCLATURE

HP_ℓ	Power required for driving auxiliaries and overcoming drive train losses

Alphabetical Symbols (Cont'd)

J_e	Engine torque
J_x	Axle torque
J_ℓ	Torque for driving auxiliaries and overcoming drive train losses
r	Gear ratio
$R_{1\ell}$, R_{1u}, $R_{2\ell}$, R_{2u}	Cut-off points 1u, 1ℓ, 2u, 2ℓ in Figure 51
RPM_e	Engine rpm
RPM_x	Axle rpm
$RPM_{1\ell}$, RPM_{1u}, $RPM_{2\ell}$, RPM_{2u}	Axle rpm at points 1u, 1ℓ, 2u, 2ℓ in Figure 51

DERIVATION

The basic equations for the transmission model are:

$$RPM_e = r\,(RPM_x) \tag{140}$$

$$J_x = r\,(J_e - J_\ell) \tag{141}$$

$$J_\ell = HP_\ell / RPM_x \tag{142}$$

MODEL DEVELOPMENT

The transmission model is entitled TRANSM and is listed in Volume II of this report. The specific model has been developed for a transmission designed for the Thermo Electron Corporation (TECO) engine. Figure 51 shows the gear-shift sequence as a function of cut-off and RPM. There are three distinct regions.

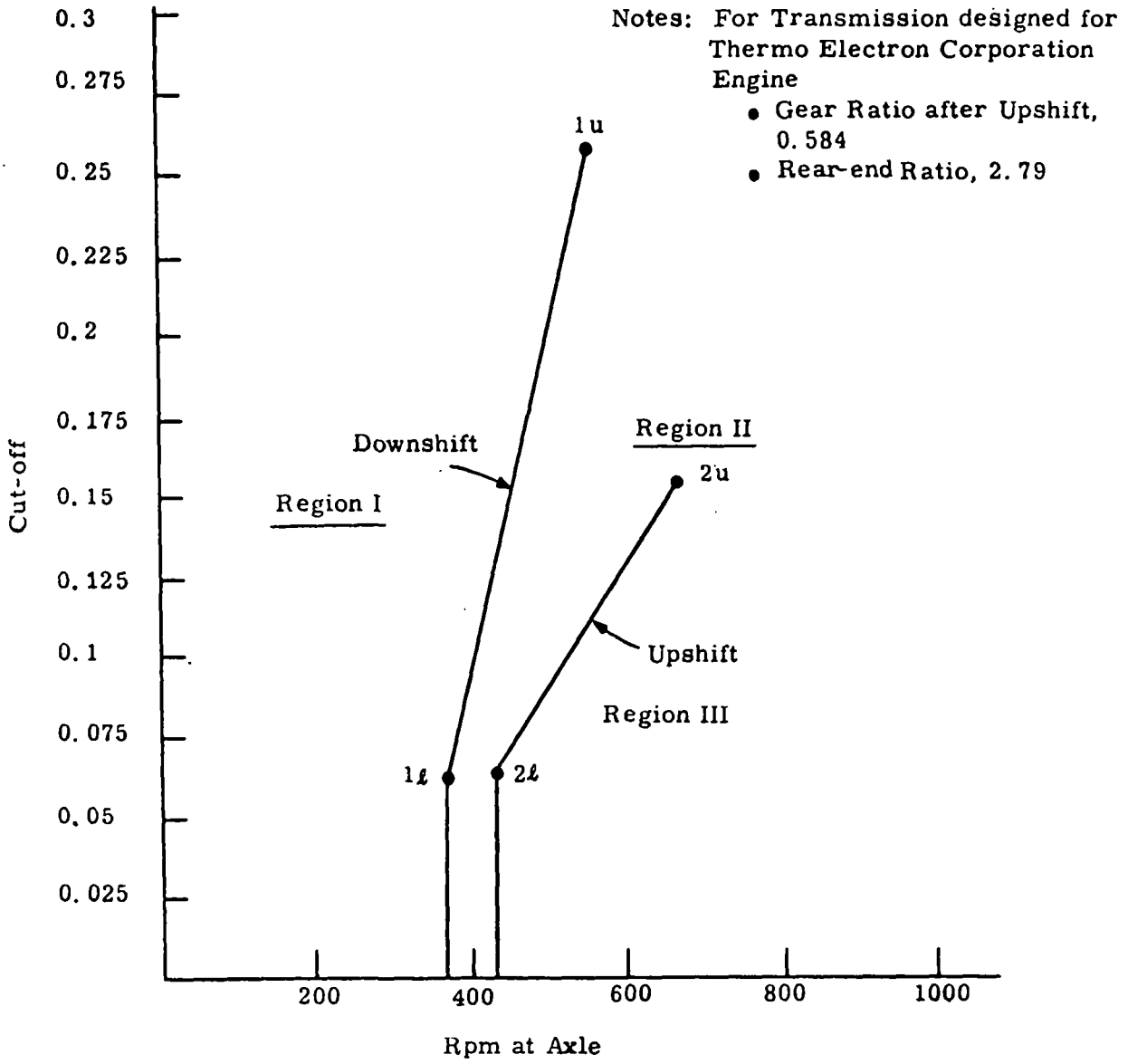

Figure 51. Transmission Gear-shift Sequence

- In Region I the gear ratio is 1.
- The ratio remains 1 as the vehicle accelerates through Region II to the upshift.
- In Region III the gear ratio is 0.584 and remains 0.584 as the vehicle decelerates through Region II to the downshift.
- There is also a rear-end ratio of 2.79; therefore, the overall ratio is the product of two values.

The power required for the transmission depends on speed and load, and in most cases is very small. The maximum power requirement observed in

the transmission data was approximately 3 hp. For simplicity, this maximum power penalty was employed over the entire range. Therefore, $HP_\ell = 3$ hp.

The input to the model is r, RPM_x, and J_e, while the output is RPM_e and J_x.

The upshift and downshift lines are automatically determined when r and RPM_x are supplied at points 1u, 1ℓ, 2u, 2ℓ (see Figure 51). In this instance,

$$R_{1\ell} = 0.065$$
$$R_{1u} = 0.26$$
$$R_{2\ell} = 0.065$$
$$R_{2u} = 0.155$$
$$RPM_{1\ell} = 370$$
$$RPM_{1u} = 550$$
$$RPM_{2\ell} = 430$$
$$RPM_{2u} = 660$$

RESULTS

The main point to be checked out in this model is the correct handling of the upshifts and downshifts. Two cases were run, one case at r = 0.035 and the other case at r = 0.15, both cases with increase and then decrease in axle speed. The results are summarized below.

Case 1: r = 0.035, J_e = 1000

	Input	Output	
	RPM_x	RPM_e	J_x
Initial	200	558	2790
	400	1116	2790
After Upshift	600	977	1629
	400	651	1629
After Downshift	200	558	2790

Case 2: $r = 0.15$, $J_e = 1000$

	Input	Output	
	RPM_x	RPM_e	J_x
Initial	200	558	2790
	500	1395	2790
After Upshift	700	1140	1629
	500	815	1629
After Downshift	200	558	2790

VEHICLE

NOMENCLATURE

Alphabetical Symbols	
A	Acceleration
A_f	Frontal area
C_d	Aerodynamic drag coefficient based on frontal area
D	Drag
D_a	Aerodynamic drag
D_g	Grade drag
D_m	Rolling and mechanical resistance
F	Tractive effort
F_m	Tractive limit
G	Grade %
J_x	Torque at axle
K_f	Traction coefficient
M	Rotational inertia
R_w	Wheel radius
V	Vehicle velocity
W	Weight of vehicle
W_n	Normal force on road

Greek Symbols

α	Rotational acceleration
ρ	Air density

DERIVATION OF BASIC EQUATIONS

The basic equation describing vehicle motion is Newton's Law:

$$A = \frac{F - D}{W} \tag{143}$$

Motion Resistance

The motion resistance is made up of aerodynamic drag, rolling and mechanical resistance, and grade drag:

$$D = D_a + D_m + D_g \tag{144}$$

The aerodynamic drag is

$$D_a = 1/2\ \rho\ V^2\ C_d\ A_f \tag{145}$$

The rolling resistance is calculated by the method specified in Reference 29.

$$D_m = \frac{W}{65}\left(1 + 1.410^{-3}\,V + 1.2110^{-5}\,(V)^2\right. \tag{146}$$

where

D_m is in pounds

W is in pounds

V is in feet per second

The grade resistance is calculated as

$$D_g = W \sin\left(\arctan\ 0.01\ G\right) \tag{147}$$

Tractive Effort

The torque applied at the rear axle must accelerate the vehicle and all the rotating parts (drive train, transmission, and expander). Therefore the tractive effort available is

$$F = \frac{J_x}{R_w} - \frac{M\alpha}{R_w} \tag{148}$$

The maximum tractive effort that can be applied (or the tractive limit) is

$$F_m = K_f W_n \tag{149}$$

where

$$W_n = W \cos \left(\arctan \left(0.01\ G \right) \right) \tag{150}$$

If F is greater than F_m, the wheels will break away from the road surface and start to slip. This is an important consideration for vapor engines because the starting torques can be high. If the wheels are slipping they accelerate at

$$\alpha = \frac{J_x - F_m R_w}{M} \tag{151}$$

If the wheels are not slipping:

$$\alpha = \frac{A}{R_w} \tag{152}$$

F is always less than or equal to F_m.

In both cases (wheel slip and no wheel slip) the linear and rotational accelerations are integrated to determine the vehicle and rotational velocities. The vehicle velocity, in turn, is integrated to determine the vehicle position.

MODEL DEVELOPMENT

The equations for vehicle motion are included in the total system model MAINSYS, listed in Volume II of this report.

The following input data are specified by the user:

$$C_d,\ A_f,\ R_w,\ M,\ W$$

The grade G and friction coefficient K_f are provided from the route profile. The acceleration A, velocity V, and vehicle position are transmitted to the driver model along with the peripheral velocity, to check for wheel slip.

ROUTE

MODEL DEVELOPMENT

The route mission profile has been prepared as a data file, entitled ROUTE, which is read by the total system model, MAINSYS. Each line of the data file indicates:

1. The next marker location (LR)
2. The grade (G)

3. Idle time (TI)
4. Reference acceleration (AR)
5. Reference velocity (speed limit) (VR)
6. Traction coefficient (KF)
7. A logic variable, to tell the driver whether to accelerate (CR = +1), decelerate (CR = -1), or cruise (CR = 0).

The driver model compares the vehicle performance with the route reference conditions and adjusts the accelerator pedal accordingly. A new line of route data is read whenever the vehicle velocity reaches the speed limit, the idle time is exceeded, or the vehicle reaches the next marker location.

The data file ROUTE, which is listed in Volume II, is repeated here in Table 10. The route profile corresponding to Table 10 is plotted in Figure 52 and includes:

1. Initial idle
2. Acceleration to 60 mph in 13.5 seconds
3. Acceleration in merging traffic
4. Cruise at various speeds
5. High-speed pass maneuver
6. Acceleration on a 5% grade

This route mission profile allows testings of some of the important vehicle performance goals in Reference 29.

It should be noted that the route profile is a forcing function but that the vehicle might not meet the required or designated performance level. That would depend upon the capability of the propulsion system.

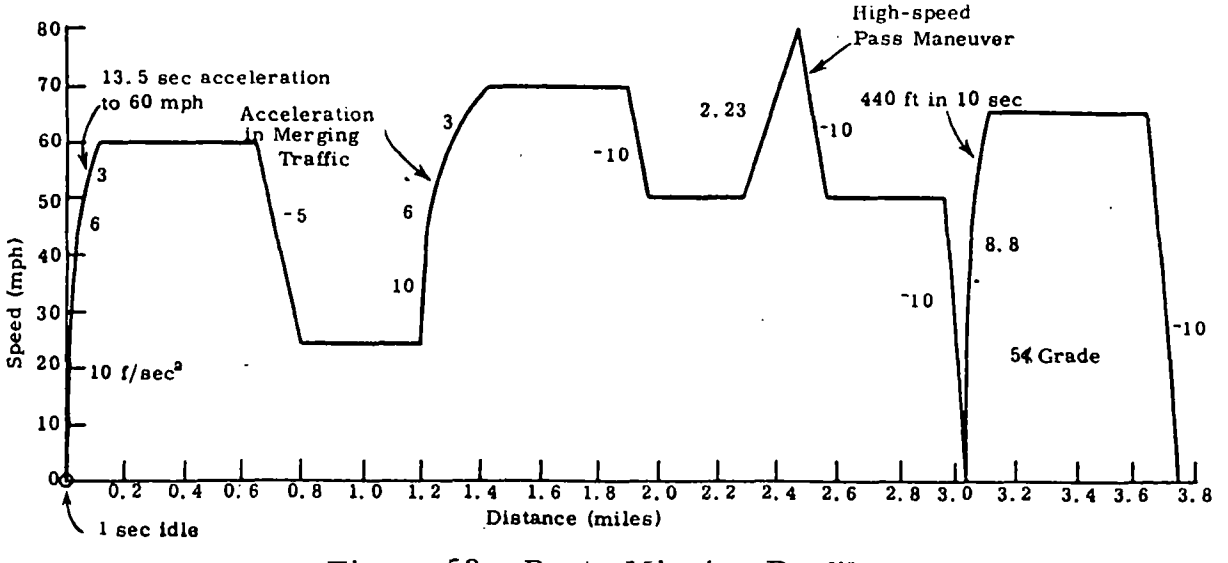

Figure 52. Route Mission Profiles

Table 10

ROUTE MISSION PROFILE

LR (miles)	G	TI (sec)	AR (ft/sec^2)	VR (mph)	KF	CR
0.65	0	1	0	0	0.5	0
0.65	0	0	10	40	0.5	1
0.65	0	0	6	50	0.5	1
0.65	0	0	3	60	0.5	1
0.65	0	0	3	60	0.5	0
1.2	0	0	-5	25	0.5	-1
1.2	0	0	3	25	0.5	0
1.93	0	0	10	40	0.5	1
1.93	0	0	6	50	0.5	1
1.93	0	0	3	70	0.5	1
1.93	0	0	3	70	0.5	0
2.3	0	0	-10	50	0.5	-1
2.3	0	0	3	50	0.5	0
2.98	0	0	2.23	80	0.5	1
2.90	0	0	-10	50	0.5	-1
2.98	0	0	3	50	0.5	0
3.65	0	0	-10	0	0.5	-1
3.65	0	0	8.8	65	0.5	1
3.65	0.05	0	3	65	0.5	0
3.65	0.05	0	-10	0	0.5	-1

DRIVER

NOMENCLATURE

Alphabetical Symbols

A_f	Frontal area
AR	Reference acceleration
AS	Accelerator setting

Alphabetical Symbols (Cont'd)

C	Torque-accelerator constant for "linear engine"
C_d	Drag coefficient based on frontal area
CR	Logic variable -- acceleration (CR = +1), cruise (CR = 0), deceleration (CR = -1)
G	Grade
J_x	Axle torque
K_f	Traction coefficient
KA	Accelerator sensitivity
LR	Next marker location
M	Rotational inertia
R_w	Wheel radius
TI	Idle time
VR	Reference velocity
W	Vehicle weight

DEVELOPMENT OF MODEL

The driver model is entitled DRIVER and is listed in Volume II of this report. The driver model closes the loop between the vehicle, propulsion system, and route. The driver receives the following information signals:

1. Maximum idle time and elapsed idle time
2. Vehicle position and the next marker location
3. Vehicle velocity and reference velocity (speed limit)
4. Vehicle acceleration and reference acceleration
5. Wheel-slip signal

After analyzing this information, the driver model regulates either the accelerator setting or the deceleration rate. If the elapsed idle time is less than the maximum idle time, the accelerator setting is maintained at zero. If the vehicle has not yet reached the next marker location, the driver attempts to follow the current acceleration and speed limit instructions. When the vehicle reaches the next marker location, a new set of instructions are relayed to the driver.

The acceleration and speed-limit instructions are obeyed as follows. A logic variable tells the driver whether he is supposed to be accelerating,

cruising, or decelerating. If the vehicle is to accelerate, the driver attempts to reach the speed limit by adjusting the accelerator setting according to the following schedule:

$$AS = ASO + KA\,(AR - A) \tag{153}$$

where

AS = New accelerator setting

ASO = Previous accelerator setting

KA = Accelerator sensitivity

AR = Reference acceleration

A = Vehicle acceleration

If the vehicle is to cruise at the speed limit but the instantaneous velocity is less than the speed limit, the driver adjusts the accelerator setting according to Equation 153. If the vehicle velocity is greater than the speed limit, the accelerator setting is adjusted by

$$AS = ASO + KA\,(-A - AR), \tag{154}$$

and if the vehicle velocity is equivalent to the speed limit, the setting is adjusted by

$$AS = ASO + KA(-A) \tag{155}$$

If the vehicle is to decelerate, the driver sets the deceleration rate equal to the reference acceleration, AR. There is no brake-force model. It is assumed that the vehicle can decelerate at any selected rate.

All of the above considerations are superseded if the wheels are slipping. In this instance, the driver model has two options. It can either hold the accelerator setting constant or reduce it to zero. In each instance the acceleration sensitivity, KA, is decreased so that the chances of future wheel slips are reduced.

It is felt that the above driver model presents a reasonable approximation to the actual behavior of a human driver and will permit the various propulsion systems to be evaluated and compared in a consistent manner.

RESULTS

The driver, vehicle, and route models were linked together and test cases were run. The purpose of these tests was to determine if the linkages, logic, and programming were correct.

An imaginary "linear engine" was used to provide the torque for acceleration according to the schedule:

$$J_x = C\,AS$$

If the C is large the torque will be high and wheel slip will occur. Two cases were run to investigate

- Vehicle route traverse
- Wheel-slip conditions

Case 1: Vehicle Route Traverse

The purpose of this test was to determine if the driver model can hold the vehicle on a given route model.

The following data were input:

$C = 1200$ ft-lb

$M = 383$ lb ft^2

$A_f = 25$ ft^2

$C_d = 0.5$

$W = 4000$ lb

$R_w = 1$ ft

$KA = 0.03$

The route profile consisted of an acceleration to 30 mph, cruise at 30 mph, followed by deceleration to rest (Figure 53). The route data are as follows:

LR (miles)	G	TI (sec)	AR (ft/sec^2)	VR (mph)	KF	CR
2.4	0	0	7	15	0.5	1
2.4	0	0	5	30	0.5	1
2.4	0	0	5	30	0.5	0
6.1	0	0	-7	0	0.5	-1

The integration was first selected as one second; the result is shown as Vehicle Traverse 1 in Figure 53. The vehicle tracks the reference conditions well during the acceleration period, but overshoots and oscillates about the speed limit. Reducing the integration step size to 0.1 second significantly reduces the overshoot and oscillation. These results indicate that the driver model is capable of holding the vehicle on a given route profile if the engine can provide the torque.

Case 2: Wheel Slip

The purpose of this test was to check out the wheel-slip logic of the driver and vehicle model.

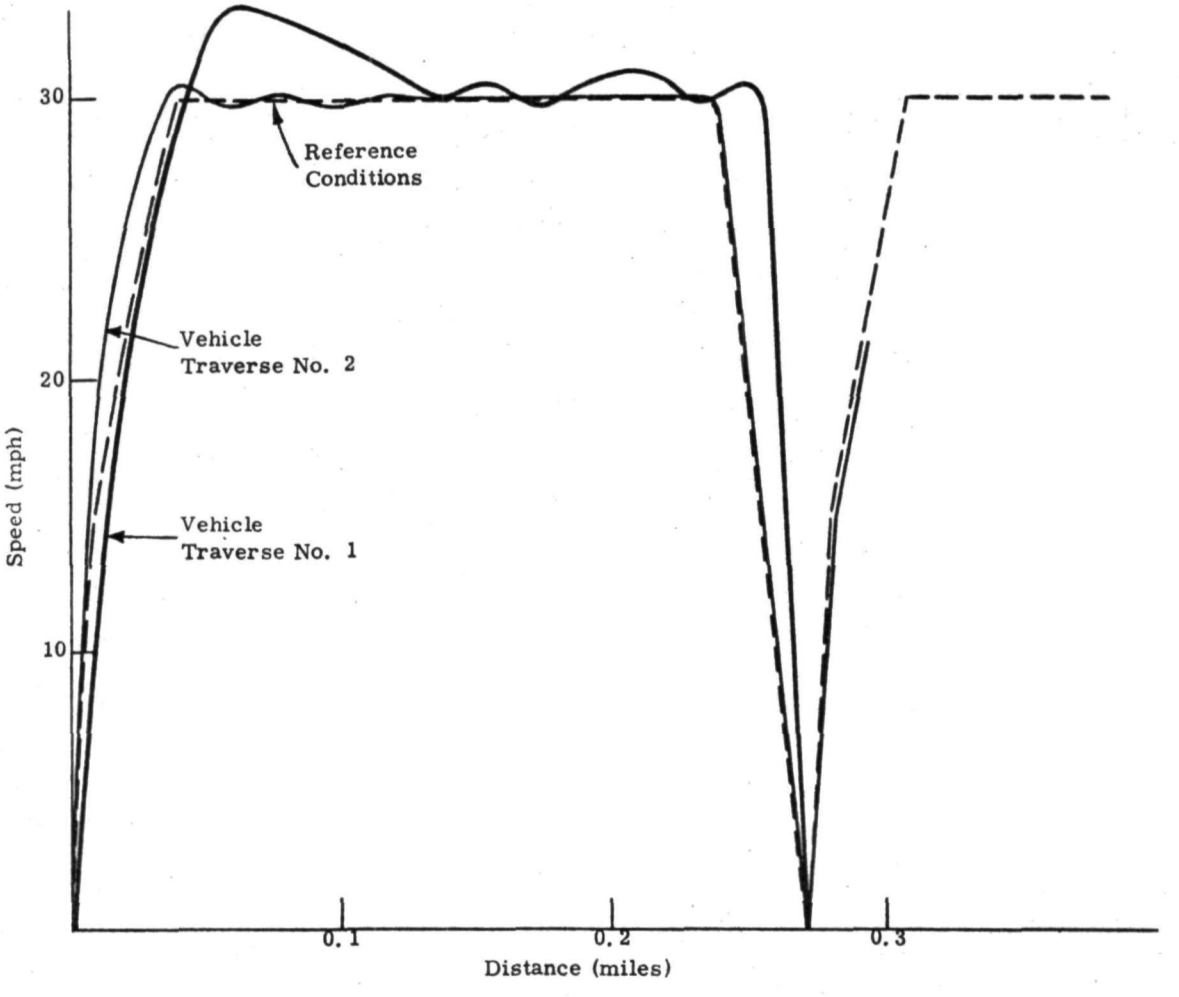

Figure 53. Comparison of Vehicle Traverse and Reference (Forcing) Conditions for a Linear Response Engine

The data were the same as in Case 1 except that C was made to equal 12, 000 foot-pounds so that the wheels would break away.

One line of data was provided for the route:

LR (miles)	G	TI (sec)	AR (ft/sec^2)	VR (mph)	KF	CR
0. 61	0	0	7	30	0. 5	1

Figure 54 shows the results. The wheels initially break away and accelerate to a high speed (the speed would not be as high in a real engine, but the fictional linear engine employed for this test is lossless). The driver model senses the wheel slip, releases the accelerator, and the engine slows down. The vehicle continues to accelerate.

In this instance the wheel speed undershoots the vehicle speed and the driver depresses the accelerator at a reduced sensitivity (KA is cut in half).

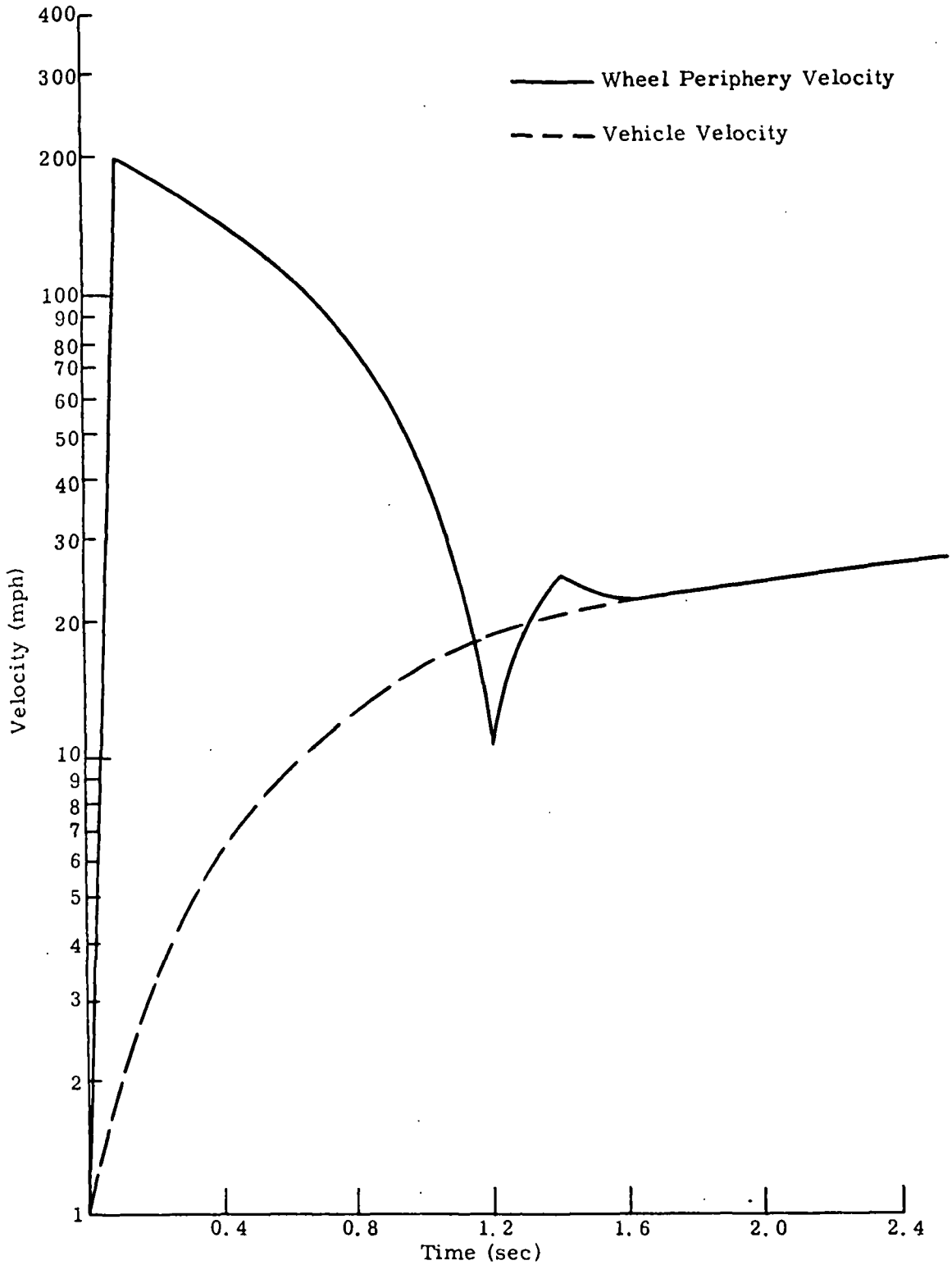

Figure 54. Response to Wheel Slip -- Driver Releases Accelerator and Reduces Acceleration Sensitivity

The wheels break away again, the accelerator sensitivity is reduced again until the wheel slip is under control. The above results illustrate the transients that the driver model is able to induce in the propulsion system.

The driver model is entitled DRIVER and is listed in Volume II of this report.

Section 5

TOTAL SYSTEM

The total system dynamic behavior depends upon the component dynamics, the control system and its dynamics, and the interaction between components and controls. The total system model therefore links the components and controls, and simulates the dynamic operation of the entire propulsion system. In order to analyze the vehicle performance in a driving situation, the propulsion system is linked to the transmission and vehicle models, and the route mission model is employed to generate system transients through the action of the driver model. The system model developed here is entitled MAINSYS, and is listed in Volume II (Users Manual) of this report.

METHOD OF SYSTEM ANALYSIS

The arrangement of component models in the system model is shown in Figure 55. The expander, the transmission, and the vehicle are joined by torque and speed linkages. The working fluid flow and properties link the expander, regenerator, condenser, pump, and vapor generator. The combus-

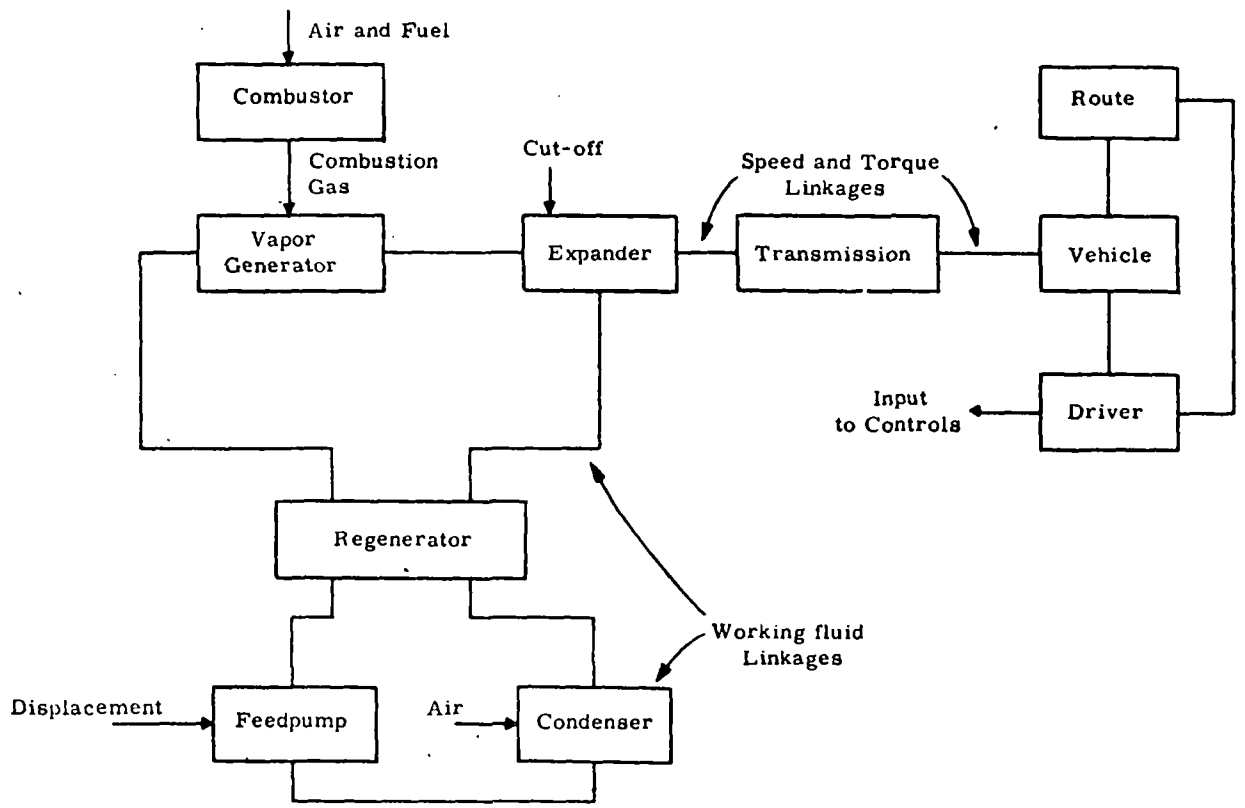

Figure 55. System Model Linkages

tion gas flow and temperature link the combustor and vapor generator. Speed, acceleration, and route conditions link the vehicle, route, and driver. The expander cut-off, pump displacement, condenser airflow, and fuel and combustor airflow are set by the controls which close the loop linking the driver to the rest of the system. The control system linkage is not shown in Figure 55.

The above arrangement provides a means of information transfer between models. The dynamic models of the components, derived earlier, predict transient behavior in response to input disturbances. The system model provides the necessary information link to change the input signals of a component in accordance with the variation in output signals of a neighboring component. Thus component interaction is maintained.

The direction of information flow depends upon the particular use of the system model; as will be shown later, the direction for deriving the total system steady-state condition differs from the direction for system transient analyses.

If the path connecting the components (duct, shaft, etc.) possesses a significant static or dynamic behavior, this should be considered when information is transferred between the components in the system model.

STEADY-STATE CONDITION

The usual first step in total system transient analysis is to derive steady-state cycle conditions and detailed distributions for each heat exchanger component at a desired power level. System transients are then superimposed on this steady-state condition.* The procedure to derive the steady-state distributions for the individual heat exchanger models was explained in the subsection "Heat Exchangers" of Section 3.

The system steady-state condition is derived as follows. Initial estimates are made for the expander cut-off, pump displacement, fuel and airflows, and some working fluid properties around the cycle (see Figure 56). The expander and pump speed are fixed.

Starting with the combustor model, the steady-state value of combustion gas temperature is obtained and transmitted to the vapor generator model. By application of the steady-state solution procedure, the pressure and enthalpy of the fluid stream at exit are obtained, as well as the detailed nodal distribution. These values are transmitted to the expander model to find the fluid flow rate and exit fluid enthalpy.

*It is not necessary to first bring the system to steady state. For example, a cold-start situation can be analyzed where the heat exchanger walls are not initially in steady state. All that is required is that the initial temperature distribution be prescribed.

In a similar manner each component is individually brought to a steady-state condition based upon the exit conditions of the previous component. The calculations proceed sequentially around the cycle in the direction of the working fluid until the vapor generator inlet is reached. The engine speed can be input to the transmission and the vehicle velocity determined.

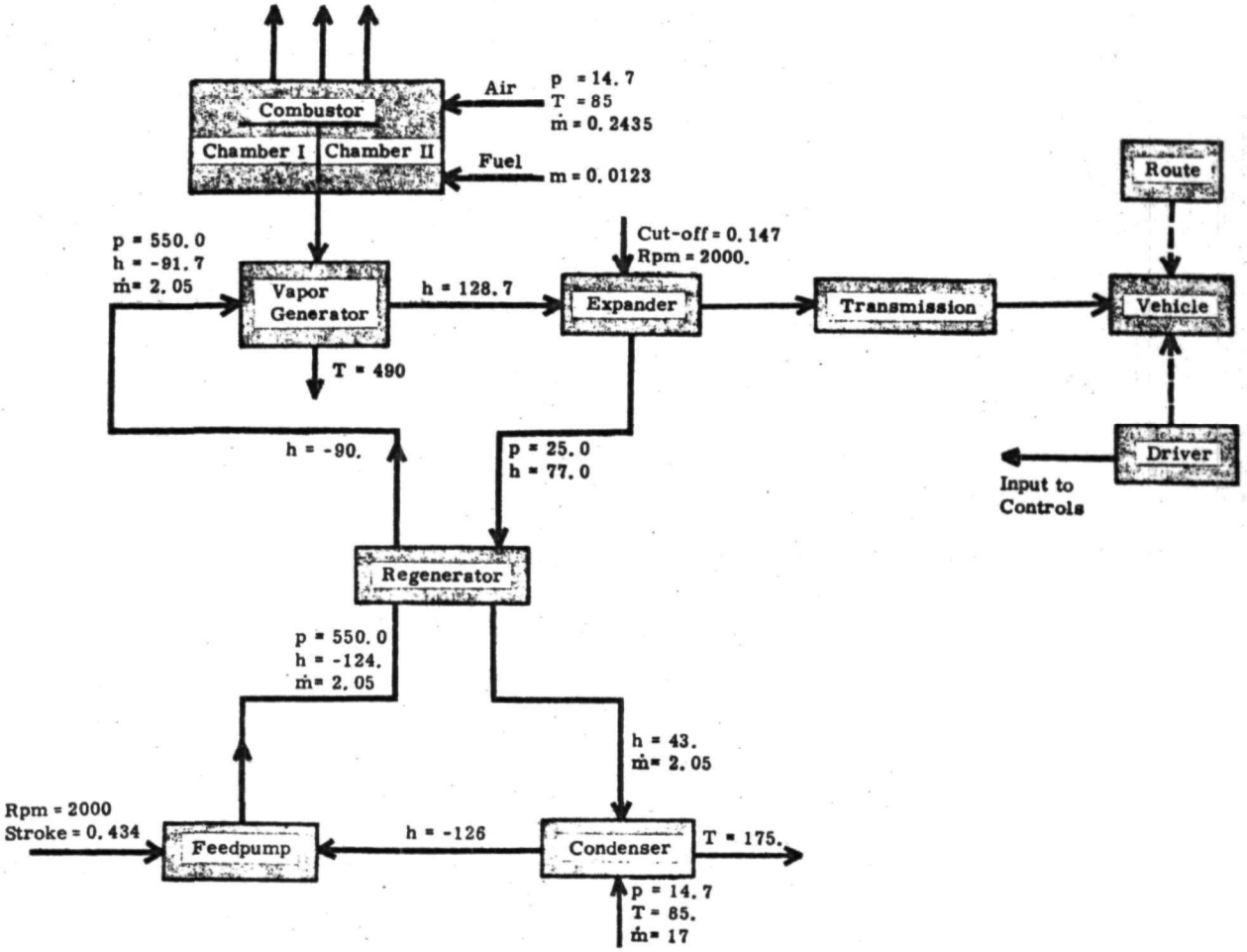

Figure 56. Total Systems Model -- Initial Estimates to Derive Cycle Design Conditions

At this point each component will be in a steady-state condition. The mass flows and fluid properties around the cycle may not match, however, because of the initial estimates on pump stroke, engine displacement, and fluid conditions. The control system can then be linked to the models so that these parameters are varied according to the control laws until the final steady-state condition is obtained.

TRANSIENT SIMULATION

After the total system model is brought to steady state at a particular operating condition corresponding to engine idle or vehicle cruise, propulsion-system transients can be analyzed. This requires a different linking of

components, which was employed in deriving the steady-state condition. This linkage is shown in Figure 57.

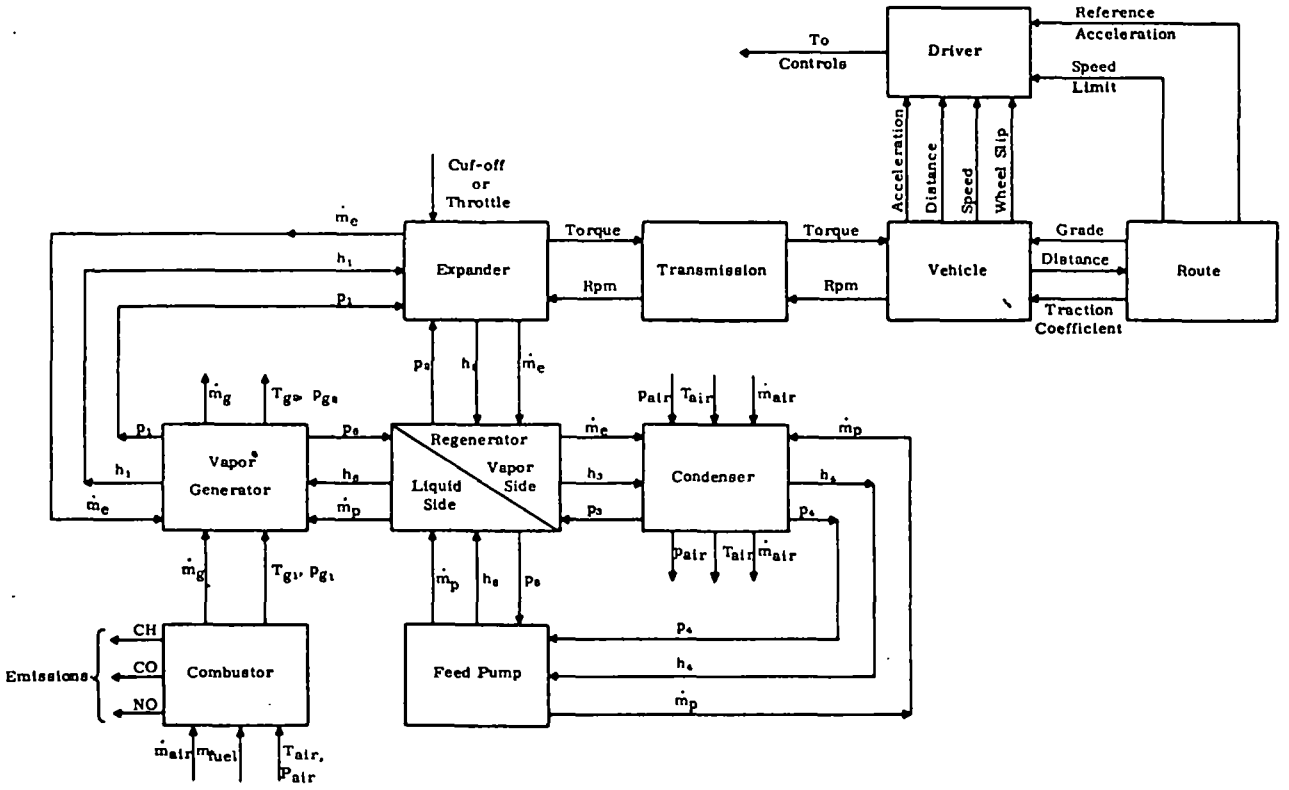

Figure 57. Dynamic System Information -- Signal Flow Diagram, Excluding Controls

The route mission information is transmitted to the driver, which acts by changing the accelerator pedal displacement. This changes other system parameters (fuel flow, feedpump stroke, expander cut-off, etc.) in accordance with the control strategy.

Initially, the cycle conditions and mass flow rates are at the steady-state condition previously derived. As the pump stroke and cut-off are adjusted by the control system, the mass flow through the pump and expander varies. This mass flow imbalance is transmitted to the vapor generator, regenerator, and condenser, causing a change in pressure in these heat exchanger components.

The new pressure levels are transmitted back to the expander and pump, and the power and torque are determined. The expander torque is conveyed through the transmission to the vehicle; this results in a change in vehicle and engine speed. The driver senses the acceleration rate and velocity of the vehicle, makes a comparison with the route mission demands, adjusts the accelerator pedal accordingly, and the transients continue.

The procedure is repeated to obtain new cycle conditions at selected time intervals. At each time interval, the new cycle conditions are stored and the effect of the next system disturbance is evaluated, starting from the cycle conditions at that time. This is continued until the route-mission traverse is completed. The cycle conditions plotted as a function of time represent the system dynamic behavior.

SYSTEM MODEL STRUCTURE

The system program, MAINSYS, is designed with a major emphasis on simplicity and flexibility. The program combines the components as shown in Figure 55. However, its modular structure and special data input arrangement makes the addition or elimination of any component (for example, regenerator) a simple task. Of course, the information signals rerouted as a result of such changes should be properly considered in the system model.

The input component design data and the initial values of various cycle parameters are organized on a component basis; hence, modification of data files is also easy. Similarly, the program output is printed on a component basis, with proper identification and clearly defined boundary values. A logic variable is available to specify the printing of additional details of the component model if these are needed. At the termination of the program, a detailed list of additional information is printed out for each fluid pass of the thermal components.

The system program can also be used,with minor changes, to study individual component transients. The changes are primarily due to the need to rearrange the direction of informational flow signals at the exit plane, as explained in Section 3 (subsection "Heat Exchanger") for the vapor generator.

RESULTS

The system program was run to derive steady-state cycle conditions under full-power design conditions. The program does not include any static or dynamic losses between the components, and the controls are not included. For the present purpose, the route and the driver models are bypassed.

Figure 56 represents the initial cycle conditions required to start the program. Figure 58 gives the cycle conditions obtained after one iteration, and Figure 59 is the actual computer print-out for this case. Since the mass flows through the expander, feedpump, and vapor generator and the fluid enthalpy values at the regenerator exit and vapor generator inlet do not match, further iterations with control interaction are required to bring the system to final steady state. After this has been accomplished, system transients can be run.

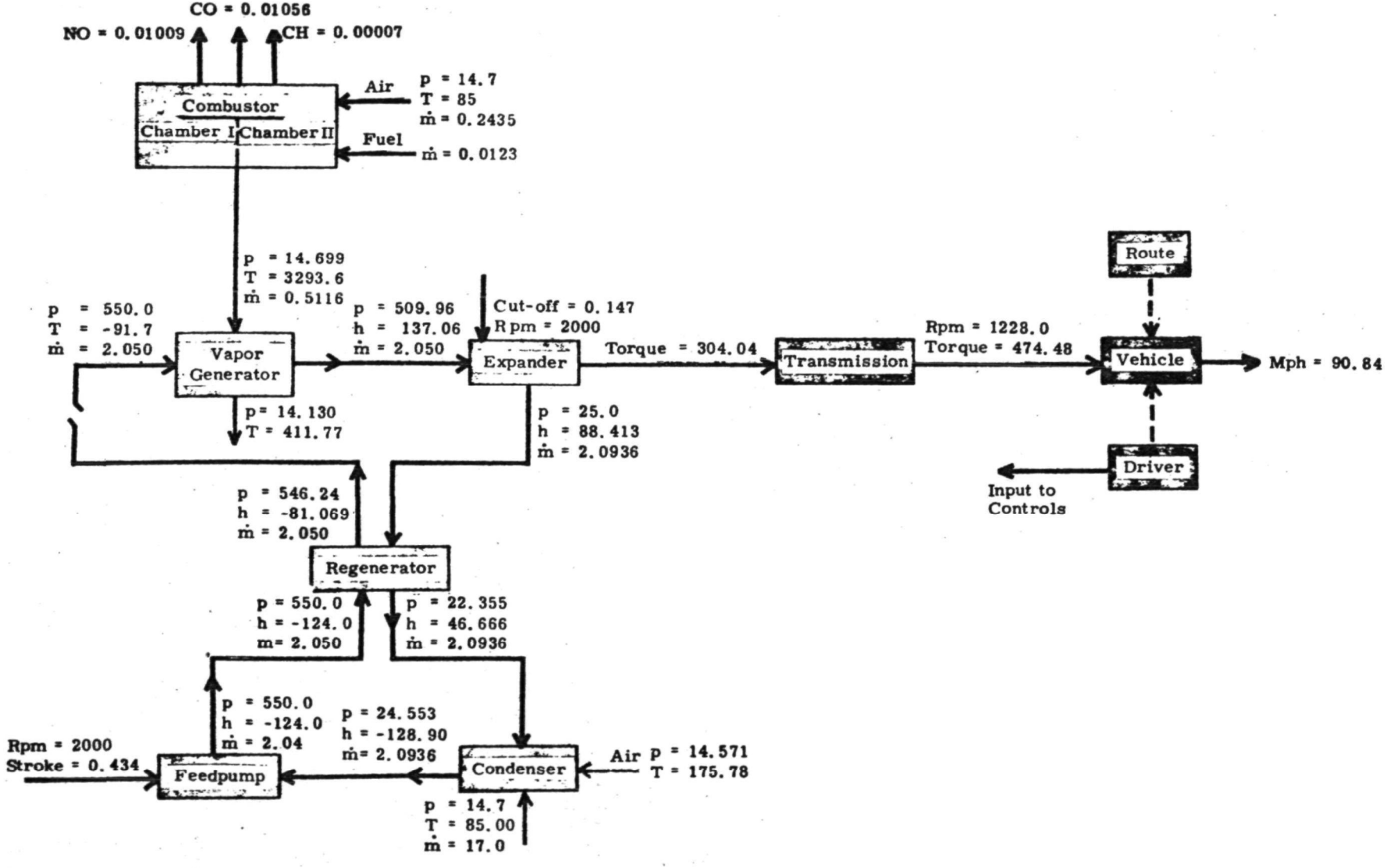

Figure 58. Total Systems Model -- Information Flow at Cycle Design Condition, Without Controls

```
AMBIENT PRES (PSIA), TEMP (F)      0.14700E 02   0.85000E 02
TIME      0.

                                        ***** COMBUSTOR *****

** FLOWS (LBS/SEC)
        AIR          0.24350E 00    FUEL        0.12300E-01

** TEMPERATURES (F)
        TUBE         0.26057E 04    SHELL       0.12491E 03
        AIR          0.12985E 03    GAS         0.32936E 04
        FLAME        0.33258E 04

** EMMISSIONS (GM/GM OF FUEL)
        NO           0.10090E-01    CO          0.10557E-01    CH          0.73214E-04

                                        ***** VAPOR GENERATOR *****

                          ***** TIME =    0.48095E-01    (TIMESTEP NO.    3 )

FLUID ENTHALPY (ENTRANCE)  =   -0.91700E 02
FLUID FLOW RATE (ENTRANCE) =    0.20500E 01
FLUID PRESSURE, SAT TEMP   =    0.55000E 03   0.52290E 03
GAS FLOW RATE (ENTRANCE)   =    0.51160E 00
GAS PRES, TEMP (ENTRANCE)  =    0.14699E 02   0.32936E 04
LUMP SIZE (COILS 1,2,3)    =    0.15600E 03   0.20400E 02   0.14000E 03

 LUMP        H2              TF              TT              TG2             H2          NPH
                                    ***** FLUID PASS NO.    1*****
   1     -0.69249E 02    0.30727E 03     0.36590E 03     0.39445E 03     0.20500E 01    1
   2     -0.48488E 02    0.35721E 03     0.40274E 03     0.42909E 03     0.20500E 01    1
                                    ***** FLUID PASS NO.    2*****
   1     -0.32335E 02    0.39693E 03     0.51016E 03     0.11879E 04     0.20500E 01    1
   2     -0.16303E 02    0.43012E 03     0.53445E 03     0.12043E 04     0.20500E 01    1
   3     -0.38375E 00    0.46025E 03     0.55743E 03     0.12199E 04     0.20500E 01    1
   4      0.15426E 02    0.48888E 03     0.57956E 03     0.12349E 04     0.20500E 01    1
   5      0.31131E 02    0.51585E 03     0.60052E 03     0.12491E 04     0.20500E 01    1
   6      0.47146E 02    0.52290E 03     0.53893E 03     0.12074E 04     0.20503E 01    2
   7      0.63172E 02    0.52290E 03     0.53689E 03     0.12060E 04     0.20510E 01    2
   8      0.79156E 02    0.52290E 03     0.53490E 03     0.12046E 04     0.20492E 01    2
   9      0.95296E 02    0.52290E 03     0.53217E 03     0.12028E 04     0.20496E 01    2
  10      0.11071E 03    0.52290E 03     0.65075E 03     0.12832E 04     0.20524E 01    2
                                    ***** FLUID PASS NO.    3*****
   1     0.11975E 03    0.53877E 03     0.56427E 03     0.83290E 03     0.20576E 01    3
   2     0.12853E 03    0.55906E 03     0.58374E 03     0.84410E 03     0.20602E 01    3
   3     0.13538E 03    0.57732E 03     0.60309E 03     0.85526E 03     0.21635E 01    3

UYY,TG1      0.16004E-01    0.84409E 03    0.32936E 04    0.12200E 04

                                    ** PRESSURE DROP RESULTS **
** GAS SIDE
  COIL        MASS FLOW          INLET P          INLET T          EXIT T          PR. DROP
    2      0.86712E-01     0.14699E 02     0.32936E 04     0.12200E 04     0.88290E-02
    3      0.57483E-01     0.14691E 02     0.12200E 04     0.84409E 03     0.15182E-01
    1      0.93018E-01     0.14675E 02     0.84409E 03     0.41177E 03     0.54579E 00

EXIT PRESSURE, TEMP    =    0.14130E 02    0.41177E 03

** FLUID SIDE
  COIL        FLOW               NPH              LENGTH          INLET PRES      PR. DROP
    1      0.20590E 01     1               0.26000E 02     0.55000E 03     0.17635E 01
    2      0.20500E 01     1               0.85000E 01     0.54824E 03     0.22646E 01
    2      0.20512E 01     2               0.85000E 01     0.54597E 03     0.17614E 02
    3      0.21080E 01     3               0.35000E 02     0.52836E 03     0.18397E 02

NCK,NX2Z,NX2          3          3          3
EXIT PRESSURE, ENTH    =    0.50996E 03    0.13706E 03

                                    ***** ENGINE *****

ENGINE SPEED, STROKE       0.20000E 04    0.14700E 00
INLET PRES, ENTHALPY       0.50996E 03    0.13706E 03
EXIT PRES, ENTHALPY        0.25000E 02    0.88413E 02
MASS FLOW (LBS/SEC)        0.20936E 01
OUTPUT TORQUE              0.30404E 03
```

Figure 59. Computer Output for System Steady-state Run (Sheet 1 of 3)

```
                                        ***** REGENERATOR *****
                        ***** TIME =       0.53987E 00          (TIMESTEP NO.    3 )

FLUID ENTHALPY (ENTRANCE)  =   -0.12400E 03
FLUID FLOW RATE (ENTRANCE) =    0.51250E 00
FLUID PRESSURE, SAT. TEMP  =    0.55000E 03    0.52290E 03
GAS FLOW RATE (ENTRANCE)   =    0.52339E 00
GAS PRES, ENTH (ENTRANCE)  =    0.25000E 02    0.88413E 02
LUMP SIZE (COILS 1,2,3,4)  =    0.10000E 03    0.10000E 03    0.10000E 03    0.50000E 02

  LUMP          H2               TF              TT              HG2             M2          NPH
                         ***** FLUID PASS NO.    7*****
   1        -0.11569E 03    0.20237E 03    0.22574E 03     0.46666E 02     0.51250E 00     1
                         ***** FLUID PASS NO.    8*****
   1        -0.10596E 03    0.22761E 03    0.25244E 03     0.54723E 02     0.51250E 00     1
                         ***** FLUID PASS NO.    9*****
   1        -0.94426E 02    0.25619E 03    0.28245E 03     0.64180E 02     0.51250E 00     1
                         ***** FLUID PASS NO.   10*****
   1        -0.87244E 02    0.28190E 03    0.31173E 03     0.74368E 02     0.51250E 00     1
   2        -0.81069E 02    0.29837E 03    0.32236E 03     0.76377E 02     0.51250E 00     1

DYY,TG1      0.17996E 00    0.27159E 03    0.30463E 03    0.34235E 03    0.38470E 03
                                  ** PRESSURE DROP RESULTS **

** GAS SIDE
  PASS      MASS FLOW        INLET P         INLET T          EXIT T          PR. DROP
   10       0.13085E 00    0.25000E 02     0.38470E 03     0.34235E 03     0.69127E 00
    9       0.13085E 00    0.24309E 02     0.34235E 03     0.30463E 03     0.66956E 00
    8       0.13085E 00    0.23639E 02     0.30463E 03     0.27159E 03     0.65029E 00
    7       0.13085E 00    0.22989E 02     0.27159E 03     0.24242E 03     0.63355E 00
EXIT PRESSURE, ENTH        0.22355E 02    0.46666E 02

** FLUID SIDE
  PASS        FLOW            NPH            LENGTH          INLET PRES       PR. DROP
    7       0.51250E 00        1          0.83333E 01     0.55000E 03     0.96143E 00
    8       0.51250E 00        1          0.83333E 01     0.54904E 03     0.94734E 00
    9       0.51250E 00        1          0.83333E 01     0.54809E 03     0.93354E 00
   10       0.51250E 00        1          0.83333E 01     0.54716E 03     0.92155E 00
EXIT PRESSURE, ENTH        0.54624E 03   -0.81069E 02

                                        ***** CONDENSER *****

                        ***** TIME =       0.18710E 00          (TIMESTEP NO.    3 )

FLUID ENTHALPY (ENTRANCE)  =    0.46666E 02
FLUID FLOW RATE (ENTRANCE) =    0.69785E-01
FLUID PRESSURE, SAT. TEMP  =    0.22355E 02    0.20899E 03
GAS FLOW RATE (ENTRANCE)   =    0.56667E 00
GAS PRES, TEMP (ENTRANCE)  =    0.14700E 02    0.85000E 02
LUMP SIZE (COILS 1,2,3)    =    0.10000E 02    0.10000E 02    0.10000E 02

  LUMP          H2               TF              TT              TG2             M2          NPH
                         ***** FLUID PASS NO.    4*****
   1         0.35026E 02    0.22481E 03    0.12382E 03     0.11523E 03     0.69785E-01     3
   2         0.42995E 01    0.20899E 03    0.18649E 03     0.16452E 03     0.69785E-01     2
   3        -0.25317E 02    0.20899E 03    0.18288E 03     0.16166E 03     0.69785E-01     2
   4        -0.55381E 02    0.20899E 03    0.17782E 03     0.15766E 03     0.69785E-01     2
   5        -0.79137E 02    0.20899E 03    0.17028E 03     0.15172E 03     0.69785E-01     2
                         ***** FLUID PASS NO.    5*****
   1        -0.87944E 02    0.20899E 03    0.18617E 03     0.17273E 03     0.69785E-01     2
   2        -0.96144E 02    0.20899E 03    0.18401E 03     0.17137E 03     0.69785E-01     2
   3        -0.10376E 03    0.20899E 03    0.18148E 03     0.16978E 03     0.69785E-01     2
   4        -0.11066E 03    0.20899E 03    0.17852E 03     0.16793E 03     0.69785E-01     2
   5        -0.11672E 03    0.20899E 03    0.17508E 03     0.16577E 03     0.69785E-01     2
                         ***** FLUID PASS NO.    6*****
   1        -0.12026E 03    0.20899E 03    0.18391E 03     0.17862E 03     0.69785E-01     2
   2        -0.12319E 03    0.20899E 03    0.18143E 03     0.17705E 03     0.69785E-01     1
   3        -0.12553E 03    0.20899E 03    0.17901E 03     0.17552E 03     0.69785E-01     1
   4        -0.12740E 03    0.20899E 03    0.17713E 03     0.17433E 03     0.69785E-01     1
   5        -0.12890E 03    0.20899E 03    0.17564E 03     0.17339E 03     0.69785E-01     1

DYY,TG1      0.62367E-01    0.85000E 02    0.15016E 03    0.16952E 03

                                  ** PRESSURE DROP RESULTS **
** GAS SIDE
  PASS      MASS FLOW        INLET P         INLET T          EXIT T          PR. DROP
    4       0.56667E 00    0.14700E 02     0.85000E 02     0.15016E 03     0.41361E-01
    5       0.56667E 00    0.14659E 02     0.15016E 03     0.16952E 03     0.43409E-01
    6       0.56667E 00    0.14615E 02     0.16952E 03     0.17578E 03     0.44149E-01
```

Figure 59. Computer Output for System Steady-state Run (Sheet 2 of 3)

```
EXIT PRESSURE, TEMP           0.14571E 02    0.17578E 03
** FLUID SIDE
  PASS           FLOW                NPH                   LENGTH           INLET PRES           PR. DROP
    4          0.69785E-01            3                  0.83333E 00       0.22355E 02         0.70980E 00
    4          0.69785E-01            2                  0.33333E 01       0.21646E 02        -0.12613E 01
    5          0.69785E-01            2                  0.41667E 01       0.22907E 02        -0.16432E 01
    6          0.69785E-01            2                  0.83333E 00       0.24550E 02        -0.86334E-01
    6          0.69785E-01            1                  0.33333E 01       0.24636E 02         0.83330E-01
EXIT PRESSURE, ENTH           0.24553E 02   -0.12890E 03


                                                   ***** FEED PUMP *****
STROKE,SPEED                 0.43400E 00    0.20000E 04
INLET PRES, TEMP             0.24553E 02    0.18733E 03
EXIT PRES                    0.55000E 03
FLOW,POWER                   0.20399E 01    0.48502E 01


                                                  ***** TRANSMISSION *****
INPUT SPEED, STROKE, TORQUE            0.12280E 04    0.14700E 00    0.30404E 03
OUTPUT SPEED, TORQUE                   0.20009E 04    0.47448E 03


                                                 ***** VEHICLE MOTION *****
VEHICLE SPEED(MPH), DISTANCE TRAVELED(MI)       0.90840E 02    0.37850E-01

END-POINT DISTRIBUTION AFTER THIS ITERATION
MAINOUT      1    1   -0.91700E 02   -0.48488E 02    0.84409E 03    0.41177E 03    0.             0.
MAINOUT      1    2   -0.48488E 02    0.11073E 03    0.32936E 04    0.12200E 04    0.             0.
MAINOUT      1    3    0.11073E 03    0.13706E 03    0.12200E 04    0.84409E 03    0.             0.
MAINOUT      2    4    0.46666E 02   -0.79137E 02    0.85000E 02    0.15016E 03    0.             0.
MAINOUT      2    5   -0.79137E 02   -0.11672E 03    0.15016E 03    0.16952E 03    0.             0.
MAINOUT      2    6   -0.11672E 03   -0.12890E 03    0.16952E 03    0.17578E 03    0.             0.
MAINOUT      3    7   -0.12400E 03   -0.11569E 03    0.27159E 03    0.24242E 03    0.54723E 02    0.46666E 02
MAINOUT      3    8   -0.11569E 03   -0.10596E 03    0.30463E 03    0.27159E 03    0.64180E 02    0.54723E 02
MAINOUT      3    9   -0.10596E 03   -0.94456E 02    0.34235E 03    0.30463E 03    0.75372E 02    0.64180E 02
MAINOUT      3   10   -0.94456E 02   -0.81069E 02    0.38470E 03    0.34235E 03    0.89527E 02    0.75372E 02
```

Figure 59. Computer Output for System Steady-state Run (Sheet 3 of 3)

Section 6

DISCUSSION AND RECOMMENDATIONS

Mathematical models required for digital simulation of the dynamics of Rankine cycle automotive propulsion systems have been developed. The following propulsion system components have been modeled:

Working fluid -- water and organic

Combustor

Vapor generator

Expander -- reciprocating and turbine

Regenerator

Condenser

Feedpump

Controls

Transmission, vehicle, driver, and route models have been developed to simulate transients produced in actual driving situations.

The dynamic models are valid over any operating range, and they have been calibrated with experimental results when such results were available. Working fluid properties and geometric and dimensional data are input quantities; hence, change of working fluid and design modifications are easily accounted for. The modular structure of the system program allows change in component arrangement or addition or elimination of any component (for example, regenerator). The programming language is FORTRAN IV and the models have been run on the General Electric 635 digital computer.

Additional important features, along with the strengths and limitations of each component model, are summarized in Table 11.

Data for a propulsion system with a reciprocating expander and organic working fluid (Ref. 1) were provided as input, and the component models were subjected to some representative open-loop transients. The component models were linked together to form a total system model, which was exercised without controls to derive the steady-state condition.

Although the main emphasis to date has been on model development rather than analysis of results, several recommendations can still be made. These are based on the experience obtained from the development of the models and the limited number of computer runs made for calibration and verification.

Table 11

SUMMARY OF COMPONENT MODELS

Component	Features	Strengths	Limitations
Working Fluid	1. Thermodynamic properties in superheated or saturated region determined through tabular interpolation. 2. Transport properties curve-fit with polynomial functions. 3. Input data for water, CP-34, and FC-75.	1. Thermodynamic models are valid for any fluid for which tabular data are available. 2. Model results in excellent agreement with standard thermodynamic tables.	Computer memory requirement for tabular data. Time required for full table search
Combustor	1. Calculates emissions and combustion gas temperature. 2. Thermal transients calculated employing lumped-parameter method. 3. Air preheated before entering combustion zone.		Emissions are based on steady-state emission data
Vapor Generator	1. Once-through monotube cross-flow configuration, with fluid passes arranged as in Reference 1. 2. Distributed parameter model. 3. Fluid change of phase (subcooled, boiling, and superheated) accounted for.	1. Vapor-generator dynamic behavior is simulated over wide nonlinear operating range. 2. Distributed parameter approach accounts for variation in properties along length of vapor generator. 3. Design modifications are easily accounted for by changing input data. 4. Forward finite-difference method gives explicit relations. Associated stability limits on distance and time step are computed in the program so that integration is always stable.	1 Complexity of vapor generator and sophistication of model adversely affects run time economy and storage requirement. 2. Effect of water jackets (Ref. 1) is accounted for by thermal storage capacity only
Condenser	1. Once-through multitube cross-flow configuration with fluid pass as in Reference 1 2. Distributed parameter model. 3. Fluid phase change accounted for.	Same as for vapor generator	Same as for vapor generator 1
Regenerator	1. Distributed parameter model. 2. Cross-flow configuration as in Reference 1. 3. Subcooled fluid in the tube. Superheated vapor outside the tube.	Same as for vapor generator, but no timewise pressure changes considered.	Same as for vapor generator 1
Expander-reciprocating	1. Quasi-steady model: speed change determined through vehicle dynamics. 2. Variable intake ratio. 3. Valve and heat losses accounted for. 4. Simple or compound expander.	Good agreement with results from Reference 1.	Small clearance and recompression

Table 11 (Cont'd)

Expander-turbine	1. Quasi-steady model: speed change determined by vehicle dynamics. 2. Single-stage axial impulse turbine. 3. Calculates off-design performance. 4. Nozzle and rotor losses accounted for.	Good correlation with expermental data	Losses would be underestimated for low specific-speed applications.
Feedpump	1. Variable stroke single-stage reciprocating pump. 2. Cavitation effects included.		
Transmission	Specific model for two-speed transmission from Reference 1.		
Vehicle	1. Motion is calculated on the basis of excess torque and road condition. 2. Air drag, grade, and traction loads are considered. 3. Wheel-slip conditions are predicted.		
Route	1. Input data in tabular form. 2. Reference velocity, acceleration, grade and idle time specified as a function of marker location.	Table can be extended to produce any driving cycle.	
Driver	Instantaneous model: physiological effects on gain not considered.		Perception-execution delay or physiological effects on gain not considered.
Controls	1. Instantaneous control models. 2. Strategy generally based on that described in Reference 1. 3. Power, working fluid, and air/fuel control relations.		

HEAT EXCHANGER DYNAMICS

The preliminary runs of the heat exchanger models (vapor generator, condenser, and regenerator) indicate that the heat exchanger transients have time constants of the order of 10 to 20 seconds. The other components (expander, pump, and controls) can be considered quasi-steady relative to the heat exchangers. Therefore the thermal inertials will determine propulsion system response. It is important to be able to accurately predict heat exchanger transients so that controls can be developed that will anticipate system changes and make appropriate adjustments.

Since heat exchanger dynamics are fairly sensitive to heat transfer coefficients, several assumptions made concerning the details of the heat transfer should be verified.

For example, the fluid capacitance of the vapor generator is related to the percentage volume occupied by the superheat region. The preliminary model results indicate that neglect of the water-jacket resistance in the TECO design resulted in a superheat region more than twice as long as calculated in Reference 1. However, the actual heat transfer mechanism in the 1/10-inch water jacket between the heat exchanger walls is not well known. By the use of the transient model this resistance can be varied parametrically in order to determine the sensitivity of the vapor generator performance to its value.

A second area where the vapor generator model can be expanded is the prediction of the heat transfer coefficient in the region where the quality is between 0.8 and 1.0. The two-phase heat transfer coefficient in the present model is based on the film boiling correlation below quality 0.8, and a linear interpolation between film boiling and convective heat transfer between qualities 0.8 and 1.0. This cut-off point is purely arbitrary and can be improved by using a better criterion, like the critical heat flux condition if such data are available.

If dynamics are found to be sensitive to the boiling-heat transfer correlation, the existence of various flow regimes -- stratified, annular, dispersed, bubble, or plug flow -- and their effect on boiling mechanisms can be included (Ref. 30).

All of the heat transfer mechanisms have been treated as quasi-steady; that is, steady-state correlations have been employed with instantaneous flow rates and fluid properties. Furthermore, standard correlations have been used which can vary from 10% to 20% when applied to different designs. Therefore it is essential to calibrate the heat exchanger models with transient experimental data for the particular designs to be analyzed.

Finally, in addition to the control system instability problems that can be caused by heat-exchanger dynamic response, the vapor generator itself may be subject to flow instabilities. Analyses of the latter were outside the scope of the present study, but they should not be ignored. Appendix IV, "Evaporator Flow Instability," of this volume gives a brief description of the effects and outlines the recommended steps for predicting stability limits.

On the basis of the above discussion, the following Recommendation 1, is made.

Recommendation 1:

- Sensitivity analyses should be carried out for

  Heat transfer coefficients

  Two-phase/vapor transition point

  Water-jacket resistance

These analyses would employ the models for parametric variation of the above items to determine their effect on steady-state and dynamic performance.

- The correlation of two-phase flow and heat transfer should be expanded to account for the various two-phase flow regimes.
- The heat exchanger models should be validated with transient experimental data.

RUN TIME ECONOMY

Figure 60 shows computer cost information for the vapor generator transient model. The data points used to construct this curve were obtained from actual computer runs with the model on the GE 635 computer.

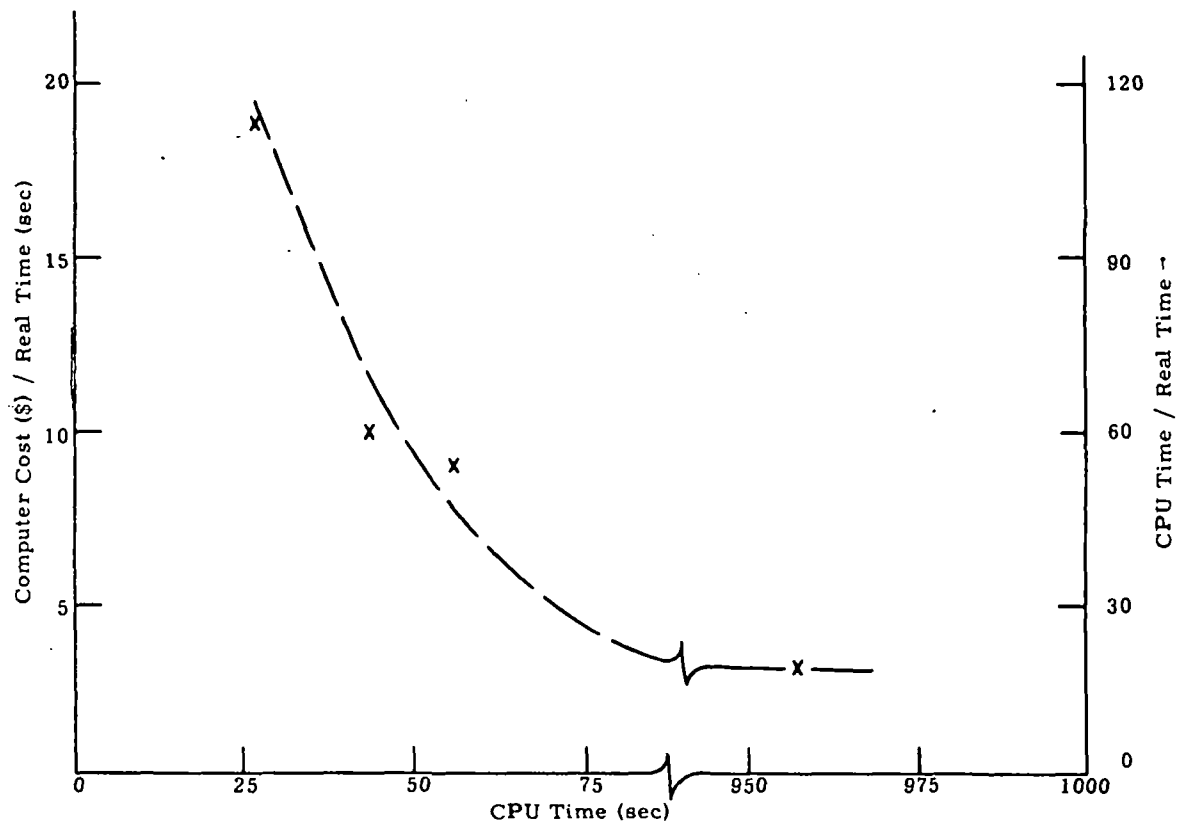

Figure 60. Computer Cost Information for Vapor Generator Transient Model

As can be seen, for a one-minute real-time transient the computer cost would be about $180. This is not an unusually high cost for the complex physical process simulated. The costs for total system transients would be of the same order of magnitude; the vapor generator model is the most costly to run and sets the time step for the rest of the system. There are several ways in which the run-time economy can be improved:

a. More efficient utilization of fluid property model

b. Using fixed time steps and lump sizes in the heat exchanger models

c. Development of "parametric models"

The heat exchanger models employ the fluid property models a large number of times. The heat exchanger models are incremented in approximately 1/100-second time steps as dictated by the stability criteria, and the fluid property models are called for each time step. Since the fluid properties do not change significantly for several time steps, the fluid property models could be used less frequently with little or no reduction in accuracy.

Furthermore, each time a fluid property model is used the entire saturated or superheated table is searched to find the appropriate fluid properties. For many transient situations the fluid properties are not expected to vary over such a wide range. An alternative search routine could therefore be employed where a selected region of the fluid property tables is searched first.

Another alternative would be to employ a binary search technique. Here the table is initially divided in half. It is then determined which half of the table contains the required fluid property; this half is, in turn, divided in half. The process is continued until the property is converged upon. More efficient utilization of the fluid property models should improve run-time economy.

The manner in which time steps and lump sizes are determined in the heat exchanger model is explained in Section 3. In summary, at a particular time the minimum lump size is determined from the stability criteria, and a node pattern is set up along the length of the heat exchanger. If the node pattern is different from that of a previous time, fluid and transport properties are determined at the new nodes by linear interpolation. The minimum time step is then determined, employing the stability criteria at each node. This procedure is repeated at each time step.

Considerable run-time economy can be achieved if a fixed time step and lump size are employed. The only requirement is that the values used to be less than as specified by the stability criteria. This can be assured by calculating the stability limits over the anticipated operating range and selecting smaller values for the fixed time step and lump size. The sections of the model which calculate the stability limits can then be bypassed when transient runs are made. If by chance the stability limits are exceeded during a run it will be immediately obvious, as the solutions will rapidly diverge. A simple limit check can be employed to stop the program if this happens.

A final method that can be employed to reduce run time and costs is to develop a set of "parametric models."

The dynamic component models are exercised for several transients at different power levels. The resulting open-loop performance is plotted parametrically and curve-fit with appropriate functions. The curve fits are programmed and then employed as models. It should be noted that the parametric models are not simple or approximate, involving a number of restrictions. They provide a valid representation of process dynamics over a limited range. Parametric models are more economical than the full-range dynamic models in situations requiring continual repeated use.

In summary of the above discussion the following, Recommendation 2, is made.

Recommendation 2:

In order to improve run-time economy it is recommended that

- Fluid property models be utilized more efficiently.
- Fixed time steps and lump sizes be employed in the heat exchanger models.
- Parametric models be developed.

CONTROL DEVELOPMENT AND SYSTEM DYNAMICS

Since the control performance depends directly on the process dynamics, a valid dynamic model of the inherently complex behavior of the Rankine cycle is required. The nature of system dynamics imposes the constraint on control dynamics. The optimum control approach would utilize the major features of system dynamics, would maintain desired operating conditions during any normal working range, and would be fail-safe under unusual working situations.

Over the wide operating range inherent in route mission situations, the process dynamics may differ significantly. The detailed, nonlinear models developed maintain all important dynamic features of the system at any power level. Hence, the models developed are an extremely powerful and useful tool which should be employed for the control system development.

By the use of parametric models, the detailed control dynamics can be investigated at reasonable cost. Here the individual loops can first be checked out analytically for stability and then for response. Following that, the complete system can be checked for interaction effects due to control dynamics using the parametric models. A subsequent check of the controls with dynamics on the complete detailed model would then be desirable.

Recommendation 3:

The following control systems development plan is recommended.

- The instantaneous control models that have been developed should be employed to bring the total system to steady state at the design condition, and small perturbation transients around this point should be analyzed. This will establish the basic validity of the control scheme.
- Acceptable limits on the variation of system parameters during transients should be established (e. g., the variation in expander mass flow demand during driving situations, assuming a droop in boiler pressure).
- The full-range dynamic models should be used to derive limited-range parametric models as described above.
- The instantaneous control scheme should be modified to include control dynamics. The controls should be developed by means of the parametric models.
- The final control scheme should be checked out with the full-range dynamic models.

Following this, route mission profiles can be traversed in order to determine fuel economy and emissions in grams per mile. The main advantage of this approach is in the minimal use of the full-range dynamic model and the economies achieved thereby. Furthermore, the parametric models will visually display the essential features of component dynamics and will help guide the control development.

APPLICATION TO SYSTEM DEVELOPMENT

Automobiles are always in transient operation; hence, development of propulsion systems requires thorough understanding of process dynamics so that control systems can be developed to insure desired performance over the total operating range. This is especially critical for maintaining low emission levels in spite of rapidly changing load conditions. To avoid costly and time-consuming development cycles, system simulation can and should be used in the early stages to uncover major problem areas in operation and control.

The models developed under the present program are highly flexible and general. They can be used to simulate the dynamics of (a) the water-based system with reciprocating expander, and (b) the organic-working-fluid system with turbine expander as well as (c) the organic fluid system with reciprocating expander for which they were checked out. The models can be easily modified and used to study the effect of transients typical of each system.

Recommendation 4:

The models should be employed for transient analysis of the systems and components under development by the Environmental Protection Agency, and the results used to support and guide the design and experimentation.

APPENDIX I

Appendix I

PARAMETRIC PROPULSION SYSTEM DESIGNS

In order to employ the dynamic model for simulation of Rankine cycle performance, dimensional and geometric data for the propulsion systems must be provided as input. Such data can come from existing system designs or can be generated by the use of the parametric design programs discussed in this Appendix.

These programs were calibrated with the Thermo Electron Corporation engine design -- simple reciprocating expander with CP-34 as working fluid (Ref. 1) -- and then employed to prepare preliminary designs for three other systems:

- Simple reciprocating engine with water as the working flud
- Turbine engine with FC-75 as the working fluid
- Compound reciprocating engine with water as the working fluid

Each system was designed for approximately 105 horsepower. The boiler conditions (pressure and temperature) at design were chosen fairly arbitrarily (reasonable values without exceeding the stability limits of the working fluid). Similarly, the condenser conditions at design were selected to give reasonable condensing temperatures.

These values could be optimized for high efficiency, but that was not the purpose here. The fluid properties around the cycle at design and the expander sizes were determined by the use of the programs EEFF (for the simple reciprocating expander), ECOMP (for the compound expander), and TSIZE (for the rotating expander). These programs are listed in Volume II, the Users Manual. The results are listed in Tables 12 to 15.

The components were sized on the basis of the design cycle conditions. The combustor, vapor generator, condenser, and regenerator dimensions are presented as Tables 16 to 22. These were determined by the use of the programs BLSIZ1 (for single-phase flow regimes of the vapor generator), BLSIZ2 (for two-phase flow regime of the vapor generator), CONDSZ (for the condenser), and RGSIZE (for the regenerator). These programs are listed in Volume II.

The heat exchanger components were sized using a computerized NTU (number of thermal units) method. In order to check the NTU method, the programs were run for the Thermo Electron system and the results compared to those given in the TECO report. This comparison is also shown in the tables.

Table 12

CYCLE DESIGN CONDITIONS FOR RECIPROCATING ENGINE WITH CP-34 AS WORKING FLUID

Location	Pressure (psia)	Temperature (°F)	Enthalpy (Btu/lb)	Specific Volume (ft^3/lb)
Boiler Exit	500	550	123	0.187
Engine Exit	25	348	77	4.05
Regenerator Vapor Exit	25	230	43	3.4
Condenser Exit	25	196	-126	0.016
Pump Exit	500	199	-124	0.016
Regenerator Liquid Exit	500	285	-90	0.018

Mass Flow Rate: 7301 lb/hr

Engine: 4 cylinders, 4.42-in. bore, 3-in. stroke
Design conditions: 2000 rpm, 127 indicated mean effective pressure, 0.137 intake ratio, 107.6 hp

Boiler: Heat rate $1.56\ 10^8$ Btu/hr, efficiency (higher heating value) 82.5%

Regenerator: Heat rate $2.468\ 10^6$ Btu/hr

Condenser: Heat rate $1.236\ 10^6$ Btu/hr

Pump: 5.2 hp at design

Cycle Efficiency: 16.8%

Table 13

CYCLE DESIGN CONDITIONS FOR RECIPROCATING ENGINE WITH WATER AS WORKING FLUID

Location	Pressure (psia)	Temperature (°F)	Enthalpy (Btu/lb)	Specific Volume (ft^3/lb)
Boiler Exit	1000	820	1401	0.702
Engine Exit	24	237	1098	16.1
Condenser Exit	24	217	185	0.0167
Pump Exit	1000	219	189	0.0167

Mass Flow Rate: 939 lb/hr

Engine: 4 cylinders, 2.78-in. bore, 3-in. stroke
Design conditions: 2000 rpm, 306 indicated mean effective pressure, 0.137 intake ratio, 105.3 hp

Boiler: Heat rate $1.139\ 10^6$ Btu/hr, efficiency (higher heating value) 82.5%

Condenser: Heat rate $8.575\ 10^5$ Btu/hr

Pump: 1.26 hp at design

Cycle Efficiency: 23.3%

Table 14

CYCLE DESIGN CONDITIONS FOR TURBINE ENGINE WITH FC-75 WORKING FLUID

Location	Pressure (psia)	Temperature (°F)	Enthalpy (Btu/lb)	Specific Volume (ft^3/lb)
Boiler Exit	220	446	130	0.0553
Turbine Exit	7.35	374	121	
Regenerator Vapor Exit	7.35	230	78.6	2 49
Condenser Exit	7.35	177	36.7	0 01
Pump Exit	220	177	37.2	0 01
Regenerator Liquid Exit	220	329	79.4	

Mass Flow Rate: 30,770 lb/hr

Engine: Single-stage impulse turbine, 7.65-in. diameter, 0.6-in. blade height, 0.012-in. tip clearance, 10° nozzle angle, 0.392-in^2 throat area, 2.62-in^2 exit area

Design conditions: 12,872 rpm, 0.548 speed ratio, 2.63 Mach number, 105 hp

Boiler: Heat rate $1.55\ 10^6$ Btu/hr, efficiency (higher heating value) 82.5%

Regenerator: Heat rate $1.3\ 10^6$ Btu/hr

Condenser: Heat rate $1.285\ 10^6$ Btu/hr

Pump: 6.6 hp at design

Cycle Efficiency: 16.1%

Table 15

CYCLE DESIGN CONDITIONS FOR COMPOUND ENGINE WITH WATER AS WORKING FLUID

Location	Pressure (psia)	Temperature (°F)	Enthalpy (Btu/lb)	Specific Volume (ft^3/lb)
Boiler Exit	1000	820	1401	0.702
First-stage Engine Exit	250	475	1248	2.08
Second-stage Engine Exit	22.8	235	1093	16.6
Condenser Exit	22.8	215	183	0 0167
Condenser-Pump Exit	250	216	184	0 0167
Feedwater Heater Exit	250	442	422	0.019
Boiler-Pump Exit	1000	444	425	0.019

Mass Flow Rate: First stage: 1240 lb/hr
Second stage: 962 lb/hr

Engine: First stage: 2 cylinders, 2.68-in. bore, 3-in. stroke
Design conditions: 2000 rpm, 361 indicated mean effective pressure, 0.37 intake ratio

Second stage: 2 cylinders, 4.05-in. bore, 3-in. stroke
Design conditions: 2000 rpm, 132 indicated mean effective pressure, 0.37 intake ratio

Hp at design: 106.6

Boiler: Heat rate $1.21\ 10^6$ Btu/hr, efficiency (higher heating value) 82.5%

Condenser: Heat rate $8.76\ 10^5$ Btu/hr

Pumps: Condenser pump, 0.4 hp at design
Boiler pump, 1.31 hp at design

Cycle Efficiency: 24.9%

Table 16

COMBUSTOR DESIGNS

Design Conditions
82.7% boiler-burner effectiveness
21,600 Btu/lb, higher-heating-value fuel
3330°F combustion-gas temperature
19.8 air/fuel ratio

As in TECO design, two combustion chambers with equal heat release rates are employed.

	Reciprocating Engine with CP-34	Reciprocating Engine with Water	Compound Reciprocating Water	Turbine Engine with FC-75
Heat Release at Design (Btu/hr)	$1.91\ 10^6$	$1.38\ 10^6$	$1.46\ 10^6$	$1.88\ 10^6$
Heat Release Maximum (Btu/hr)	$2.1\ 10^6$	$1.51\ 10^6$	$1.60\ 10^6$	$2.06\ 10^6$
Fuel Rate at Design (lb/sec)	0.0245	0.0178	0.0187	0.0242
Fuel Rate Maximum (lb/sec)	0.0275	0.0194	0.0205	0.0267
Air Rate at Design (lb/sec)	0.485	0.362	0.371	0.479
Air Rate Maximum (lb/sec)	0.534	0.385	0.466	0.529
Burner Length (in.)	17	12	13	16.7
Burner Diameter (in.)	7	7	7	7
Burner Weight (lb)	3.15	2.22	2.34	3.1
Shell Length (in.)	17	12	13	16.7
Shell-Burner Hydraulic Diameter (in.)	4	4	4	4
Shell Weight (lb)	6.8	4.8	5.16	6.7
Combustion Gas-Burner Wetted Area (in^2)	374	263	284	368
Shell-Air Wetted Area (in^2)	454	320	346	446
Air-Burner Wetted Area (in^2)	374	263	284	368

Table 17

RECIPROCATING ENGINE SYSTEM WITH CP-34 AS A WORKING FLUID

	Coil 1	Coil 2	Coil 3
Working Fluid			
Flow rate (lb/sec)	2.05	2.05	2.05
Inlet temperature (°F)	290	520	515 (0.525 qual
Exit temperature (°F)	390	515 (0.525 qual.)	550
Pressure (psi)	550	540	500
Combustion Gas			
Flow rate (lb/sec)	0.51	0.51	0.51
Inlet temperature (°F)	1190	3330	1896
Exit temperature (°F)	462	1896	1190
Tube Diameter			
Outer (in.)	1.315	1.315	1.315
Inner (in.)	0.930	0.930	0.930
Extended Surface, Outer	Ball Matrix	Finned	None
Ball diameter (in.)	3/32	--	--
Matrix thickness (in.)	0.5	--	--
Matrix porosity	0.39	--	--
Outer fin height (in.)	--	0.356	--
Outer fin thickness (in.)	--	0.012	--
Outer fin spacing	--	10	--
Extended Surface, Inner	None	Finned	None
Inner fin height (in.)	--	0.120	--
Inner fin thickness (in.)	--	0.0312	--
Inner fin number	--	16	--
Tube spacing (pitch) (in.)	2.28	2.23	1.42
Tube length calculated (ft)	21.6	Liquid, 8.1 2-phase, 5	2-phase, 24 2 Gas, 13.8
Tube length, TECO design (ft)	26	Liquid, 10 2-phase, 7	2-phase, 22.4 Gas, 12

Table 18

SIMPLE RECIPROCATING ENGINE SYSTEM
WITH WATER AS WORKING FLUID

	Vapor Generator Design		
	Coil 1	Coil 2	Coil 3
Working Fluid			
Flow rate (lb/sec)	0.253	0.253	0.253
Inlet temperature (°F)	220	545 (0 qual.)	545
Exit temperature (°F)	545	545 (1 qual.)	820
Pressure (psi)	1000	1000	1000
Combustion Gas			
Flow rate (lb/sec)	0.369	0.369	0.369
Inlet temperature (°F)	1274	3330	1776
Exit temperature (°F)	330	1776	1274
Tube Diameter			
Outer (in.)	1	1	1
Inner (in.)	0.9	0.9	0.9
Extended Surface, Outer	Ball Matrix	Finned	None
Ball diameter (in.)	3/32	--	--
Matrix thickness (in.)	0.5	--	--
Matrix porosity	0.39	--	--
Outer fin height (in.)	--	0.356	--
Outer fin thickness (in.)	--	0.012	--
Outer fin spacing	--	10	--
Extended Surface, Inner	None	Finned	None
Inner fin height (in.)	--	0.120	--
Inner fin thickness (in.)	--	0.0312	--
Inner fin number	--	16	--
Tube spacing (pitch) (in.)	2	2.0	1.1
Tube length (ft)	61	8.3	19

Table 19

TURBINE ENGINE SYSTEM WITH FC-75 AS WORKING FLUID

	Vapor Generator Design	
	Coil 1	Coil 2
Working Fluid		
Flow rate (lb/sec)	8.55	8.55
Inlet temperature (°F)	362	402
Exit temperature (°F)	402	446
Pressure (psi)	220	220
Combustion Gas		
Flow rate (lb/sec)	0.503	0.503
Inlet temperature (°F)	1850	3330
Exit temperature (°F)	400	1850
Tube Diameter		
Outer (in.)	1	1
Inner (in.)	0.9	0.9
Extended Surface, Outer	Ball Matrix	Ball Matrix
Ball diameter (in.)	3/32	3/32
Matrix thickness (in.)	0.5	0.5
Matrix porosity	0.39	0.39
Outer fin height (in.)	--	--
Outer fin thickness (in.)	--	--
Outer fin spacing	--	--
Extended Surface, Inner	None	None
Inner fin height (in.)	--	--
Inner fin thickness (in.)	--	--
Inner fin number	--	--
Tube spacing (pitch) (in.)	2	2
Tube length (ft)	15	4.5

Table 20

COMPOUND RECIPROCATING ENGINE SYSTEM
WITH WATER AS WORKING FLUID

	Vapor Generator Design		
	Coil 1	Coil 2	Coil 3
Working Fluid			
Flow rate (lb/sec)	0.345	0.345	0.345
Inlet temperature (°F)	445	545 (0 qual.)	545
Exit temperature (°F)	545	545 (1 qual.)	820
Pressure (psi)	1000	1000	1000
Combustion Gas			
Flow rate (lb/sec)	0.39	0.39	0.39
Inlet temperature (°F)	1102	3330	1755
Exit temperature (°F)	702	1755	1102
Tube Diameter			
Outer (in.)	1	1	1
Inner (in.)	0.9	0.9	0.9
Extended Surface, Outer	Ball Matrix	Finned	None
Ball diameter (in.)	3/32	--	--
Matrix thickness (in.)	0.5	--	--
Matrix porosity	0.39	--	--
Outer fin height (in.)	--	0.356	--
Outer fin thickness (in.)	--	0.012	--
Outer fin spacing	--	10	--
Extended Surface, Inner	None	Finned	None
Inner fin height (in.)	--	0.120	--
Inner fin thickness (in.)	--	0.0312	--
Inner fin number	--	16	--
Tube spacing (pitch) (in.)	2	2	1.1
Tube length (ft)	7.75	9	49.5

Table 21

CONDENSER DESIGNS

Flat Tubes with Louvered Fins	
Number of Parallel Tubes	30
Frontal Height	19.9 in.
Tube Width, Outer	0.75 in.
Tube Width, Inner	0.69 in.
Tube Height, Outer	0.206 in.
Tube Height, Inner	0.146 in.
Tube Spacing (Pitch)	0.664 in.
Fin Number	14/in.
Fin Height	0.465 in.
Fin Thickness	0.0025 in.
Metal - Tubes	Steel
Metal - Fins	Copper
Frontal Width	50 in.

	Reciprocating Engine with CP-34	Reciprocating Engine with Water	Compound Reciprocating Engine - Water	Turbine Engine with FC-75
Design Heat Rate (Btu/hr)	$1.23\ 10^6$	$0.857\ 10^6$	$0.876\ 10^6$	$1.51\ 10^6$
Working Fluid				
Flow rate (lb/sec)	2.03	0.261	0.267	8.54
Quality, in	1	1	1	1
Quality, out	0	0	0	0
Condenser Temperature (°F)	216	237	235	177
Pressure (psi)	25	24	23	7.35
Air				
Flow rate (lb/sec)	17	11.8	12	20.7
Inlet temperature (°F)	95	95	95	95
Tube Length (in.)				
Calculated	240	167	174	384
TECO design	200	--	--	--
Condenser thickness	3.75	3	3	6

Table 22

REGENERATOR DESIGNS

Designs Based Upon TECO Regenerator
Liquid Flow Inside Tubes, Gas Flow Across Tube Banks

Number of Flow Sections	4
Tube Banks	25 in. long, 4 tubes high
Tube Diameter, Outer	0.550 in.
Tube Diameter, Inner	0.5 in.
Tube Spacing (Pitch)	0.85 in.
Outer Surface	Ball Matrix
Matrix Porosity	0.35
Ball Diameter	0.0625 in.
Matrix Thickness	0.29 in.(CP-34), 0.55 in. (FC-75)
Matrix Height	0.3 in.
Metal	Steel

	CP-34 System	FC-75 System
Flow Rate (lb/sec)	2.05	8.54
Gas Side		
Inlet temperature (°F)	348	374
Exit temperature (°F)	230	230
Pressure (psi)	25	7.35
Liquid Side		
Inlet temperature (°F)	199	177
Exit temperature (°F)	285	322
Pressure (psi)	540	220
Tube Length (in.)		
Calculated	456	1334
TECO design	400	--

It can be seen that the NTU method does not accurately duplicate the TECO results in all cases. In fact, in some instances it differs by about 25 percent. This is probably due to the fact that the heat exchanger effectiveness correlations employed in these programs did not properly represent extended-surface heat exchangers (fins and ball-matrix). It should be noted that in the case of the bare surfaces the agreement is much better.

The NTU method is probably adequate for the purpose -- to roughly size the heat exchanger components so that the dynamic models can be checked out for the various systems.

In any case, if the dimensions derived for these components are grossly incorrect it will be immediately apparent in the dynamic modeling and modifications can be made.

The instantaneous control equations have been derived for the reciprocating expander with CP-34 as working fluid in Section 3 (subsection "Controls") of this volume. Employing the same techniques, the following instantaneous control equations apply for the reciprocating expander with water as the working fluid specified as the preceding paragraphs.

For Intake Ratio and Feed Pump

$$IR = 0.8\ AO$$

where

IR = Intake ratio
AO = Operator's input

The following limits apply:

$$\text{MAX IR} = 0.8 \text{ for } 0 \leq \text{RPM} \leq 342.5 \tag{157}$$

$$\text{MAX IR} = \frac{274}{\text{RPM}} \text{ for RPM} > 342.5 \tag{158}$$

$$\text{MIN IR} = 0.8 \text{ for } 0 \leq \text{RPM} \leq 285 \tag{159}$$

$$\text{MIN IR} = 0.05333\ (300\text{-RPM}) \text{ for } 285 \leq \text{RPM} < 300 \tag{160}$$

$$\text{MIN IR} = 0 \text{ for RPM} > 300 \tag{161}$$

The pump-stroke equation, based on 5% pressure drop, is

$$S_p = 1.25\ (IR) - \frac{(P_b - 1001.42)}{50} \tag{162}$$

APPENDIX II

where

S_p = Normalized pump stroke

IR = Intake ratio

P_b = Boiler outlet pressure psi

For Fuel Air Control

$$Q_f^* = 3.42836 + 0.00070\ Q_b + 0.00011\ Q_b^2 - 4.09780\ 10^{-8}\ Q_b^3 \quad (163)$$

where

Q_f^* = fuel flow (lb/hr) at 820°F boiler outlet temperature

Q_b = boiler inlet flow (lb/hr)

and

$$Q_f = Q_f^* + K_b\ (T_b - 820°) \quad (164)$$

where

$$K_b = -2.125 + 0.00118\ Q_b$$

Q_f = fuel flow (lb/hr) for small deviations (± 10°F) off 820°F boiler outlet temperature (°F)

T_b = boiler outlet temperature

The maximum fuel flow limit is 77 pounds per hour, and Q_f can never go negative. The air fuel relationship is

$$Q_A = 19.8\ Q_f \quad (165)$$

where Q_A is airflow rate (lb/hr).

Appendix II

STABILITY AND ERROR CRITERIA FOR FINITE-DIFFERENCE SOLUTION OF PARTIAL DIFFERENTIAL EQUATIONS

NOMENCLATURE

Alphabetical Symbols

A	Flow cross-section area
H	Enthalpy by finite-difference solution
h	Enthalpy by actual solution
$\dot{m}$	Mass flow rate
n	Node position n
$\dot{Q}$	Heat addition
t	Time
v	Specific volume
w	Discretization error
x	Distance
λ	$= \left(\frac{\dot{m}v}{A} \frac{\Delta t}{\Delta x}\right)$

The finite-difference approximation of a partial differential equation (PDE) should satisfy convergence criteria. The difference between the finite-difference solution (H) and the solution of PDE (h) at any grid point is known as the local discretization error, w, defined as

$$w = h - H$$

The convergence requires that $w \to 0$ as the grid spacing Δx and Δt tend to zero; this requirement will give stability criteria. During computation, since only a finite number of digits can be retained by the computer, the round-off error is introduced. Generally, this error grows in direct proportion to the grid refinement.

To obtain the stability criteria, examine the following energy equation:

$$\dot{m} \frac{\partial h}{\partial x} + \frac{A}{v} \frac{\partial h}{\partial t} = \dot{Q} \qquad (166)$$

For simplicity assume $\dot{m}$ and $\dot{Q}$ constants for the given grid and for a given time interval Δt. From Taylor's series expansion, supposing that h possesses a sufficient number of derivatives,

$$h\,(n+1, t) = h\,(n, t) + \Delta x\,\frac{\partial h}{\partial x} + \frac{(\Delta x)^2}{2!}\,\frac{\partial^2 h}{\partial x^2} + 0\left[(\Delta x)^3\right]$$

$$h\,(n+1, t+\Delta t) = h\,(n+1, t) + \Delta t\,.\,\frac{\partial h}{\partial t} + \frac{(\Delta t)^2}{2!}\,\frac{\partial^2 h}{\partial t^2} + 0\left[(\Delta t)^3\right]$$

Then

$$\dot{m}\,\frac{\partial h}{\partial x} = \frac{\dot{m}}{\Delta x}\left[h\,(n+1, t) - h\,(n, t) - \frac{(\Delta x)^2}{2!}\,\frac{\partial^2 h}{\partial x^2} - 0\left[(\Delta x)^3\right]\right]$$

$$\frac{A}{v}\,\frac{\partial h}{\partial t} = \frac{A}{v}\,\frac{1}{\Delta t}\left[h\,(n+1, t+\Delta t) - h\,(n+1, t) - \frac{(\Delta t)^2}{2!}\,\frac{\partial^2 h}{\partial t^2} - 0\left[(\Delta t)^3\right]\right] \qquad (167)$$

where the derivatives are evaluated at $((n+1)\,\Delta x,\ t)$

From Equations 166 and 167, the PDE can be represented as

$$\dot{m}\,\frac{\partial h}{\partial x} + \frac{A}{v}\,\frac{\partial h}{\partial t} - \dot{Q} = \frac{A}{v}\,.\,\frac{1}{\Delta t}\left[h\,(n+1, t+\Delta t) - h\,(n+1, t) - \frac{(\Delta t)^2}{2!}\,\frac{\partial^2 h}{\partial t^2} - 0\left[(\Delta t)^3\right]\right.$$

$$\left. + \frac{\dot{m} v}{A}\,\frac{\Delta t}{\Delta x}\left\{h\,(n+1, t) - h\,(n, t) - \frac{(\Delta x)^2}{2!}\,\frac{\partial^2 h}{\partial x^2} - 0\left[(\Delta x)^3\right]\right\} - \frac{\dot{Q} v\,\Delta t}{A}\right] \qquad (168)$$

From Dusinberre's explicit finite-difference approximation of Equation 166 (using H to denote the approximate solution),

$$H\,(n+1, t+\Delta t) = \left(\frac{\dot{m} v}{A}\,\frac{\Delta t}{\Delta x}\right) H\,(n, t) + \left(1 - \frac{\dot{m} v}{A}\,\frac{\Delta t}{\Delta x}\right) H\,(n+1, t) + \frac{Q v\,\Delta t}{A} \qquad (169)$$

From the definition of discretization error w, and from Equations 168 and 169, and using $\lambda = (\dot{m} v/A)(\Delta t/\Delta x)$,

$$w\,(n+1, t+\Delta t) = \lambda\, w\,(n, t) + (1-\lambda)\, w\,(n+1, t) + \frac{\dot{Q} v \Delta t}{A} + Z\,(n+1, t) \qquad (170)$$

where

$$Z\,(n+1, t) = \frac{(\Delta t)^2}{2!}\,\frac{\partial^2 h}{\partial t^2} + \lambda\,\frac{(\Delta x)^2}{2!}\,\frac{\partial^2 h}{\partial x^2} + 0\left[(\Delta t)^3\right] + 0\left[(\Delta x)^3\right]$$

If $0 < \lambda \leq 1$, the coefficients λ and $(1 - \lambda)$ are non-negative, and the inequality is

$$\left|w\,(n+1, t+\Delta t)\right| \leq \lambda\left|w\,(n, t)\right| + (1-\lambda)\left|w\,(n+1, t)\right| + \left|\frac{\dot{Q} v\,\Delta t}{A}\right| + \left|Z\,(n+1, t)\right| \qquad (171)$$

It can be proved that, provided $0 < \lambda \leq 1$, the discretization error is $0[(\Delta x)^2]$ and $0[(\Delta t)^2]$, and thus the explicit finite-difference representation converges as $\Delta x \to 0$ and $\Delta t \to 0$.

Note that Dusinberre's stability criterion is equivalent to the convergence criteria developed above. It can be shown that, for a linear partial differential equation, stability is a necessary and sufficient condition for convergence.

APPENDIX III

Appendix III

HEAT TRANSFER AND PRESSURE DROP RELATIONS

NOMENCLATURE

Alphabetical Symbols	
A	Flow area
B	Used in fin efficiency equation
b	Fin height
C_f, f	Friction factor
C_p	Specific heat
D	Hydraulic diameter
d	Tube diameter
E	Fin (or ball matrix) effectiveness
G	Volumetric flow rate
h	Heat transfer coefficient
k	Conductivity
K_1	Entrance expansion coefficient
K_2	Exit expansion coefficient
$\dot{m}$	Mass flow rate
n	Number of fins per inch
p	Pressure
Pr	Prandtl number
R	Matrix porosity (based on flow area)
Re	Reynolds number
S	Wetted area
T	Temperature
t	Tube spacing
w	Fin width
x	Quality
y	Length
η	Fin efficiency

Alphabetical Symbols Cont'd

μ	Viscosity
ρ	Density

Subscripts

bTi	Bare inner tube wall
b_{To}	Bare outer tube wall
e	Fins above
eTi	Finned inner wall
eTo	Finned outer wall
f	Working fluid
g	Combustion gas
gTo	Combustion gas and tube outer wall
k	Fuel
L	Liquid phase
m	Matrix
Ti	Tube inner wall
Tif	Tube inner wall and working fluid
v	Vapor phase

The heat transfer and pressure drop relations used for the Thermo Electron vapor-generator case are listed below.

HEAT TRANSFER COEFFICIENTS

BETWEEN WORKING FLUID AND INNER TUBE WALL (h_{Tif})

Single-phase Flow

$$h_{Tif} = (0.023)\left(\frac{G_f D_{Ti}}{\mu_f}\right)^{0.8}\left(\frac{C_{pf}\mu_f}{k_f}\right)^{0.4}\frac{k_f}{D_{Ti}} \qquad (172)$$

where the fluid properties are evaluated at the average fluid bulk temperature at a particular location.

Two-phase Flow

The heat transfer coefficient is broken up into two components (Ref. 31):

$$h_{Tif} = h_1 + h_2$$

The convective heat transfer coefficient, h_1, is defined as:

$$h_1 = (0.023) \quad (Re_\ell)^{0.8} \quad (Pr_\ell)^{0.4} \quad \frac{k_L}{D_{Ti}} \quad F \tag{173}$$

where

$$Re_\ell = \frac{G_f D_{Ti}}{\mu_L}$$

$$Re_\ell = \frac{C_{pL} \mu_L}{k_L} \tag{173a}$$

$$F = \text{Function (XT)}$$

$$XT = \left(\frac{x}{1 - x}\right)^{0.9} \quad \left(\frac{\rho_L}{\rho_V}\right)^{0.5} \quad \left(\frac{\mu_V}{\mu_L}\right)^{0.1}$$

and

$$\begin{aligned} XT &\leq 0.1 && \text{Function} = 1 \\ 0.1 < XT &\leq 0.4 && \text{Function} = 1.996\,(XT)^{0.3} \\ 0.4 < XT &\leq 2 && \text{Function} = 2.730\,(XT)^{0.643} \\ 2 < XT & && \text{Function} = 2.584\,(XT)^{0.721} \end{aligned} \tag{173b}$$

The boiling heat transfer coefficient, h_2, is defined as:

$$h_2 = \frac{(0.00122)\, k_L^{0.79}\, C_{pL}^{0.45}\, \rho_L^{0.49}\, (32.2)^{0.25}\, (\Delta T)^{0.24}\, (\Delta p)^{0.75}\, s}{\sigma^{0.5}\, \mu_L^{0.29}\, (\mu_V - \mu_L)^{0.24}\, \rho_V^{0.24}} \tag{174}$$

where

$$\Delta T = T_{Ti} - T_f$$

$$\Delta p = p_v (T_{Ti}) - p_V (T_f) \tag{174a}$$

$$s = \text{Function } Re_\ell\, (F^{1.25})$$

where F is as defined in Equation 173a and

$$
\begin{aligned}
10{,}000 &< Re_\ell F^{1.25} < 20{,}000;\ s = 2.282 - 0.15\ \ell n\,(Re_\ell F^{1.25}) \\
20{,}000 &\le Re_\ell F^{1.25} < 200{,}000;\ s = 3.343 - 0.257\ \ell n\,(Re_\ell F^{1.25}) \\
200{,}000 &\le Re_\ell F^{1.25} < 4\ 10^5;\ s = 2.032 - 0.150\ \ell n\,(Re_\ell F^{1.25}) \\
4\ 10^5 &\le Re_\ell F^{1.25};\ s = 0.1
\end{aligned}
\qquad (174b)
$$

Further,

$$
\sigma(T) = 0.2317\ 10^{-3} \left(\frac{1 - \frac{T}{584}}{0.818} \right)^{1.318} \qquad (175)
$$

The above two-phase heat transfer correlation for h_{Tif} is valid up to a quality of 0.8; for qualities between 0.8 and 1.0,

$$
\begin{aligned}
h_3 &= 0.023 \left(\frac{G_f D_{Ti}}{\mu_v} \right)^{0.8} \left(\frac{C_{pV}\ \mu_v}{k_v} \right)^{0.4} \frac{k_v}{D_{Ti}} \\
h_4 &= (h_1 + h_2)\ \text{(at } x = 0.8\text{, from Equations 173 and 174)}
\end{aligned}
\qquad (176)
$$

and

$$
h_{Tif} = h_3 + (x - 0.8)\,(h_4 - h_3)/0.2 \qquad (176a)
$$

Fins In Tube

If the inside of the tube is finned, the heat transfer coefficient becomes:

$$
h_{Tif} = E_{Ti}\ \frac{S_{eTi}}{S_{bTi}}\ h_{bTi} \qquad (177)
$$

where

$$
\frac{S_{eTi}}{S_{bTi}} = 1 + n_{Ti}\ (2b_{Ti})\ /\ \pi d_{Ti} \qquad (178)
$$

$$
E_{Ti} = \eta_{Ti}\ \frac{S_e}{S_{eTi}} + \frac{S_{bTi}}{S_{eTi}} \qquad (179)
$$

$$\frac{S_e}{S_{eTi}} = \frac{n_{Ti}(2b_{Ti} + w_{Ti})}{\pi d_{Ti} + n_{Ti}(2b_{Ti})} \quad (180)$$

$$\eta_{Ti} = \frac{\tanh(B_{Ti} b_{Ti})}{B_{Ti} b_{Ti}} \quad (181)$$

$$B_{Ti} = \sqrt{\frac{h_{bTi}^2}{k_{eTi} w_{Ti}}} \quad (182)$$

BETWEEN COMBUSTION GAS AND OUTER TUBE WALL (h_{gTo})*

Bare Tube

$$h_{gTo} = 0.237 \left[Re_g^{-0.4} Pr_g^{-2/3}\right] C_{pg} G_g \quad (183)$$

where

$$Re_g = \frac{G_g D_g}{\mu_g} \quad (184)$$

$$Pr_g = \frac{\mu_g C_{pg}}{k_g} \quad (184a)$$

Finned Tube

$$h_{bTo} = 0.1632 \left[Re_g^{-0.388} Pr_g^{-2/3}\right] C_{pg} G_g \quad (185)$$

Then

$$h_{gTo} = E_{To} \frac{S_{eTo}}{S_{bTo}} h_{bTo} \quad (186)$$

where

$$\frac{S_{eTo}}{S_{bTo}} = 1 + 2b_{To} n_{To} + \frac{2b_{To}^2}{d_{To}} n_{To} + \frac{2n_{To} w_{To} b_{To}}{d_{To}} \quad (186a)$$

$$E_{To} = \eta_{To} \frac{S_e}{S_{eTo}} + \frac{S_{bTo}}{S_{eTo}} \quad (186b)$$

*Only convective heat transfer relations are given here. The radiative effect, if important, should be included.

$$\frac{S_e}{S_{eTo}} = \frac{2n_{To}\left(b_{To} + b_{To}^2/d_{To} + w_{To}\,(1 + 2b_{To}/d_{To})\right)}{1 + 2n_{To}\,(b_{To} + b_{To}^2/d_{To} + w_{To}\,b_{To}/d_{To})} \quad (186c)$$

$$\eta_{To} = \frac{\tanh\left(B_{To}\,b_{To}\right)}{B_{To}\,b_{To}} \quad (186d)$$

$$B_{To} = \sqrt{\frac{h_{bTo}\,2}{k_{eTo}\,w_{To}}} \quad (186e)$$

Ball Matrix Between Tubes

$$h_{bTo} = 0.23\,(Re_g^{-0.3}\,Pr_g^{-2/3})\,G_g\,C_{pg} \quad (187)$$

$$h_{gTo} = E_m\,h_{bTo}\,5.249 \quad (188)$$

$$E_m = \frac{\tanh\,(z)}{z} \quad (189)$$

$$z = 3.63\,(1.94\,10^{-2})\,B_m \quad (190)$$

$$B_m = \frac{h_{bTo}}{k_m\,D_m} \quad (191)$$

PRESSURE DROP

WORKING FLUID

Single-phase Flow

$$\Delta p_f = \frac{2f\,G_f^2}{D_{Ti}\,\rho_f} \quad (192)$$

If $(Re_f) = \frac{G_f\,D_{Ti}}{\mu_f} < 3000$

$$f = 16/Re_f$$

If $3000 \leq Ref < 20{,}000$

$$f = 0.0791/Re_f^{0.25}$$

If 20,000 ≤ Ref

$$f = 0.046/Re_f^{0.2}$$

Two-phase Flow -- Martinelli-Nelson correlation (Ref. 30, p. 79)

$$\Delta p = \Delta p_1 + \Delta p_2 \tag{193}$$

where Δp_1 = friction pressure drop

Δp_2 = acceleration pressure drop

$$\Delta p_1 = \frac{\Delta p_1}{\Delta p_L} \Delta p_L$$

where Δp_L is the pressure drop as if all the fluid is liquid at the saturation temperature, and

$$\frac{\Delta p_1}{\Delta p_L} = (\phi)^2 (1 - x)^{1.8} \tag{194}$$

where x is the average quality in length Δy

$$\phi = \text{Function (XT)} \tag{195}$$

where XT is defined in the section on two-phase-flow heat transfer. The functional relationship between ϕ and XT is:

$$\ln \phi = 1.4516 - 8.688\ 10^{-4}\ \ell n\,(XT) + 5.463\ 10^{-6} \left[\ell n\,(XT)\right]^2 - 0.4784 \left[\ell n\,(XT)\right]^3 \tag{196}$$

The acceleration pressure drop is:

$$\Delta p_2 = 4G_f^2 \left(\frac{1 - x_2}{\rho_{L2}} - \frac{(1 - x_1)}{\rho_{L1}} + \frac{x_2}{\rho_{V2}} - \frac{x_1}{\rho_{V1}} \right) \tag{197}$$

where the subscripts 1 and 2 refer to locations in the tube.

COMBUSTION GAS (Ref. 32)

$$\Delta p = \frac{G_g^2}{\rho_{g_1}^2} (K_1 + 1 - \sigma^2) + 2 \frac{\rho_{g_1}}{\rho_{g_2}} - 1 + f \frac{S}{A} \rho_{g_1} \left(\frac{1}{\rho_{g_1}} + \frac{1}{\rho_{g_2}} \right) - (1 - \sigma^2 - K_2) \frac{\rho_{g_1}}{\rho_{g_2}} \tag{198}$$

K_1, K_2, and σ are defined below; subscripts 1 and 2 refer to axial locations.

Bare Tube

$$\sigma = (t_{To} - d_{To})/t_{To} \tag{199}$$

$$\frac{S}{A} = 4\frac{d_{To}}{D_{To}} \tag{200}$$

$$f(C_f, Re_g) = C_f (Re_g)^{-0.18} \tag{201}$$

$$C_f(z) = 0.3906\ z - 0.3321 \tag{202}$$

$$z = t_{To}/d_{To} \tag{203}$$

$$\left.\begin{aligned} Re_g &= \frac{G_g D_{To}}{\mu_g} \\ K_1 &= 0 \\ K_2 &= 0 \end{aligned}\right\} \tag{204}$$

Finned Tube

$$\sigma = \frac{t_{To} - d_{To} - 2n_{To}\, b_{To}\, w_{To}}{t_{To}} \tag{205}$$

$$\frac{S}{A} = \frac{4(d_{To} + 2b_{To})}{D_{To}} \tag{206}$$

$$\left.\begin{aligned} f(Re_g) &= 0.151\,(Re_g)^{-0.346} \\ K_1(\sigma) &= 0.395\ \sigma^3 + 0.685\ \sigma^2 + 0.065\ \sigma + 0.8 \\ K_2(\sigma) &= -0.87\ \sigma^3 + 1.573\ \sigma^2 - 2.46\ \sigma + 1 \end{aligned}\right\} \tag{207}$$

Ball-matrix Tube

$$\sigma = R_m \tag{208}$$

$$\frac{S}{A} = \frac{4\,(0.0417)}{D_{To}} \tag{209}$$

$$\left.\begin{aligned} f\,(Re_g) &= 78.63\,Re_g^{-1.179} + 1.397\,Re_g^{-1.452} \\ K_1 &= 0 \\ K_2 &= 0 \end{aligned}\right\} \tag{210}$$

HYDRAULIC DIAMETERS

Hydraulic diameters are defined as $\frac{4A}{S/\Delta y}$.

INNER TUBE

Bare Tube

$$D_{Ti} = d_{Ti}$$

Finned Tube

$$D_{Ti} = \frac{\pi d_{Ti}^{\,2}}{4} - n_{Ti}\,w_{Ti}\,b_{Ti} \Big/ (\pi d_{Ti} + 2n_{Ti}\,b_{Ti}) \tag{211}$$

OUTER TUBE

Bare Tube

$$D_g = \frac{4\,(t_{To} - d_{To})}{\pi} \tag{212}$$

Finned Tube

$$D_g = \frac{4\,(t_{To} - d_{To} - 2n_{To}\,w_{To}\,b_{To})\,(d_{To} + 2b_{To})}{\pi n_{To}\,(d_{To}\,b_{To} + 2b_{To}^{\,2} + 2w_{To}\,b_{To}) + \pi d_{To}} \tag{213}$$

Ball-matrix Tube

$$D_g = \frac{\frac{4\,R_m}{6\,(1 - R_m)}}{d_s} \tag{214}$$

FLOW RATES

$$G = \dot{m}/A \tag{215}$$

WORKING FLUID

Bare Tube

$$G_f = 4\dot{m}_f/\pi d_{Ti}^2 \tag{216}$$

Finned Tube

$$G_f = \dot{m}_f \Big/ \left(\frac{\pi d_{Ti}^2}{4} - n_{Ti}\, w_{Ti}\, b_{Ti} \right) \tag{217}$$

COMBUSTION GAS

Bare Tube

$$G_g = \frac{(\dot{m}_a + \dot{m}_k)}{(t_{To} - d_{To})\, L_{To}} \tag{218}$$

Finned Tube

$$G_g = \frac{(\dot{m}_a + \dot{m}_k)}{(t_{To} - d_{To} - 2n_{To}\, w_{To}\, b_{To})\, L_{To}} \tag{219}$$

Ball-matrix Tube

$$G_g = \frac{(\dot{m}_a + \dot{m}_k)}{(t_{To} - d_{To})\, R_m\, L_{To}} \tag{220}$$

APPENDIX IV

Appendix IV

EVAPORATOR FLOW INSTABILITY

Under various conditions, some of which have been relatively well defined and analyzed, static, dynamic, or compound flow instabilities can exist in evaporators. These instabilities can lead to either high-frequency (acoustic) pressure oscillations or low-frequency pressure and flow oscillations under subcritical or near-critical thermodynamic conditions. They have caused premature burnout or mechanical evaporator failure when various means now available for avoiding unstable operation have not been introduced.

Static instabilities, such as the chugging oscillation, occur mostly with alkali liquid metals and with fluorocarbons, where large superheat is required for nucleation and where the boiling curve hysteresis sustains the oscillation. Dynamic instabilities, such as acoustic or density wave instabilities, can occur at low (5 - 30 Hz) or high (> 1000 Hz) frequencies; the low frequencies are usually associated with long evaporators. The dynamic instabilities can be associated with large-amplitude (100-psi amplitude in a 500-psia system) pressure oscillations.

The primary phenomena leading to static instabilities can be predicted by using steady-state criteria or correlations. The threshold of static instability can thus be predicted. For dynamic instabilities linearized solutions of the constitutive equations, together with carefully taken experimental data, have permitted the correct definition of several stable and unstable operating regions. These methods of analysis (Refs. 33 - 36) at least allow the designer to predict whether he is clearly stable or unstable or if he is in a "grey zone".

The following steps are therefore recommended for predicting evaporator stability or alleviating existing instabilities:

1. Determine system or loop instability by using Ledinegg criterion. Check for static instability, using steady-state correlations, to avoid or alleviate instabilities caused by boiling crises (dry wall), flow pattern transition, etc.
2. Check for the onset of dynamic (density wave) instabilities by using a simplified analytical model (Ref. 35) or empirical correlations (Ref. 37).
3. Validate the prediction from step 2, above, by a dynamically instrumented and controlled (single-tube) experiment carried out at the phase density ratio of interest. Since the amplitude of oscillations in a multitube evaporator will be less than that in a single-tube unit, this procedure should result in a conservative design.

4. Use the analytical model in step 2 and the instrumented experimental test section in step 3 to define system or control changes required to alleviate existing instabilities.

APPENDIX V

Appendix V

REFERENCES

1. Morgan, D. T., and Raymond, R. J., Conceptual Design Rankine-cycle Power System with Organic Working Fluid and Reciprocating Engine for Passenger Vehicles, Department of Health, Education and Welfare Final Report, Contract No. CPA 22-69-132, Thermo Electron Corporation, Waltham, Massachusetts, June 1970.

2. Meyer, C. A., et al., Thermodynamic and Transport Properties of Steam (1967 ASME Steam Tables), second edition, The American Society of Mechanical Engineers, New York, N. Y., 1967.

3. Yarrington, R. M., and Kay, W. B., "Thermodynamic Properties of Perfluoro-2 Butyltetrahydrofuran," Journal of Chemical Engineering Data, Vol. 5, No. 1, January 1960, pp. 24-29.

4. Fluorinert Branch Electronic Liquids Technical Information, Bulletin of the Minnesota Mining and Manufacturing Company, St. Paul, Minn., 1965.

5. The Extrapolation of FC-75 Thermodynamic Data to Low Pressures and Temperatures, Barber-Nichols Engineering Company Report, Arvada, Colorado, March 1971.

6. CP-34: Thermodynamic Fluid Candidate, Bulletin of Monsanto Company, St. Louis, Mo., August 1968.

7. Evaluation of FC-75 as a Rankine Cycle Working Fluid, Barber-Nichols Engineering Company Technical Report No. 100168, Arvada, Colorado, October 1968.

8. Shapiro, A. H., The Dynamics and Thermodynamics of Compressible Fluid Flow, Ronald Press, New York, N. Y., 1953, Chapter 4.

9. Foa, J. V., Elements of Flight Propulsion, John Wiley and Sons, Inc., New York, N. Y., 1960, Chapter 9.

10. Marks, L. S., Mechanical Engineers Handbook, McGraw-Hill Book Company, Inc., New York, N. Y., 1941, p. 1229.

11. Barber, R. E., "Effect of Pressure Ratio on the Performance of Supersonic Turbine Nozzles," Proceedings of the Fourth Intersociety Energy Conversion Engineering Conference, American Institute of Chemical Engineers, Washington, D. C., September 1969.

12. Total Environmental Facility, Interim Test Report on TIPI/TEF Breadboard System, for Fairchild Hiller Company, Bayshore, N. Y., by Barber-Nichols Engineering Company.

13. Takahashi, Y., Rabins, M. J., and Auslander, D. M., Control and Dynamic Systems, Addison - Wesley Publishing Company, Inc., Reading, Mass., 1970, pp. 291-296.

14. Campbell, D. P., Process Dynamics, John Wiley and Sons, Inc., New York, N. Y., 1958, Chapter 4.

15. Dusinberre, G. M., Heat Transfer Calculations by Finite Differences, International Textbook Company, Scranton, Pa., 1961.

16. Brown, F. T., "A Unified Approach to the Analysis of Uniform One-dimensional Distributed Systems," Paper No. 66-WA/AUT-20, presented at the American Society of Mechanical Engineers Winter Annual Meeting, 1966.

17. Wyngaard, J. C., and Schmidt, F. W., "A Comparison of Methods for Determining the Transient Response of a Shell-and-tube Heat Exchanger," Paper No. 64-WA/HT-20, presented before American Society of Mechanical Engineers.

18. Cima, R. M., and London, A. L., "The Transient Response of a Two-fluid Counterflow Heat Exchanger -- the Gas-Turbine Regenerator" (Paper No. 57-A-135), Transactions ASME, Vol. 80, July 1958, pp. 1169-1179.

19. Adams, J., Clark, D. R., Louis, J. R., and Spanbauer, J. P., "Mathematical Modeling of Once-through Boiler Dynamics" (paper No. 31-TP-65-177), IEEE Transactions on Power Apparatus and Systems, Vol. 84, February 1965, pp. 146-156.

20. Paschkis, V., and Hlinka, J., "Electric Analogy Studies of the Transsient Behavior of Heat Exchangers," Transactions of the New York Academy of Sciences, Vol. 19, 1957, pp. 714-730.

21. deMello, F. P., "Plant Dynamics and Control Analysis," Paper No. 63-1401 presented at National Power Conference, Institute of Electrical and Electronic Engineers and American Society of Mechanical Engineers, Cincinnati, Ohio, September 22-25, 1963.

22. Korol'kov, V. P., "Concerning the Dynamics of Vapor-Liquid Heat Exchangers," Heat Transfer - Soviet Research, Vol. 2, No. 3, May 1970, pp. 74-82.

23. Silvey, T.I., and Barker, J.R., "Hybrid Computing Techniques for Solving Parabolic and Hyperbolic Partial Differential Equations," Computer Journal, Vol. 13, No. 2, May 1970.

24. Hellman, S.K., Habetter, G., and Babrov, H., "Use of Numerical Analysis in the Transient Solution of Two-dimensional Heat Transfer Problem with Natural and Forced Convection," Transactions of the ASME, Vol. 78, August 1956, pp. 1155-1161.

25. Brown, D.H., "Transient Thermodynamics of Reactors and Process Apparatus," Advances in Nuclear Engineering, Vol. II, Part 2, 1957, Pergamon Press, New York, N.Y., pp. 526-534.

26. Baumeister, T., Mechanical Engineers Handbook, sixth edition, McGraw-Hill Book Company, Inc., New York, N.Y., 1964, pp 4-72.

27. Low Emission Burner for Rankine Engines for Automobiles, Department of Health, Education and Welfare Technical Report, Contract No. EHS-70-106, Solar Division, International Harvester Company (final report in preparation).

28. Study of Continuous-flow Combustion Systems for External Combustion Vehicle Power Plants, Department of Health, Education and Welfare Final Report,Contract No. CPA 22-69-129, The Marquardt Company, June 1970.

29. Vehicle Design Goals -- Six Passenger Automobile, Advanced Automotive Power Systems Program, Office of Air Programs, Environmental Protection Agency, Revision C, May 1971.

30 Tong, L.S., Boiling Heat Transfer and Two-phase Flow, John Wiley and Sons, Inc., New York, N.Y., 1965.

31. Chen, J.C., "A Correlation for Boiling Heat Transfer to Saturated Fluids in Convective Flow," Paper No. 63-HT-34, presented at Heat Transfer Conference, American Society of Mechanical Engineers and American Institute of Chemical Engineers, Boston, Mass., August 11-14, 1963.

32. Kays, W.M., and London, A.L., Compact Heat Exchangers, McGraw-Hill Book Company, Inc., San Francisco, Calif., 1964, p. 33.

33. Boure, J.A., and Mihaila, A., The Oscillatory Behavior of Heat Channels, Parts I and II, Report No. CEA-R-3049 (in French), Commissariat a l'Energie Atomique, Grenoble, France, September 1966.

34. Yadigaroglu, G., and Bergles, A.E.,"An Experimental and Theoretical Study of Density-wave Oscillation in Two-phase Flow, Massachusetts Institute of Technology Report No. DSR 74629-3, 1969.

35. Zuber, N., "An Analysis of Thermally Induced Flow Oscillations in the Near Critical and Super Critical Thermodynamic Region," General Electric Company, Corporate Research and Development Report No. 67-C-173, May 1967.

36. Friedly, J.C., "Some Aspects of Predicting Two-phase Flow Instabilities," General Electric Company, Corporate Research and Development, Report No. 68-C-436, November 1968.

37. Edeskuty, F.J., and Thurston, R.S., "Similarity of Flow Oscillations Induced by Heat Transfer in Cryogenic Systems," EURATOM Report, Proceedings, Symposium on Two-phase Flow Dynamics, Eindhoven, Netherlands, 1967, pp. 551-567.